Glutamate Ligation in the Ni(II) and Co(II) Responsive *Escherichia coli* Transcriptional Regulator, RcnR

Carolyn E. Carr,[§,†] Francesco Musiani,[‡] Hsin-Ting Huang,[§] Peter T. Chivers,[¶] Stefano Ciurli,[‡] and Michael J. Maroney[*,§]

§Department of Chemistry, University of Massachusetts, Amherst, Massachusetts 01003, United States

‡Laboratory of Bioinorganic Chemistry, Department of Pharmacy and Biotechnology, University of Bologna, Bologna, Italy

¶ Departments of Biosciences and Chemistry, Durham University, United Kingdom.

ABSTRACT: *Escherichia coli* RcnR (resistance to cobalt and nickel regulator, *Ec*RcnR), is a metal-responsive repressor of the genes encoding the Ni(II) and Co(II) exporter proteins RcnAB by binding to P_{rcnAB}. DNA-binding affinity is weakened when the cognate ions Ni(II) or Co(II) bind to *Ec*RcnR in a six-coordinate site that features a $(N/O)_5S$ ligand donor-atom set in distinct sites: while both metal ions are bound by the N-terminus, Cys35, and His64, Co(II) is additionally bound by His3. On the other hand, the non-cognate Zn(II) and Cu(I) ions feature a lower coordination number, have a solvent-accessible binding site, and coordinate protein ligands that do not include the N-terminal amine. A molecular model of apo-*Ec*RcnR suggested potential roles for Glu34 and Glu63 in binding Ni(II) and Co(II) to *Ec*RcnR. The roles of Glu34 and Glu63 in metal binding, metal selectivity and function were therefore investigated using a structure/function approach. X-ray absorption spectroscopy (XAS) was used to assess the structural changes in the Ni(II), Co(II), and Zn(II) binding sites of Glu $\rightarrow$ Ala and Glu $\rightarrow$ Cys variants at both positions. The effect of these structural alterations on the regulation of $P_{rcn}A$ by *Ec*RcnR in response to metal binding was explored using LacZ reporter assays. These combined studies indicate that while Glu63 is a ligand for both metal ions, Glu34 is a ligand for Co(II) but possibly not for Ni(II). The Glu34 variants affect the structure of the cognate metal sites, but they have no effect on the transcriptional response. In contrast, the Glu63 variants affect both the structure and transcriptional response, although they do not completely abolish the function of *Ec*RcnR. The structure of the Zn(II) site is not significantly perturbed by any of the Glu variations. The spectroscopic and functional data obtained on the mutants were used to calculate models of the metal site structures of *Ec*RcnR bound to Ni(II), Co(II) and Zn(II). The results are interpreted in terms of a switch mechanism, in which a subset of the metal binding ligands is responsible for the allosteric response required for DNA release.

Transition metals are essential for the function of a wide variety of proteins and are thus critical for the maintenance of proper cellular metabolism.[1-3] However, excessive metal levels are toxic.[4-8] It is therefore imperative that cells tightly regulate their intracellular metal content, which is often achieved by employing a cellular trafficking system composed of metal-binding proteins. The complexity of these systems is dependent on the requirements of the cell and on the metal ion in question. Typically, transition metal trafficking systems are equipped with importers, exporters, metallochaperones and accessory proteins required for metal insertion and metallocenter assembly, as well as regulatory proteins that control the cellular levels of the other trafficking proteins.[9] A common arrangement in bacteria employs metal-responsive transcriptional regulators to control the expression of metal importers and exporters.[2, 4, 10] These transcriptional regulators are metal-specific, responding only to a single "cognate" metal or a limited number of such metals. How these proteins distinguish cognate metal(s) from non-cognate metals with similar physical properties is not completely understood.[2, 9-15]

E. coli has no confirmed cobalt-containing proteins,[16] and while it can utilize vitamin-B_{12} if it is available, it cannot synthesize it *de novo*.[17-19] In contrast, *E. coli* requires nickel for the active sites of at least three anaerobically expressed hydrogenases, and thus has a dedicated nickel trafficking system for maintaining nickel homeostasis.[20-23] This trafficking system consists of an importer, NikABCDE,[24, 25] chaperones (*e.g.* HypA for hydrogenase-3),[26-28] accessory proteins involved in hydrogenase metallocenter assembly (HypB and SlyD),[29, 30] and an exporter, RcnAB.[31, 32] In addition, there are two homotetrameric transcriptional regulators: *Ec*NikR,[33, 34] which controls the expression of the Ni(II) importer NikABCDE by increasing the affinity for DNA in the Ni(II)-bound form, and *Ec*RcnR,[35, 36] which controls the expression of the Ni(II) and Co(II) exporter RcnAB by binding to DNA in the apo-form and decreasing the affinity for DNA when

bound to either Ni(II) or Co(II). RcnAB and RcnR are so far the only known proteins involved in Co(II) trafficking in *E. coli*.

RcnR is a founding member of a family of entirely α-helical transcriptional regulators.[37] This family is now known to be widespread across prokaryotes and senses a wide variety of substrates, including Cu(I) (CsoR and RicR),[38, 39] Ni(II) (RcnR and InrS),[35, 40] sulfide (CstR),[41] and formaldehyde (FrmR).[42, 43] *Ec*RcnR recognizes a TACT-G_6-N-AGTA DNA sequence, of which there are two in the *rcnA-rcnR* intergenic region.[44] In addition to its recognition sequence, tetrameric *Ec*RcnR interacts with the flanking DNA regions, leading to DNA wrapping.[44]

*Ec*RcnR binds a variety of metal ions *in vitro*, but only Ni(II) and Co(II) binding results in transcription of *rcnAB in vivo*.[44] Previous studies have established that cognate and non-cognate metals are distinguished in part by coordination number, a common feature of specific metal recognition in other metal-responsive transcriptional regulators,[10, 45, 46] as well as by ligand selection.[47, 48] Cognate metals were shown to bind to *Ec*RcnR in six-coordinate sites composed of $(N/O)_5S$ ligand donor-atoms, while non-cognate metals consistently showed lower coordination numbers.[35] Ligand selection also plays a role in the *Ec*RcnR response. *Ec*RcnR binds both cognate and non-cognate metals using the only cysteine in the protein, Cys35,[35] but cognate metals are distinguished from non-cognate metals by inclusion of the N-terminal amine in the coordination complex, thus accounting for the difference in coordination number of cognate versus non-cognate metals.[47] Consistent with this model, when the Co(II)-binding His3 residue was mutated to a Glu residue, Zn(II) can occupy a six-coordinate binding site and the protein is now responsive to Zn(II) in the cell.[47]

The Co(II)- and Ni(II)-bound forms of EcRcnR are distinguished in at least two ways: His3 is a ligand for Co(II) and not for Ni(II), and, in addition, the M-S(Cys35) distance differs greatly depending on the metal ion (Ni(II) = 2.6 Å and Co(II) = 2.3 Å).[47, 48] It has been previously suggested that metal/small molecule binding residues can be identified in members of the CsoR/RcnR family of transcriptional regulators by utilizing a W-X-Y-Z fingerprint motif.[37, 49] In EcRcnR, these positions are filled by His3, Cys35, His60, and His64, although His3 is not a Ni(II) ligand. However, there appears to be diversity in metal site structures and functions across the currently known members of the CsoR/RcnR family of transcriptional regulators. Two recently reported phylogenetic analyses and sequence alignments of the CsoR/RcnR family members reveal no clear distinction between the amino acids in the canonical W-X-Y-Z fingerprint that denotes first coordination sphere residues of this family for Ni(II) and Cu(I) sensors.[49, 50] For example, the Ni(II) sensor RcnR contains some of the same fingerprint motifs as the Cu(I) binding proteins CsoR and RicR, yet has a different metal binding motif than InrS, another known Ni(II)-responsive protein. Thus, as previously observed,[50] fingerprint analysis of this family of regulators is a poor way to identify the cognate metals. Metal site structures also do not help to identify the cognate metals, as SyInrS and EcRcnR both respond to Ni(II) binding but adopt distinct four-coordinate planar and octahedral geometries, respectively.[35, 40] Thus, each protein employs different structure/function relationships, although there is an emerging trend in terms of protein function in that regulators of importers (*e.g.,* InrS, NikR) employ four-coordinate Ni(II) sites, while regulators of exporters, such as RcnR, employ six-coordinate Ni(II) sites.

No structure of EcRcnR is yet available, but the protein shows homology to CsoR, a tetrameric copper sensing transcriptional regulator of the same family.[51] Recent structural bioinformatics

studies have provided a computational model of apo-EcRcnR in the tetrameric state,[52] in agreement with experimental data.[35] The structural model is consistent with the presence of three α-helices in each monomer (Figure 1A). The three α-helices form large contact surfaces that contribute to the building up of the dimer and the tetrameric oligomer is obtained by dimerization of the two dimers through the N-terminal helices. Figure 1B shows that the model of apo-EcRcnR features a large number of putative metal-binding residues localized at the interface between two monomers in the vicinity of Cys35 from one chain: the N-terminal amine, the imidazole rings of His3, His64 and His67, as well as His60, known to be involved in metal binding, are all found in this region. In addition, Glu34 and Glu63 are also located in this potential metal loading region (Figure 1B), and their carboxylate groups could act as ligands for Co(II) and Ni(II). Although not strictly conserved in the CsoR/RcnR family of transcriptional regulators, these glutamate residues lie in X-space and Z-space in the W-X-Y-Z spatial motif.

In order to test the involvement of the these two residues in metal-binding and effects on DNA-affinity, X-ray absorption spectroscopy (XAS) was used to assess the metal site structure in Co(II), Ni(II), and Zn(II) complexes of the EcRcnR variants E34A-RcnR and E63A-RcnR (loss of ligand variations) as well as E34C-RcnR and E63C-RcnR (ligand substitution variations). The results of XAS analysis confirm that both of these carboxylates are ligands in the Co(II) complex, while for Ni(II), only Glu63 unambiguously acts as a ligand. Neither Glu residue is found to be involved in Zn(II) binding. Promoter-lacZ fusion transcription reporter assays show that Glu34 is not critical for EcRcnR function, while Glu63 RcnR variants show a decreased response to both Ni(II)- and Co(II)-binding. The structures of EcRcnR bound to Ni(II), Co(II) and Zn(II) were modeled according to the spectroscopic and functional experimental data, providing a working hypothesis for understanding the geometrical arrangement of the metal-

binding ligands, a type of information not available from EXAFS analysis alone. The structures identify other putative ligands, and further understanding of the relationships between the metalation state and the DNA-binding capability of *Ec*RcnR.
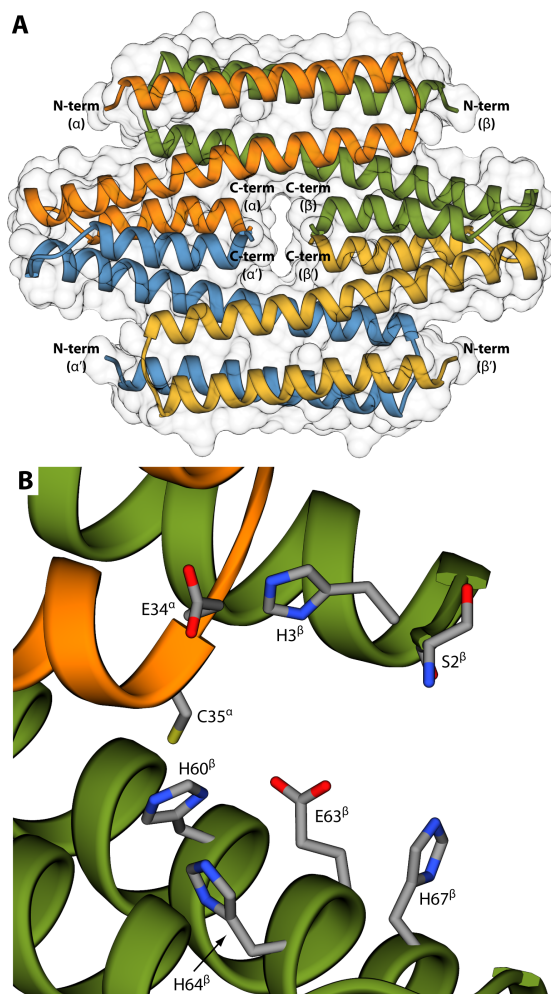
Figure 1: (A) Ribbon schemes and solvent-excluded surfaces of the tetrameric apo-*Ec*RcnR model structure.[52] (B) Details of the proposed metal binding region at the interface between two monomer chains (α, orange and β, green). Atoms are colored according to atom type.

MATERIALS AND METHODS

EcRcnR mutagenesis

Point mutations for producing E34A-, E34C-, E63A-, and E63C-*Ec*RcnR protein variants were introduced into the wild-type *Ec*RcnR gene on a pET22-b vector (pRcnR[36]) using the QuikChange (Stratagene) site-directed mutagenesis method. The same method and primers were used in order to introduce the point mutations on to the pJI114[35, 36, 44] vector for LacZ transcriptional assays. The mutations for E34A-RcnR and E34C-RcnR were made using PCR and employing the primers atgctcgacgagccgcacgcatgcgctgcagttttac and atgctcgacgagccgcactgttgcgctgcagttttac and their reverse complements, respectively. The mutation for the E63A-RcnR variant was made using the primers cgggaagtgattaaaggtcatctgacggcacacatc and catccccctggtgaacgatgtgtgccgtcag, while the mutation for the E63C-RcnR variant was made using the primers cgggaagtgattaaaggtcatctgacgtgccacatc and catccccctggtgaacgatgtggcacgtcag. The presence of the desired mutation was confirmed in each case via sequencing at GENEWIZ Inc. (South Plainfield, NJ).

RcnR expression and purification

Expression of all *Ec*RcnR variants was performed as previously described.[47, 48]

Chromatographic purification of *Ec*RcnR employed an AKTA-FPLC system (Amersham Biosciences). Lysate from 1 L of cells was loaded onto a 5 mL HiTrap Heparin HP column (GE Life Sciences) equilibrated with 20 mM HEPES, 1 mM TCEP, 5 mM EDTA, 10% glycerol, 300 mM NaCl at pH 7.0 (buffer A). The protein was washed with buffer A and then eluted in one step using 30% buffer B (20 mM HEPES, 1 mM TCEP, 5 mM EDTA, 10% glycerol, 1 M NaCl

at pH 7.0). The protein was eluted in four 5 mL fractions and the fraction containing *Ec*RcnR, as determined by SDS-PAGE, was then split into two 2.5 mL fractions and loaded on a 120 mL HiLoad 16/60 Superdex 75 (GE Life Sciences) column equilibrated with buffer A. Fractions were collected on the basis of absorbance at 280 nm. An SDS-PAGE gel was used to determine which fractions contained *Ec*RcnR. The fractions containing *Ec*RcnR were exchanged into buffer B containing 200 mM NaCl and loaded onto a 5 mL SP Sepharose HP column. The column was washed with buffer C (20 mM HEPES, 1 mM TCEP, 5 mM EDTA, 10% glycerol, 50 mM NaCl at pH 7.0) and then the protein was eluted in a single step using 40% buffer B and 60% buffer C in three fractions. The purity of the fractions was checked using SDS-PAGE. Fractions containing *Ec*RcnR were estimated to be >90% pure and were used without further purification. The expected molecular weights of the purified proteins were confirmed using electrospray ionization mass spectrometry (ESI-MS) using an ABI-SCIEX QSTAR-XL equipped with a turbo-spray ESI source in sequence with an Agilent 1100 HPLC system with a BioBasic-8 (Thermo Scientific) column for salt removal. Alternatively, samples were measured by direct injection following exchange into 200 mM ammonium acetate using Zeba desalting column. The calculated/observed monomer molecular weights of wild-type (10002.7/10002.6 Da), E34A- (9944.7/9945.0 Da), E34C- (9976.7/9975.9 Da), E63A- (9944.7/9945.1 Da), and E63C- (9976.7/9976.8 Da) *Ec*RcnR proteins confirm that the desired proteins were obtained.

Preparation of metal complexes

All proteins were concentrated to ~150 μM except where noted, and the solution was exchanged twice using a buffer containing 20 mM HEPES, 300 mM NaBr, 1 mM TCEP, 10% glycerol at pH 7.0 (buffer M). The exchange was performed using 10 mL Zeba spin desalting columns (Thermo Scientific) with a 7 kDa molecular weight cutoff to remove EDTA and exchange NaCl

for NaBr. The two samples in NaCl (E63A-RcnR with Co(II) and Ni(II)) were prepared using the same procedure except for the use of 300 mM NaCl instead of NaBr in the buffer. NaBr was used in XAS experiments to distinguish cysteine S-donors from Cl$^-$ ligands in the EXAFS analysis, and to identify solvent accessible sites when Br$^-$ binding to the metal occurs. Protein concentrations were confirmed using the experimentally determined extinction coefficient $\varepsilon_{276} =$ 2530 M^{-1} cm^{-1} from protein denatured with 8 M guanidine hydrochloride.[35] Four aliquots of a 50 mM stock solution in water providing a total of 2.5 equivalents of Ni(OAc)$_2$ or Co(OAc)$_2$ (Fisher Scientific) or 1.5 equivalents of Zn(OAc)$_2$ (J. T. Baker) were added to the apo-EcRcnR solutions to produce the respective metal complexes. The concentrations of the metal ion stock solutions were determined by using a Perkin-Elmer Optima DV4300 ICP-OES instrument. The protein samples were allowed to equilibrate overnight with the added metal ions before being incubated with Chelex (Sigma Aldrich) beads for ~30 minutes to remove nonspecifically bound metal ions. The protein solutions were then analyzed for metal content by ICP-OES. This analysis was performed by preparing a 1 ppm sample of the EcRcnR protein complexes using the previously determined protein concentrations. The metal:protein (monomer) ratios for samples prepared in buffer M were as follows: WT-EcRcnR, 1.2:1 for Ni(II), 0.8:1 for Co(II), 0.7:1 for Zn(II); E34A-EcRcnR, 0.4:1 for Ni(II), 0.6:1 for Co(II), 0.5:1 for Zn(II); E34C-EcRcnR, 0.2:1 for Ni(II), 1:1 for Co(II), 0.7:1 for Zn(II); E63A-EcRcnR, 0.4:1 for Ni(II), 0.3:1 for Co(II), 0.3:1 for Zn(II); E63C-EcRcnR, 0.5:1 for Ni(II), 0.2:1 for Co(II), 0.6:1 for Zn(II).

X-ray Absorption Spectroscopy (XAS)

Samples of the metallated proteins were concentrated to ~1-4 mM and a total volume of ~50 μL in buffer M (unless otherwise noted) using microspin concentrators (Millipore). The

concentrated samples were injected into polycarbonate XAS sample holders wrapped in kapton tape, and then rapidly frozen in liquid nitrogen and stored at -80 °C.

XAS data for the Co(II) E63C-*Ec*RcnR complex and Ni(II) complexes of WT-, E34A-, E34C-, E63A-, E63C-*Ec*RcnR, and Zn(II) complexes of E34C-, E63A-, and E63C-*Ec*RcnR were collected on beam line X3B at the National Synchrotron Light Source (NSLS), Brookhaven National Laboratories (Upton, NY). Data for the Co(II) complexes of WT-, E34A- E34C- E63A-, and E63A- (in NaCl buffer), for the Ni(II) complex of E63A- in NaCl buffer, and for the Zn(II) complex of WT- and E34A-*Ec*RcnR complexes were collected at the Stanford Synchrotron Radiation Laboratory (SSRL) on beam line 9-3. For data collected at NSLS, the samples were cooled to ~50 K using a He displex crysostat, and data was collected under ring conditions of 2.8 GeV and 120-300 mA using a sagittally focusing Si(111) double-crystal monochromator. X-ray fluorescence was collected using a 30-element Ge detector (Canberra). Scattering was minimized by placing a Z-1 filter between the sample chamber and the detector. For data collected at SSRL, the samples were cooled to ~10 K using a liquid helium cryostat (Oxford Instruments). The ring conditions were 3 GeV and 450-500 mA. Beam line optics included a Si(220) double-crystal monochromator. X-ray fluorescence data was collected using a 100-element detector (Canberra) at beam line 9-3 or a 30 element detector (Canberra) at beam line 7-3. Soller slits with a Z-1 element filter were placed between the sample chamber and the detector to minimize scattering.

Internal energy calibration was performed by collecting spectra simultaneously in transmission mode on the corresponding metal foil to determine the first inflection point on the edge, which was set to 7709.5 eV for Co(II), 8331.6 eV for Ni(II), or 9660.7 eV for Zn(II). X-ray absorption near-edge structure (XANES) data were collected from -200 to +200 eV relative to the metal K-

edge. Extended X-ray absorption fine structure (EXAFS) data were collected to $15k$ above the reference edge energy.

Data Reduction and Analysis

The SixPack software[53] program was used to remove bad channels, average the data, and to perform energy calibrations, in addition to data reduction and normalization. Edge normalization and background subtraction was performed using a Gaussian pre-edge function and a seven spline point quadratic polynomial between $k = 2$ Å^{-1} and $k = 14$ Å^{-1} for the post-edge region, followed by normalization of the edge jump.

The Artemis software program was used for EXAFS analysis. Artemis employs the IFFEFIT engine to fit EXAFS data using parameters generated by FEFF6. [54, 55] The data were converted to k-space using the relationship: $k = [\frac{2m_e(E-E_0)}{\hbar^2}]^{1/2}$. The k^3-weighted data were Fourier-transformed over a k-range of 2-12.5 Å^{-1} using a Kaisser-Bessel window for all data sets, and fit in r-space using an S_0 value of 0.9. The r-space spectra shown in the figures are not phase-corrected.

The Artemis software program was used for EXAFS analysis by utilizing the EXAFS equation with parameters generated using FEFF6.[54, 55] The EXAFS equation is defined as:

$$\chi(k) = \sum_i \frac{N_i f_i(k) e^{-2k^2\sigma_i^2}}{kr_i^2} \sin[2kr_i + \delta_i(k)]$$

where $f(k)$ is the scattering amplitude, $\delta(k)$ is the phase-shift, N is the number of neighboring atoms, r is the distance to the neighboring atoms, and σ^2 is the disorder to the nearest neighbor.

Data sets were fit with separate sets of Δr_{eff} and σ^2 for the sulfur, nitrogen, and imidazole rings with initial values of 0.0 Å and 0.003 Å^2, respectively. Each fit was initiated with a universal E_0 (7723 eV for Co, 8340 eV for Ni, and 9670 eV for Zn) and an initial ΔE_0 of 0 eV, the latter of which was allowed to vary for each fit. In order to assess multiple-scattering contributions from histidine imidazole ligands, fits were performed over an r-space range of 1-4 Å. Histidine ligands were fit as geometrically rigid imidazole rings with varied angles of rotation, α, with α being defined as the rotation around an axis perpendicular to the plane of the ring and going through the coordinated nitrogen. In this manner, the distances of the five non-hydrogen atoms in the imidazole ring were fit in terms of a single metal-N bond distance for various angles ($\alpha = 0 - 10°$).[56-58] Multiple-scattering parameters for imidazole ligands bound to nickel, cobalt and zinc were generated using the FEFF6 software package with the initial input obtained from average bond lengths and angles gathered from crystallographic data, as previously described.[56, 59] All paths with relative amplitudes larger than 16% of the pathway with maximum intensity were included.

To assess the goodness of fit from different fitting models, the fit parameters χ^2, reduced χ^2 (r χ^2), and r-factor were minimized. Increasing the number of adjustable parameters is generally expected to improve the R-factor; however χ^2 may go through a minimum, the increase indicating that the model is overfitting the data. These parameters are defined as follows:

$$\chi^2 = \frac{N_{\text{idp}}}{N_{\varepsilon^2}} \sum_{N}^{i=1} (\{\text{Re}[\tilde{\chi}_{\text{data}}(R_i) - \tilde{\chi}_{\text{theory}}(R_i)]\}^2 + \{\text{Im}(\tilde{\chi}_{\text{data}}(R_i)) - \tilde{\chi}_{\text{theory}}(R_i)]\}^2)$$

and

$$r\chi^2 = \frac{\chi^2}{N_{\text{idp}} - N_{\text{var}}}$$

where N_{idp} is the number of independent data points defined as $N_{\text{idp}} = \frac{(2\Delta r \Delta k)}{\pi}$, Δr is the fitting range in r-space, Δk is the fitting range in k-space, N_{ε^2} is the number of uncertainties to minimize, Re() is the real part of the EXAFS Fourier-transformed data and theory functions, Im() is the imaginary part of the EXAFS Fourier-transformed data and theory functions, and $\tilde{\chi}(R_i)$ is the Fourier-transformed data or theoretical function.

Additionally, IFEFFIT calculates the R-factor for each fit, which is directly proportional to χ^2 and is the root-mean-square difference between the data and calculated fit, and given by:

$$R = \frac{\sum_{i=1}^{n}\{[\text{Re}[\tilde{\chi}_{\text{data}}(R_i) - \tilde{\chi}_{\text{theory}}(R_i)]\}^2 + \{\text{Im}(\tilde{\chi}_{\text{data}}(R_i)) - \tilde{\chi}_{\text{theory}}(R_i)]\}^2)}{\sum_{i=1}^{n}\{[\text{Re}(\tilde{\chi}_{\text{data}}(R_i))]^2 + [\text{Im}(\tilde{\chi}_{\text{data}}(R_i))]^2\}}$$

Magnetic susceptibility measurements.

Evans' NMR method[60] was used to measure the magnetic susceptibility of Ni(II) complexes (2.25 mM Ni(II) WT-*Ec*RcnR and 0.939 mM E63C-*Ec*RcnR) that were buffer exchanged into 20 mM HEPES,150 mM NaCl, 1 mM TCEP, 5% glycerol, pH 7.0 in 90% H_2O/10% D_2O. The protein solutions (400 μL) were placed into an NMR tube and a coaxial insert containing the 10% deuterated buffer was placed inside the NMR tube. Relative shifts between the DSS (4,4-dimethyl-4-silapentane-1-sulfonic acid) reference peak at 0 ppm and the peak shifted due to the magnetic properties of the protein sample in the outer NMR tube were used to calculate μ_{eff} using equations:[61, 62]

$$\chi_g = \frac{-3\Delta v}{4\pi v_o m}$$

$$\chi_M = \chi_g M$$

$$\chi'_M = \chi_M - \Sigma \chi_L$$

$$\mu_{eff} = 2.83\sqrt{\chi'_M T}$$

where χ_g is the gram susceptibility in cgs units, χ_M is the molar susceptibility, χ_M' is the molar susceptibility corrected for the diamagnetic contribution of the protein, μ_{eff} is the magnetic moment in Bohr Magnetons, m is the concentration of the sample in g/mL, Δv is the peak separation in Hz, v_o is the frequency of the spectrometer in Hz (400.132471 x 10^6 Hz), M is the molecular weight of the protein in g/mol, χ_L is the diamagnetic correction for the protein, and T is the temperature (298 K). The diamagnetic correction was determined by measuring Δv for apo-protein at the same concentrations and using that to calculate the molar susceptibility of apo-protein.

LacZ reporter assays

LacZ reporter assays were carried out as previously described[63] with the following modifications. Starter cultures of *E. coli* strain PC113 (Δ*rcnR*) cells containing WT or mutant *rcnR* genes on the *rcnR-PrcnA-lacZ* plasmid (pJI114)[36] were grown aerobically overnight at 37 °C in Luria-Bertani broth (LB) with chloramphenicol. These cultures were used to inoculate duplicate cultures in 2.0 mL LB with chloramphenicol in sterile culture tubes. These cultures were grown aerobically to an OD_{600} ~0.3-0.7 and then placed on ice to arrest cell growth. The OD_{600} of each culture was recorded prior to placing 200 μL of culture into a 2.0 mL micro-centrifuge tube containing 800

μL of the LacZ assay buffer.[63] For metal induction experiments, cells were treated in the same way, except that before the addition of cells to the duplicate cultures, a maximal concentration of metal that resulted in < 10% inhibition of growth was added to each culture (300 μM $Zn(OAc)_2$, 130 μM $CoCl_2$, or 700 μM $NiCl_2$). Metal titration experiments were performed identically to the metal induction experiments. Metal was added to each individual culture with a range of 0 – 180 μM $CoCl_2$ and 0 – 900 μM $NiCl_2$. All experiments were performed in quadruplicate. Statistical significance was determined by performing a one-way ANOVA statistical analysis followed by Dunnett's test for multiple comparisons.

Fluorescence Anisotropy

5' TAMRA (5-carboxytetramethylrhodamine) labeled oligonucleotide GATTCTACTCCCCCCCAGTACCTG and non-labeled complementary strand CAGGTACTGGGGGGGGAGTAGAATC were annealed by heating a 10 μM solution of each strand in 10 mM HEPES, 150 mM NaCl, 5 mM EDTA, pH 7.0 to 95 °C and then cooling overnight. WT-, E63A-, and E63C-*Ec*RcnR were prepared in 10 mM HEPES, 150 mM NaCl, 5 mM EDTA, 1 mM TCEP, pH = 7.0 (FA buffer). A final DNA concentration of 10 nM was prepared in FA buffer in a 1 cm fluorescence cuvette (Firefly Scientific). *Ec*RcnR was then titrated into the cuvette, and changes in anisotropy were measured using a QuantaMaster-7 2003 fluorimeter (Photon Technology International) fitted with polarizing filters (excitation: 543 nm, emission: 575 nm, averaging time: 10 s, independent replicates: 3). The data was fit using DynaFit[64] using a one-step model where one *Ec*RcnR tetramer binds to one DNA molecule.

Computational studies

A model structure for tetrameric apo-*Ec*RcnR has been previously calculated by homology modeling using all available crystal structures of CsoR (PDB codes: 2HH7, 3AAI, 4M1P, and 4ADZ), a copper-dependent transcription factor belonging to the same family of DNA-binding proteins as RcnR[52] To model the metal-bound forms of *Ec*RcnR, the same procedure was repeated, using Modeller v9.12[65] with the same template structures and sequence alignments, and incorporating the additional experimental information available from EXAFS analysis of the metal complexes of WT-*Ec*RcnR to guide the calculations (see Table 3 for details), in analogy with a published protocol.[66] In particular, for each modeled structure, four metal ions were included in the calculation (one per subunit), in agreement with the prior characterization[35] as well as with the metal content analyses carried out in this study. The van der Waals parameters for Co(II), Ni(II), were derived from the Zn(II) parameters included in the CHARMM22 force field implemented in the Modeller v9.12 package by applying a scale factor calculated on the basis of the ionic radius of each metal ion. In all modeling calculations that included metal ions, constraints were imposed using a Gaussian-shaped energy potential for distances, angles and dihedrals in order to correctly position the metal ions (M) with respect to the experimentally identified ligated residues (see Table 3). Symmetry restraints were also applied in the calculation in order to obtain four symmetrically identical monomers. The best model was selected on the basis of the lowest value of the DOPE score in Modeller. [67] A loop optimization routine was used to refine the regions that showed higher than average energy as calculated using the DOPE score. The results of the PROCHECK analysis [68] for the final model were fully satisfactory ($\geq$ 97.5% most favored regions, $\leq$ 2.5% additional allowed regions). The molecular (solvent-excluded) surfaces and graphics of *Ec*RcnR model structures were calculated using the UCSF Chimera package (see supporting information for additional details).[69]

RESULTS

Metal Site Structural Analysis

X-ray absorption spectroscopy (XAS) was used to examine the metal site structures of complexes of WT-*Ec*RcnR and its Glu34 and Glu63 variants in order to elucidate whether these two residues are first coordination sphere ligands and if they are involved in distinguishing cognate (*i.e.*, Co(II) and Ni(II)) from non-cognate (*e.g.*, Zn(II) and Cu(I)) metals.

X-ray absorption near-edge structure (XANES) analysis was used to provide information regarding the coordination number and geometry of the metal centers. Metal ions with vacancies in the 3d orbitals, such as Co(II) and Ni(II), exhibit features below the edge energy that involve 1s → 3d electronic transitions. This transition is symmetry-forbidden in centrosymmetric geometries, and thus the intensities of these features (peak areas) provide a measure of the centrosymmetric character of the metal site. Peak areas are smaller for more centrosymmetric geometries, such as octahedral and square-planar, and larger for non-centrosymmetric geometries, such as tetrahedral and square-pyramidal. [70, 71] For geometries lacking one or more axial ligands (planar or pyramidal), a 1s → $4p_z$ electronic transition is observed that can be used to distinguish between centrosymmetric geometries, *e.g.*, square-planar and octahedral, and between five-coordinate pyramidal and trigonal bipyramidal complexes. [71] Being a d^{10} metal, Zn(II) lacks vacancies in the 3d manifold and thus no 1s → 3d transition is possible. However, in this case, the intensity of the white line as well as number of transitions that follow the absorption edge are affected by coordination number and ligand type, allowing a qualitative analysis of the XANES spectra to be made for Zn(II).[72, 73] XANES data for WT-*Ec*RcnR and its Glu34 and Glu63 variants are summarized in Table 1 and Figure 2. (Additional fits useful in

18

developing the final models are shown in Supporting Information Tables S1 – S17. Enlargements of pre-edge features can be found in Figure S3).

At energies higher than the metal K-edge, extended X-ray absorption fine structure (EXAFS) analysis was used to provide metal-ligand distances with an accuracy of ~ 0.02 Å, information on the identity of the scattering atoms ($Z \pm 2$), and a second estimate on the coordination number (~20% total number of ligands) that is complementary to the XANES analysis. The EXAFS spectra and best fits are summarized in Figures 3 – 6 and Table 1. Comprehensive fitting tables are included in the supporting information (Tables S1-17).

XAS of Co(II) complexes.

A single pre-edge feature at ~7710 eV that is associated with a 1s → 3d transition (Figure 2) is observed for the Co(II) complexes of both E34A- and E34C-*Ec*RcnR proteins. The relatively small peak areas (Table 1) indicate that the Co(II) centers in these complexes have centrosymmetric ligand arrangements. [71, 74] This, coupled with the lack of any other pre-edge feature, is consistent with an octahedral geometry in all cases. Thus, there is no obvious change in geometry associated with the variation of Glu34 or Glu63 as compared to WT-*Ec*RcnR. [75, 76] However, the XANES spectra for WT, E34A-, E34C-, E63A- and E63C -*Ec*RcnR are non-overlapping, and thus indicative of some change in the Co(II) coordination sphere. These differences were addressed by EXAFS analysis.
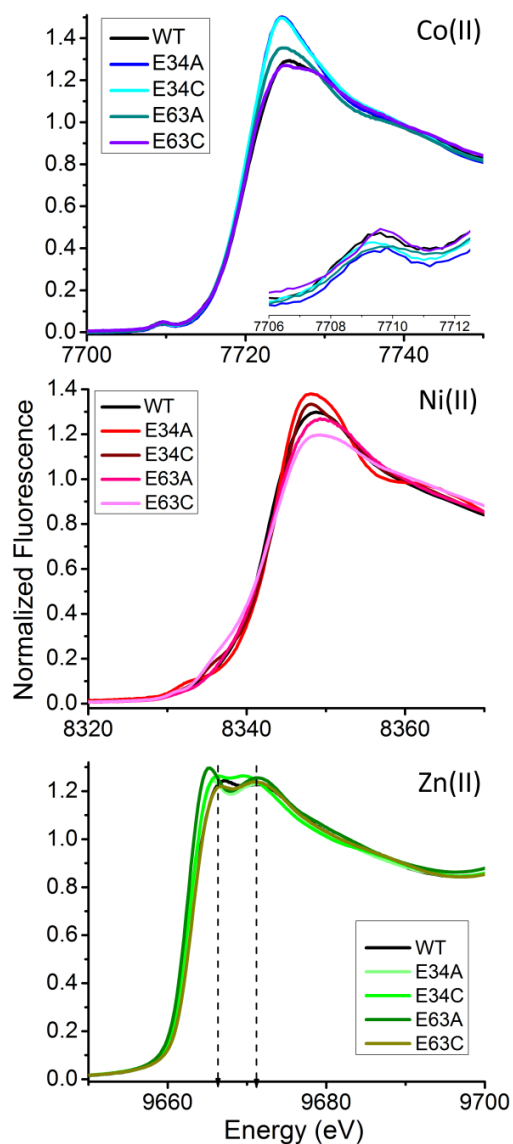
Figure 2: K-edge XANES spectral overlays for metal complexes of WT-*Ec*RcnR and Glu variants in buffer with 20 mM HEPES, 300 mM NaBr, 1 mM TCEP and 10% glycerol (pH 7.0). The inset shows the pre-edge region for clarity.

EXAFS analysis of Co(II) E34A-*Ec*RcnR (Table 1, Figure 3A) is consistent with a six-coordinate site, in agreement with the XANES analysis, and the best fit features two histidine imidazole ligands, two N/O-donors, a bromide ion from the buffer and a sulfur-donor that

indicates coordination of Cys35. Incorporation of the Br⁻ ligand indicates the presence of an

open coordination site, or solvent-exchangeable ligand, in the E34A-*Ec*RcnR complex that does

not exist in WT-*Ec*RcnR. In addition to the replacement of a N/O-donor ligand with a Br⁻, the

E34A-*Ec*RcnR site has a long Co-S bond at 2.54(4) Å, that is significantly altered compared to

the Co-S distance in the Co(II) WT-*Ec*RcnR complex (2.20 Å), and more closely resembles the

WT-*Ec*RcnR Ni(II)-SCys35 bond distance (2.63 Å). The resulting [Co(His)$_2$(N/O)$_2$(Cys)Br]

complex is consistent with the role of Glu34 as a Co(II) ligand in WT-*Ec*RcnR.
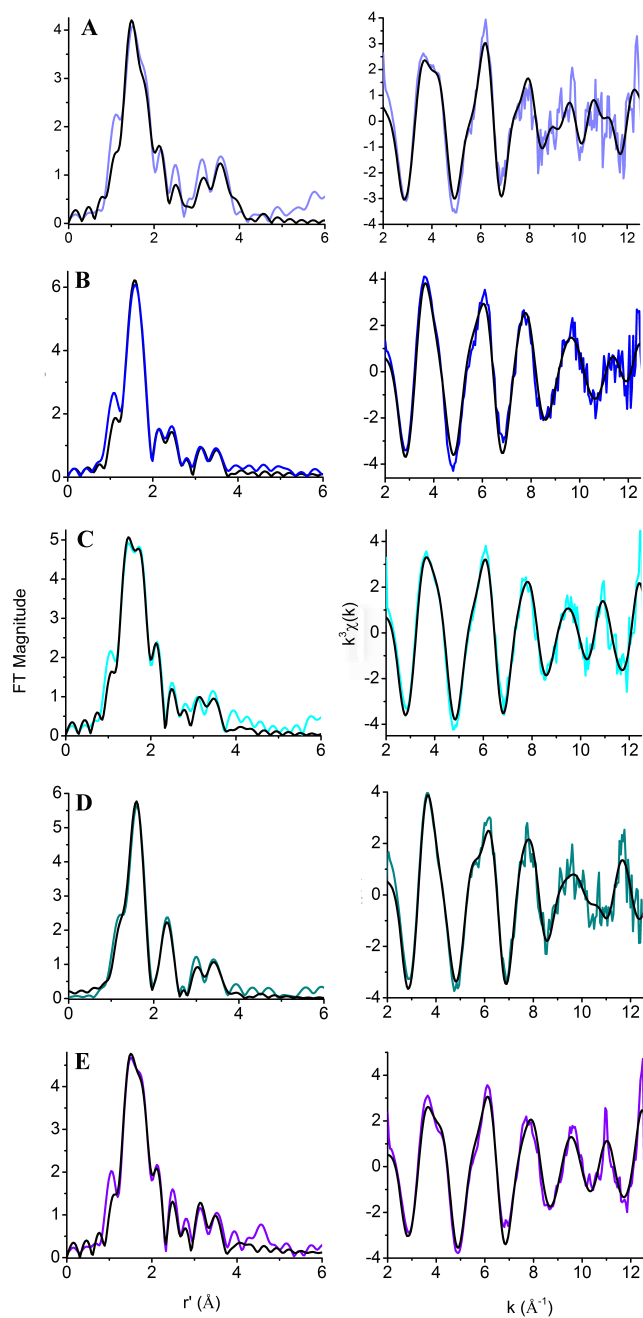
Figure 3: K-Edge EXAFS spectra for the Co(II) complexes of (A) WT-, (B) E34A-, (C) E34C-, (D) E63A-, and (E) E63C-*Ec*RcnR in buffer containing 20 mM HEPES, 300 mM NaBr, 1 mM TCEP and 10% glycerol (pH 7.0). Left: Fourier-transformed EXAFS data (colored lines) and fits (black lines). Right: unfiltered k^3-weighted EXAFS spectra and fits. Metric details for the fits

shown are in bold face type in Table 1.

The EXAFS analysis of Co(II) E34C-*Ec*RcnR is consistent with a six-coordinate complex, and therefore also consistent with the XANES analysis (Table 1, Figure 3B). The major change in the structure with respect to Co(II) WT-*Ec*RcnR is the inclusion of two S-donor ligands (Cys34 and Cys35), one at a longer distance (2.61(4) Å) and one at a shorter distance (2.36(4) Å). The data are best fit by a model that includes two His imidazole ligands, and features a split N/O shell, where the difference in the M-N/O distances between the two shells (0.15 Å) is at the calculated resolution of the data set ($r = \frac{\pi}{2 \times \Delta k} = 0.15$) and thus significant. Although it is not possible to identify which Cys residue is responsible for the long vs. short Co-S distances, the resulting [Co(His)$_2$(N/O)$_2$(Cys)$_2$] complex also supports the assignment of Glu34 as a Co(II) ligand in Co(II) WT-*Ec*RcnR.

The EXAFS analysis of the Co(II) E63A-*Ec*RcnR spectrum yields similar results to Co(II) E34A-*Ec*RcnR. The EXAFS analysis is consistent with a six-coordinate geometry, in agreement with the XANES analysis. The best fit includes four N/O-donors, two of which can be modeled as histidine imidazole ligands, one long Cys35 S-donor, and one Br$^-$, which replaces a N/O-donor ligand in the WT Co(II) site (Table 1 and Figure 3C). The Co-SCys35 distance (2.50(2) Å) is considerably longer than that observed for Co(II) WT-*Ec*RcnR, and approaches the distance found in the Ni(II) WT-*Ec*RcnR complex, as was the case for the Co(II) E34A-*Ec*RcnR complex (*vide supra*). The resulting [Co(His)$_2$(N/O)$_2$(Cys)Br] complex differs from that found for Co(II) E34A-*Ec*RcnR only by small differences in Co-L distances. Thus, the data are consistent with Glu63 acting as a Co(II) ligand in the Co(II) WT-*Ec*RcnR complex.

The best fits of Co(II) E63A-*Ec*RcnR in NaBr buffer suggest that the Co-Br distance is shorter than the Co-S distance. In an attempt to confirm this assignment, the experiment was repeated using a buffer containing 300 mM NaCl instead of NaBr (SI Tables S1 and S2; Figure S1 and S2). In this case, the data analysis is consistent with a [Co(His)$_2$(N/O)$_2$(Cys)Cl] complex, the major differences being substitution of Br$^-$ by a Cl$^-$ ligand. The latter is indistinguishable from an S-donor ligand and was therefore fit using S parameters, (see Table 1). However, the Co-S/Cl distances in the Cl$^-$ complex are shorter (2.42 Å) and longer (2.66 Å) than the putative Co-Br$^-$ and Co-S distances, and so no definitive assignment can be made. Regardless, the results are consistent with Glu63 coordination to Co(II) in WT-*Ec*RcnR.

Table 1: XAS Analysis for Metal Complexes of WT-, Glu34-, and Glu63-RcnR Variants in Buffer with 300 mM NaBr [a]

	XANES Analysis				EXAFS Analysis				
Sample	K-edge energy (eV)	1s → 3d peak area (x10^2 eV)	1s → 4p$_z$ observed	Coord #	Shell	r (Å)	σ^2 (x10^{-3} Å^2)	ΔE_0 (eV)	%R
					WT-RcnR				
Co(II)	7720.2	6(1)	No	6	1 N/O	1.97(4)	2(3)	-2(2)	4.1
					2 N/O	2.20(4)	0(2)		
					1 S	2.20(6)	5(6)		
					1 Im 0°	2.09(4)	4(3)		
					1 Im 10°	2.09(3)	2(3)		
Ni(II)	8342.7	2(1)	No	6	2 N/O	2.07(2)	2(2)	4(1)	3.8
					1 N/O	2.21(3)	3(4)		
					1 S	2.63(2)	6(2)		
					1 Im 0°	2.07(3)	3(2)		
					1 Im 10°	2.02(6)	6(5)		
Zn(II)	9663.0	NA	NA	4/5	**1 N/O**	**1.94(3)**	**7(4)**	**-4(1)**	**1.2**
					1 S	**2.30(2)**	**7(3)**		
					1 Br	**2.41(1)**	**5(1)**		
					1 Im 0°	**1.99(2)**	**0(3)**		
					1 Im 10°	**2.10(2)**	**1(2)**		
					1 S	2.30(2)	5(2)	-5(1)	1.5
					1 Br	2.41(1)	5(1)		
					1 Im 0°	2.07(2)	2(1)		
					1 Im 0°	1.95(2)	0(2)		
					E34A-RcnR				
Co(II)	7720.6	6(1)	No	6	1 N/O	2.02(1)	5(1)	2(2)	1.7

					1 N/O	2.16(1)	6(1)		
					1 S	2.54(4)	1(4)		
					1 Br	2.50(3)	3(3)		
					1 Im 0°	2.02(7)	6(9)		
					1 Im 0°	2.16(8)	6(11)		
Ni(II)	8343.9	10(1)	No	7	1 N/O	2.04(1)	13(1)	7(1)	3.2
					2 N/O	2.19(2)	9(2)		
					1 S	2.60(2)	3(2)		
					1 Im 0°	1.94(2)	9(1)		
					1 Im 0°	2.10(2)	3(2)		
					2 N/O	**2.07(1)**	**9(1)**	**7(1)**	**3.2**
					2 N/O	**2.22(2)**	**7(2)**		
					1 S	**2.61(1)**	**3(1)**		
					1 Im 0°	**1.94(2)**	**8(1)**		
					1 Im 0°	**2.11(2)**	**7(1)**		
Zn(II)	9663.0	NA	NA	4/5	**1 N/O**	**1.98(4)**	**7(6)**	**-3(1)**	**1.9**
					1 S	**2.28(3)**	**9(4)**		
					1 Br	**2.43(1)**	**6(1)**		
					1 Im 0°	**2.11(2)**	**2(2)**		
					1 Im 0°	**1.98(2)**	**1(2)**		
					1 S	2.27(3)	8(3)	-4(2)	2.9
					1 Br	2.42(1)	6(1)		
					1 Im	1.96(1)	2(1)		
					1 Im	2.09(2)	2(2)		

<div align="center">E34C-RcnR</div>

Co(II)	7720.4	6(1)	No	6	1 N/O	1.99(3)	1(3)	3(2)	1.5
					1 N/O	2.14(2)	4(2)		
					1 S	2.36(4)	7(4)		
					1 S	2.61(4)	8(4)		
					1 Im 0°	2.17(4)	1(3)		
					1 Im 0°	2.01(3)	1(2)		
Ni(II)	8344.3	5(2)	Yes	5	1 N/O	2.04(2)	1(2)	1(2)	2.5
					1 S	2.29(2)	3(2)		
					1 S	2.56(3)	9(3)		
					1 Im 0°	1.94(3)	2(3)		
					1 Im 0°	2.08(3)	1(2)		
Zn(II)	9662.9	NA	NA	4/5	**1 N/O**	**2.02(3)**	**6(5)**	**-2(1)**	**1.1**
					1 S	**2.29(1)**	**3(2)**		
					1 Br	**2.41(1)**	**7(1)**		
					1 Im	**1.99(3)**	**3(5)**		
					1 Im	**2.11(4)**	**3(5)**		
					1 S	2.27(2)	3(2)	-3(2)	2.3
					1 Br	2.41(1)	6(1)		
					1 Im	1.97(2)	1(3)		
					1 Im	2.09(3)	0(3)		

<div align="center">E63A-RcnR</div>

Co(II)	7720.6	5(1)	No	6	2 N/O	2.08(2)	2(2)	-2(1)	2.6
					1 S	2.50(2)	4(2)		
					1 Br	2.45(2)	1(2)		
					1 Im 5°	2.03(3)	4(3)		
					1 Im 10°	2.16(6)	7(7)		
Co(II)[b]	7720.2	6(1)	No	6	1 N/O	1.95(5)	5(6)	-2(2)	2.6
					1 N/O	2.11(3)	0(3)		
					1 S/Cl	2.66(5)	8(4)		
					1 S/Cl	2.42(4)	8(4)		
					1 Im 0°	2.00(2)	2(2)		

					1 Im 0°	2.15(2)	2(1)		
Ni(II)	8343.5	>0.5	No	6	2 N/O	2.02(2)	3(2)	3(1)	3.5
					1 S	2.50(4)	2(4)		
					1 Br	2.44(4)	3(4)		
					1 Im 0°	2.03(3)	2(3)		
					1 Im 10°	2.16(2)	1(2)		
Ni(II)*	8343.1	>0.5	No	6	2 N/O	2.01(3)	3(3)	3(2)	3.8
					1 S	2.38(5)	9(6)		
					1 S (Cl⁻)	2.59(3)	5(3)		
					1 Im 0°	2.01(8)	9(7)		
					1 Im 10°	2.08(5)	3(6)		
Zn(II)	9662.7	NA	NA	4/5	**1 S**	**2.23(2)**	**9(3)**	**-3(1)**	**1.1**
					1 Br	**2.40(1)**	**4(1)**		
					1 Im 0°	**2.05(1)**	**6(2)**		
					1 Im 0°	**2.17(2)**	**2(3)**		
					1 Im 0°	**1.93(1)**	**4(1)**		
					1 N/O	1.99(3)	6(4)	-4(2)	1.0
					1 S	2.24(3)	14(5)		
					1 Br	2.40(1)	4(0)		
					1 Im 0°	2.09(1)	2(1)		
					1 Im 0°	1.96(2)	1(1)		
					1 S	2.23(2)	9(3)	-5(1)	1.8
					1 Br	2.40(1)	4(1)		
					1 Im	2.07(1)	3(1)		
					1 Im	1.94(1)	2(1)		
				E63C-RcnR					
Co(II)	7720.6	7(1)	No	6	2 N/O	2.12(3)	9(4)	-3(1)	1.8
					1 S	2.28(2)	9(3)		
					1 S	2.52(3)	5(2)		
					1 Im 0°	2.14(2)	0(2)		
					1 Im 0°	1.98(1)	1(1)		
Ni(II)	8342.9	<0.5	Yes	5	1 N/O	2.04(2)	1(2)	0(2)	3.7
					1 S	2.30(3)	4(3)		
					1 S	2.55(4)	8(4)		
					1 Im 0°	1.94(4)	2(3)		
					1 Im 0°	2.08(4)	2(4)		
Zn(II)	9663.0	NA	NA	4/5	**1 S**	**2.29(3)**	**6(4)**	**-1(2)**	**3.4**
					1 Br	**2.40(2)**	**8(3)**		
					1 Im 0°	**2.17(3)**	**4(3)**		
					1 Im 0°	**2.05(2)**	**7(2)**		
					1 Im 0°	**1.93(2)**	**4(2)**		
					1 N/O	1.96(3)	1(2)	-1(2)	4.4
					1 S	2.29(2)	3(2)		
					1 Br	2.42(2)	9(3)		
					1 Im 0°	2.05(2)	0(1)		

[a]The numbers in parentheses are the estimated uncertainties in the corresponding variables. These uncertainties are calculated by Artemis and reflect the change in the variable that will result in an increase in χ_2 of 1. EXAFS fits in bold type are shown in Figures 2-5. [b]Sample prepared in buffer with 20 mM Hepes, 300 mM NaCl, 1mM TCEP and 10% glycerol (pH 7.0).

The results of EXAFS analysis for the Co(II) E63C-*Ec*RcnR complex (Table 1, Figure 3D) also resemble those obtained for the corresponding E34C-*Ec*RcnR complex, and is also consistent with the formation of a [Co(His)$_2$(N/O)$_2$(Cys)$_2$] complex with similar metric parameters. Thus, the results from both variants confirm the role of Glu63 as a Co(II) ligand in WT-*Ec*RcnR.

XAS of Ni(II) complexes.

The pre-edge features of the Ni(II) complexes of E34A- and E34C-*Ec*RcnR are very different from each other, and distinct from the six-coordinate Ni(II) WT-*Ec*RcnR complex. Both Glu34 variants exhibit a peak associated with a 1s → 3d transition located at ~8330 eV (Figure 2 and SI Figure S3). The peak area for the E34A-*Ec*RcnR Ni(II) complex is very large (~ 10 x 10^{-2} Å^2), indicating a non-centrosymmetric geometry. Coupled with the absence of a peak associated with a 1s → 4p$_z$ transition, the XANES is consistent with a seven-coordinate geometry, as suggested by the EXAFS analysis (*vide infra*). The peak area for the Ni(II) E34C-*Ec*RcnR complex is ~ 5 x 10^{-2} Å^2, and together with the presence of a shoulder associated with a 1s → 4p$_z$ transition at ~8336 eV, is most consistent with a five-coordinate pyramidal complex. [74,75,77]
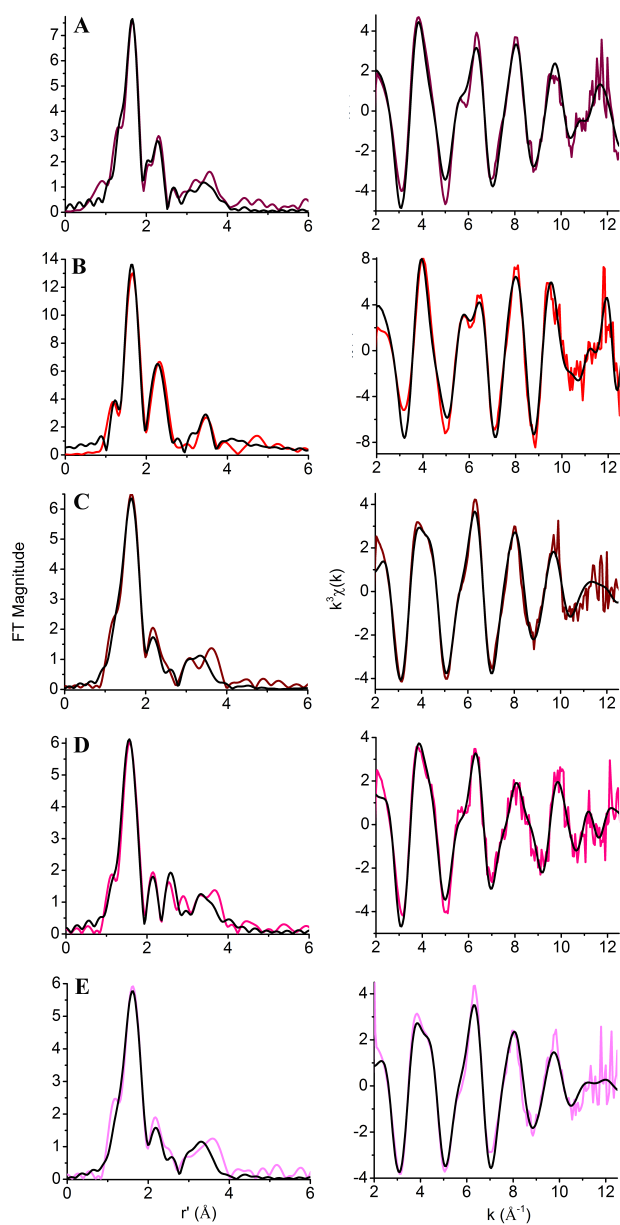
Figure 4: K-Edge EXAFS spectra for the Ni(II) complexes of (A) WT-, (B) E34A-, (C) E34C-, (D) E63A-, and (E) E63C-*Ec*RcnR in buffer containing 20 mM HEPES, 300 mM NaBr, 1 mM TCEP and 10% glycerol (pH 7.0). Left: Fourier-transformed EXAFS data (colored lines) and fits (black lines). Right: unfiltered k^3-weighted EXAFS spectra and fits. Metric details for the fits

shown are in bold face type in Table 1.

Neither of the Ni(II) complexes of the E63A- nor E63C-*Ec*RcnR variants have a visible 1s → 3d transition. As the peak is too small to be observed, it indicates that both complexes feature centrosymmetric Ni(II) environments. The E63A-*Ec*RcnR Ni(II) complex does not feature any other visible pre-edge feature, consistent with an octahedral geometry. On the other hand, the spectrum of the Ni(II) complex of E63C-*Ec*RcnR has a small shoulder that is associated with a 1s → 4p$_z$ transition. This feature is not consistent with six-coordinate, trigonal-bipyramidal, or tetrahedral geometries. The presence of this shoulder is consistent with a five-coordinate pyramidal Ni(II) site, but the small 1s → 3d transition is not. This situation could arise if, for example, the sample is a mixture of four-coordinate planar and six-coordinate Ni(II) sites, which would exhibit a feature associated with a 1s → 4p$_z$ transition from the planar component, but have a small 1s → 3d peak area since that is characteristic of both geometries, and could average to five ligands in the EXAFS analysis (*vide infra*). Regardless of the exact coordination number, this variant shows a tendency toward loss of ligands in at least some of the Ni(II) sites, a trend that was also observed for the Ni(II) E34C-*Ec*RcnR complex (*vide infra*).

The analysis of the EXAFS spectrum of the E34A-*Ec*RcnR Ni(II) complex is best fit with a ligand environment that is composed of two histidine imidazole ligands, four additional N/O-donor ligands in two resolved shells, and a long (~2.61(1) Å) Cys35 S-donor. This yields a total of seven scattering atoms (Table 1 and Figure 4A). Although a six-coordinate complex would be within the error of coordination number determination by EXAFS analysis (± 20%), a centrosymmetric arrangement of ligands is inconsistent with the large 1s → 3d transition observed in the XANES spectrum. A seven-coordinate geometry is most consistent with both the EXAFS and XANES analyses, although a highly distorted six-coordinate complex cannot be

ruled out. A six-coordinate fit of the EXAFS was attempted, but resulted in an unacceptably high σ^2 value for the first shell N-donor ligands. A seven-coordinate fit resulted in acceptable values for all parameters. In all other aspects, the E34A-*Ec*RcnR Ni(II) site is essentially unaltered from Ni(II) WT-*Ec*RcnR (Table 1). In addition, the complex does not bind exogenous Br⁻, as expected for a 'loss of ligand' variant. Replacement of Glu34 by a water molecule in preference to Br⁻ cannot be ruled out in principle, though it would be inconsistent with the incorporation of Br⁻ in Co(II) complexes of E34A- and E63A-*Ec*RcnR (*vide supra*), and with the Ni(II) complex of E63A-*Ec*RcnR (*vide infra*). Moreover, the substitution of Glu34 by water would modify the charge on the metal center, and would be expected to significantly alter the XANES spectrum, in contrast with the observation.

In contrast to the data obtained for the Ni(II) E34A-*Ec*RcnR complex, the EXAFS data from Ni(II) E34C-*Ec*RcnR indicates a decrease in the coordination number from six to five (Table 1, Figure 4B). This change in coordination is consistent with the XANES result, which indicated a five-coordinate pyramidal geometry. In addition to a change in coordination number, the EXAFS analysis reveals that the Ni(II) center in E34C-*Ec*RcnR has two S-donor ligands (Cys34 and Cys35), with one long, WT-like, Ni-S distance at 2.56(3) Å, and a shorter Ni-S bond at 2.29(2) Å. The resulting [Ni(His)₂(N/O)(Cys)₂] complex minimally results from substitution of Glu34 by Cys and loss of an N/O-donor ligand. This could be interpreted as resulting from the substitution of a bidentate carboxylate by Cys. However, neither the E34A- nor the E34C-*Ec*RcnR Ni(II) sites give unambiguous results for simple 'loss of ligand' or 'ligand substitution' variations.

The EXAFS data for the Ni(II) E63A-*Ec*RcnR site is best fit by a six-coordinate model featuring four N/O-donors, two of which are imidazole ligands (Tables 1, and Figure 4C). The coordination sphere is completed by a bromide ion from the buffer and a Ni-SCys35 bond

(2.50(2) Å) that is shorter than in the WT-*Ec*RcnR Ni(II) complex (2.63(2) Å). This [Ni(His)$_2$(N/O)$_2$(Cys)Br] complex results from replacement of Glu63 by Br$^-$ in Ni(II) WT-*Ec*RcnR, similarly to what is observed in the Co(II) complex of E63A-*Ec*RcnR, and consistent with Glu63 acting as a ligand to Ni(II), as well as to Co(II), in WT-*Ec*RcnR.

As was the case for E34C-*Ec*RcnR, the analysis of the EXAFS spectrum of the Ni(II) complex of E63C-*Ec*RcnR (Figure 4D) is consistent with coordination of a second S-donor and a reduced coordination number. The resulting five-coordinate [Ni(His)$_2$(N/O)(Cys)$_2$)] complex involves the loss of two N/O-donor ligands relative to the WT-*Ec*RcnR structure, one of which is replaced by the Cys63 S-donor, and resulting in one long (2.55(4) Å) and one short (2.30(3) Å) Ni-S distance. The large number of structural changes makes it difficult to unambiguously determine which S-donor belongs to which cysteine residue. But, taken together, the results of both Glu63 variants are clearly consistent with ligation of Glu63 in the Ni(II) WT-*Ec*RcnR complex.

XAS of Zn(II) complexes.

The ratio of the normalized intensities of the two post-edge XANES features for the Zn(II) complexes of WT-*Ec*RcnR and all variants are ~1.3, which is consistent with either four- or five-coordinate Zn(II) sites.[71] XANES spectra of all Zn(II) complexes (Figure 2) exhibit features at 9666.6 and 9671.0 eV that are associated with 1s → 4p transitions, and are consistent with a
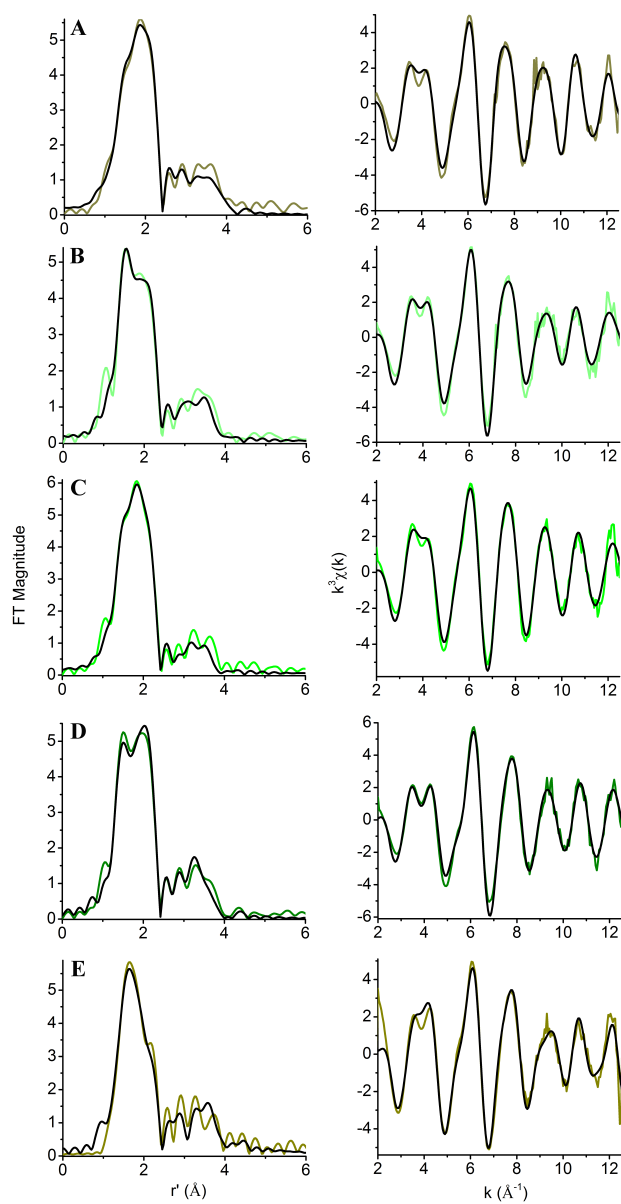
Figure 5: K-Edge EXAFS spectra for the Zn(II) complexes of (A) WT-, (B) E34A-, (C) E34C-, (D) E63A-, and (E) E63C-*Ec*RcnR in buffer containing 20 mM HEPES, 300 mM NaBr, 1 mM TCEP and 10% glycerol (pH 7.0). Left: Fourier-transformed EXAFS data (colored lines) and fits (black lines). Right: unfiltered k^3-weighted EXAFS spectra and fits. Metric details for the fits shown are in bold face type in Table 1.

Zn(II) center coordinated by a combination of N/O-donors together with heavier scattering donor-atom ligands, such as sulfur or bromide. [72]

The results of the analysis of the EXAFS data for Zn(II) complexes of E34A- and E34C-*Ec*RcnR (Table 1, Figure 5A and B) are generally consistent with the qualitative XANES analysis, and indicate that the Zn(II) sites in these variants are essentially identical, and very similar to the Zn(II) complex in WT-*Ec*RcnR. The best fits in all cases include two His ligands, one N/O-donor ligand, one Br$^-$ ligand and one S-donor. The resulting five-coordinate [Zn(His)$_2$(N/O)(Cys)Br] complexes demonstrate that Glu34 is not a ligand for Zn(II) in WT-*Ec*RcnR.

The EXAFS analysis of Zn(II) E63A-*Ec*RcnR is indicative of a site composed of three N/O-donors, one S-donor from Cys35 and a bromide from the buffer (Table 1), and is consistent with expectations based on the XANES analysis (*vide supra*). However, unlike the Zn(II) complex of WT-*Ec*RcnR, where EXAFS data can be modeled as a [Zn(His)$_2$(N/O)(Cys)Br] complex (Table 1), the best models for the Zn(II) sites in E63A- and E63C-*Ec*RcnR contain three histidine imidazole ligands, [Zn(His)$_3$(Cys)Br] (Table 1, Figure 5C and D). Attempts to fit the EXAFS spectrum for the E63A Zn(II) site using two imidazole ligands and 1 N/O ligand, in analogy with the WT case, result in slightly lower values of %R and reduced χ^2, but also yield a very large value of σ^2 for the Zn-SCys35 bond, although the Zn-S distance is unchanged between the two models (Table 1). A similar fit, involving two imidazole ligands and 1 N/O ligand, could be obtained for the Zn(II) complex of E63C-*Ec*RcnR, but the values of %R and reduced χ^2 were higher.

The Zn(II) sites in E63A- and E63C-EcRcnR show subtle structural changes (possible increased imidazole ligation) that are not consistent with Glu63 being a ligand in the WT-RcnR Zn(II) complex, but might suggest a role for Glu63 in ordering the ligands in Zn(II) site.

Electronic factors in the structures of the Ni(II) sites in EcRcnR variants.

Susceptibility measurements using the Evans NMR method were made on samples of WT- and E63C-EcRcnR Ni(II) complexes, and the parameters obtained from the spectra (SI Figure S4) and calculated values of are shown in Table 2. The results show that WT-EcRcnR contains

Table 2. Magnetic susceptibility data and calculated values for WT- and E63C-EcRcnR Ni(II) complexes.

Parameter	WT-EcRcnR	E63C-EcRcnR
$\Delta\nu$	-18.4005 Hz	-1.56944 Hz
m	0.0226 g/mL	0.00942 g/mL
M	10,061 g/mol	10,035 g/mol
χ_M	4.89×10^{-3} cgs/mol	9.97×10^{-4} cgs/mol
χ_L	4.48×10^{-6} cgs/mol	4.48×10^{-6} cgs/mol
χ_M'	4.89×10^{-3} cgs/mol	9.93×10^{-4} cgs/mol
μ_{eff}	3.42 BM	1.54 BM

a paramagnetic Ni(II) center with $\mu = 3.4$ BM, which is in the range expected for high-spin Ni(II) complexes (2.8 – 4.0 BM),[77] and consistent with a six-coordinate $S = 1$ Ni(II) center. The sample of E63C-EcRcnR has greatly reduced paramagnetism that would correspond to a Ni(II) center with $\mu = 1.5$ BM, which is too low to result from a high-spin Ni(II) complex, and indicates that most of the Ni(II) in the sample is diamagnetic (low-spin). The ratio of the molar susceptibilities of WT- to E63C-EcRcnR Ni(II) complexes indicates that the solution of the

variant is ~20% as paramagnetic as the WT-*Ec*RcnR sample, suggesting the presence of a paramagnetic impurity that might arise from a an equilibrium of five- and six-coordinate species, with the six-coordinate complex serving to provide the paramagnetism and moderate the XANES features normally associated with a five-coordinate pyramidal complex (*vide supra*).

Functional Analysis

Previous studies[35] revealed that expression of P_{rcnA} occurs only in the presence of Ni(II) and Co(II), but not upon addition of Mn(II), Fe(II), Cu(II), Zn(II), and Cd(II). The effects of the Glu → Ala and Glu → Cys variations on the metal responsiveness of *Ec*RcnR were tested using a LacZ reporter assay (Figure 6, Table S18). Statistically significant differences are indicated with stars in
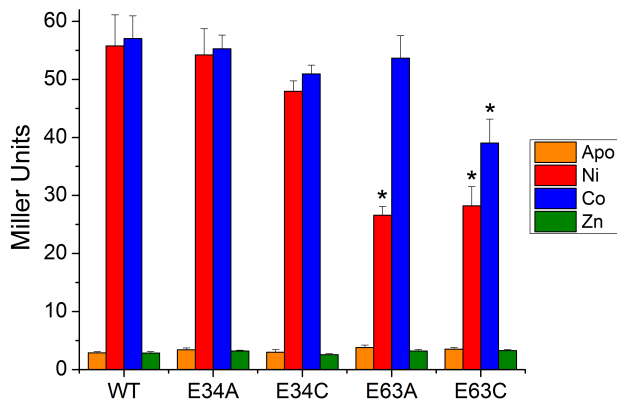
Figure 6: Results of LacZ transcription reporter assays showing the effects of the E34A-, E34C-, E63A-, and E63C-*Ec*RcnR mutations on the expression of P_{rcnA} in response to metal ions. A statistically significant difference from wild-type response is indicated by a * (p < 0.01, one-way ANOVA followed by Dunnett's test for multiple comparisons).

Figure 6. Both E34A- and E34C-*Ec*RcnR had metal ion responses that are indistinguishable from WT-*Ec*RcnR, demonstrating that ligation of Glu34 is not important to metal-induced transcription, regardless of the structural role identified by XAS analysis. On the other hand, while the E63A-*Ec*RcnR variant also shows a WT-like response to Co(II)-binding, derepression is reduced by ~50% in response to Ni(II)-binding. The E63C-*Ec*RcnR variant also shows a ~50% reduction in response to Ni(II), but also displays a 25% decrease in response to Co(II). All four variants remain unresponsive to Zn(II)-binding, indicating that metal selectivity has not been impaired by the Glu34 and Glu63 mutations. These results suggest that while mutation of both Glu34 and Glu63 affect the metal site structure, only mutation of Glu63 significantly affects the metal-responsiveness of RcnR in the cell. The data also indicate that while Glu63 may be involved in ordering the Zn(II) site (*vide supra*), this ordering imparts no obvious change to WT-*Ec*RcnR's lack of response to binding Zn(II).

The LacZ reporter assays were performed at metal concentrations that produced maximal activity without being detrimental for cell growth. Thus, even though the Glu34 mutations did not affect the functional response at maximal metal concentrations, metal titrations were performed to see if the mutations affected the LacZ activity at lower metal concentrations. In all cases, there was no difference between the response to metal of WT-*Ec*RcnR and that of the two Glu34 variants at concentrations ranging from 0 μM to 900 μM (SI Figure S5). These studies also reveal that WT-*Ec*RcnR begins to respond to Ni(II) at ~300 μM $NiCl_2$, similar to a previously reported value,[36] and to Co(II) at ~10 μM $CoCl_2$. This response is unchanged for both E34A- and E34C-*Ec*RcnR.

Protein structure and DNA Binding

No changes in the quaternary structures of the Glu variants with respect to WT-RcnR was observed by size exclusion chromatography (SI, Figure S6). Both Glu63 variants showed diminished transcriptional response to the addition of Ni(II) and Co(II). In order to test if this is due to increased DNA-binding affinity, fluorescence anisotropy measurements were performed. 5-carboxytetramethylrhodamine (TAMRA) labeled Site-2 DNA, containing one of two recognition sequences,[44] was titrated with WT-, E63A-, and E63C-EcRcnR. The apparent K_{DNA} of WT-EcRcnR is 13.64 ± 3.9 nM with no significant change in the apparent K_{DNA} of either mutant (20.75 ± 4.9 nM for E63A-EcRcnR and 17.02 ± 6.9 nM for E63C-EcRcnR) (SI, Figure S7). This indicates that the E63A- and E63C-EcRcnR variants did not alter the DNA binding affinity of the apo-RcnR proteins compared to WT, and is compelling evidence that they are correctly folded. The decrease in metal-induced transcriptional responses is not a consequence of increased DNA-binding affinity of the apo-protein.

*Computational models of metal bound WT-Ec*RcnR

In view of the data presented above regarding the role of Glu34 and Glu63 in metal binding, the initial computational models used to identify these residues as potential metal ligands [52] were refined. All three modeled metal sites feature Cys35 thiolate as a common ligand, because this is the only Cys residue in the protein and S-donor ligation is observed in the EXAFS spectra of all the metal complexes.[47, 48] In all cases, the metal ions bind at a dimer interface that connects the N-terminal portion of helix α2 of one monomer to the C-terminal portion of the same helix from the adjacent monomer. The models show that one monomer provides most of the potential metal ligands, namely the N-terminal amine, His3, His60, His64, and His67, whereas Glu34 and Cys35 are derived from the other monomer at the dimer interface. This situation is analogous to what observed in the crystal structures of Cu(I)-CsoR.[39]

Table 3. Distances, angle and dihedral constraints used to guide the modeling of *Ec*RcnR metal binding sites.*

Model	Constrained atoms	Distance (Å)
Co(II)-*Ec*RcnR	Co(II) - Ser2(NH$_2$)	2.04
	Co(II) - His3(Nδ)	2.04
	Co(II) - Glu34(Oδ1)	2.04
	Co(II) - Cys35(Sγ)	2.31
	Co(II) - Glu63(Oδ1)	2.04
	Co(II) - His64(Nε)	2.04
	His60(Nε) - Cys35(Sγ)	**3.00 ± 0.10**
Ni(II)-*Ec*RcnR	Ni(II) - Ser2(NH$_2$)	2.14
	Ni(II) - Ser2(O)	**2.14**
	Ni(II) - Cys35(Sγ)	2.63
	Ni(II) - Glu63(Oδ1)	2.14
	Ni(II) - Glu63(Oδ2)	**2.14**
	Ni(II) - His64(Nε)	2.05
Zn(II)-*Ec*RcnR	Zn(II) - Cys35(Sγ)	2.30
	Zn(II) - Glu63(Oδ1)	**2.10**
	Zn(II) - His64(Nε)	2.05
	Zn(II) - His67(Nε)	2.05
	Zn(II) - Br⁻	2.41

Bonded atoms	Constrained atoms	Angle (degrees)
M-Cys(Sγ)	M-Cys(Sγ)-Cys(Cβ)	109 ± 5
M-Glu(Oδ)	M-Glu(Oδ)-Glu(Cγ)	120 ± 5
M-His(Nδ)	M-His(Nδ)-His(Cγ)	120 ± 10
	M-His(Nδ)-His(Cε)	120 ± 10
M-His(Nε)	M-His(Nε)-His(Cδ)	120 ± 10
	M-His(Nε)-His(Cε)	120 ± 10

Bonded atoms	Constrained atoms	Dihedral (degrees)
M-His(Nδ)	M-His(Nδ)-His(Cε)-His(Nε)	180 ± 10
	M-His(Nδ)-His(Cγ)-His(Cδ)	180 ± 10
M-His(Nε)	M-His(Nε)-His(Cε)-His(Nδ)	180 ± 10
	M-His(Nε)-His(Cδ)-His(Cγ)	180 ± 10

*Distances that do not derive directly from experimental data are in bold.

All constraints are listed in the form: mean value ± 1 standard deviation. When not differently indicated, distance restraints have a standard deviation of ±0.05 Å with the respect to the equilibrium distances. No restraints were added to constrain the coordination geometry around the metal ions.

Co(II) WT-EcRcnR. The EXAFS analysis presented above provides evidence for Glu34 and Glu63 as ligands to the Co(II) site in WT-*Ec*RcnR. These results, along with prior identifications

of additional Co(II) ligands,[35, 47, 48] lead to a proposed six-coordinate $(His)_2(Glu)_2(Cys)Ser2-NH_2$ site for WT-EcRcnR. The His ligands involved are His3 and His64, the Glu ligands are Glu34, and Glu63, the Cys is Cys35, and Ser2-NH_2 represents the N-terminal amine ligand generated upon cleavage of Met1.[35] His60 was also proposed to be involved in the Co(II) binding site as a second coordination sphere residue that is H-bonded to one of the residues directly bound to the metal ion.[48] The calculation was conducted by imposing distance and angle restraints to each of the four Co(II) ions in order to bind them to Ser2-NH_2, His3, Glu63, and His64 from one chain and Glu34 and Cys35 from the second chain comprising each dimeric unit (Table 3). A preliminary calculation showed a small distortion in the His3 aromatic ring if the restraints are imposed on Nε, and so Nδ was used to bind Co(II). The result of the first modeling scheme (named Co-1) are reported in Figure 7A. The coordination geometry around the modeled Co(II) binding site is compatible with the distorted octahedral complex found by XAS analysis. The bond distances are in good agreement with those determined experimentally (Table 1 and SI Table 3). The only Co(II) binding residue in the vicinity of His60, which is known to contribute to this binding site without interacting directly with the metal ion, is Cys35, and therefore a new model named Co-2 was prepared with the same constraints as Co-1 plus an additional distance restraint of 3.00 ± 0.10 Å between Cys35 and His60(Nε) to model a His60 – Cys35 H-bond. The results of the Co-2 calculation are reported in Figure 7B. The Co(II) binding site is unchanged with respect to the Co-1 model and His60 is found in a good orientation to perform a H-bond with Cys35.
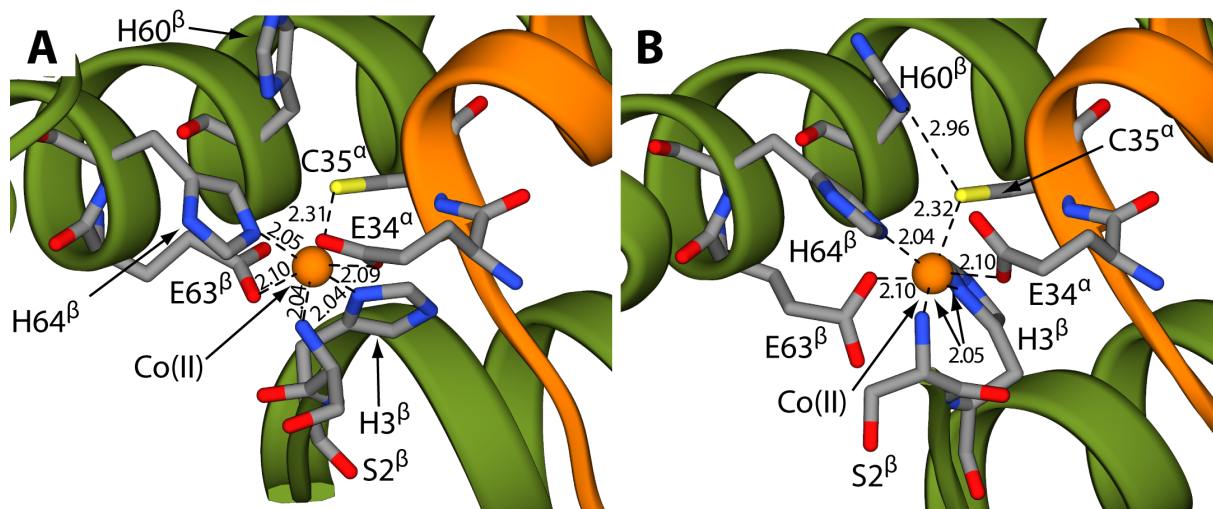
Figure 7. Panels **A** and **B** report the results for Co-1, Co-2 modeling, respectively. The *Ec*RcnR backbone is reported as ribbons colored by polypeptide chain, with chain α in orange and chain β in green. Putative metal binding residues are reported as sticks colored accordingly to atom types (labeled with single letter amino acid code, residue number, and polypeptide chain identification α or β). The Co(II) ion is showed as an orange sphere. The reported distances are in Angstroms.

Ni(II) WT-EcRcnR. The analysis of the XAS data for the Ni(II) complex with *Ec*RcnR is consistent with a $(N/O)_5S$ center with one or two histidine ligands and contributions from one cysteine ligand. One ligand has been experimentally identified to be the Ser2 N-terminal amine, while site-directed mutagenesis was used to identify other metal ligand residues as Cys35, Glu63, and His64. His3 was specifically excluded as a Ni(II) ligand. The aim of our modeling calculation was to identify other putative Ni(II) ligands in order to complete the coordination sphere of the ion. In the first modeling scheme (named Ni-1) each Ni(II) ion was constrained to coordinate Ser2-NH_2, Glu63, and His64 from one chain together with Cys35 from the second chain of each dimeric unit. In this model, the metal ion is coordinated in a distorted four-coordinate planar geometry with Ser2-NH_2 trans to His64 and Cys35 trans to Glu63 (Figure 8A).
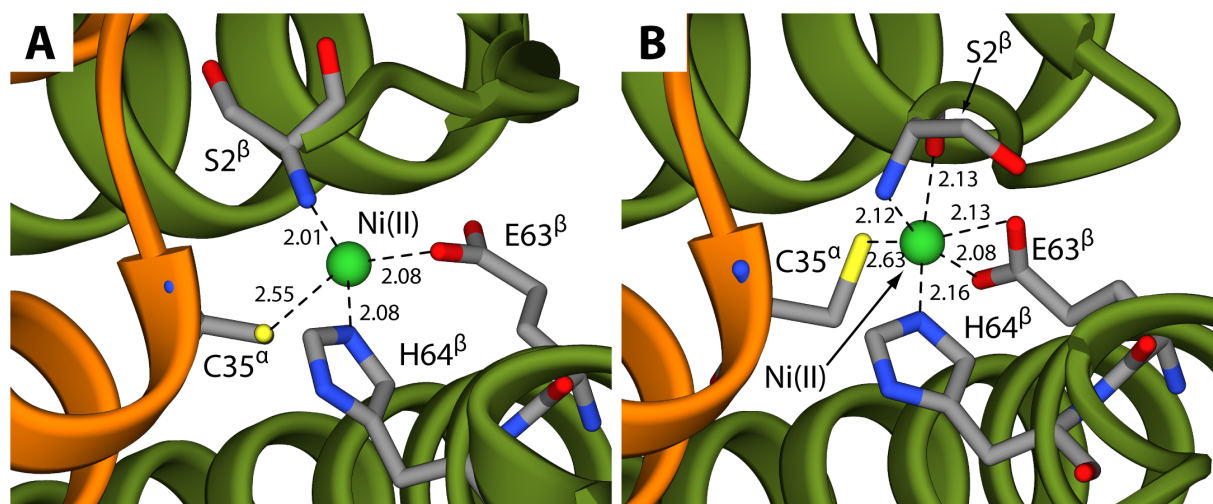
Figure 8. Panels **A** and **B** report the results for Ni-1 and Ni-2 modeling, respectively. The

*Ec*RcnR backbone is reported as ribbons colored accordingly to the protein chain, as in Figure 7.

Putative metal binding residues are reported as sticks colored accordingly to atom types. The

Ni(II) ions are shown as green spheres. The reported distances are in Angstroms.

The constraints used in the Ni-1 calculation lead to a model that does not fill the Ni(II)

coordination sphere as determined by the XAS data (Figure 8A). This consideration prompted us

to prepare a second modeling scheme (named Ni-2) in which Glu63 was imposed as a bi-dentate

ligand. This still would leave one empty position, which is filled by the carbonyl oxygen of Ser2.

The results of the Ni-2 calculation are reported in Figure 8B. The Ni(II) ion is coordinated in a

highly distorted octahedral geometry, consistent with the XANES analysis (*vide supra*). The

calculated bond distances in this case are also in agreement with those determined

experimentally by EXAFS analysis (Table 1 and Table 3).

Zn(II) WT-EcRcnR. The fitting of the XAS data for the Zn(II) complex with *Ec*RcnR is

consistent with a $(N/O)_2SBr$ or with a $(N/O)_3SBr$ center, with two histidine ligands and

contributions from one cysteine sulfur and one bromide derived from the buffer (Figure 9). The

histidine and the cysteine residues appear to be His67 and Cys35, while His3 and the N-terminal amine are not involved in Zn(II) binding. Thus, the aim of our modeling calculation was to identify other putative Zn(II) ligands in order to complete the coordination sphere of the ion and give hints on the coordination number. The present study also indicated that neither Glu34 nor Glu63 are ligands to Zn(II), with Glu63 having a marginal role in ordering the Zn(II) site (Figures 9 and S8). Multiple Zn(II) models were attempted and are discussed in detail in the supporting information. Among these, only model Zn-2b accurately reproduces the experimentally determined coordination number and ligand identity. In this model, Cys35, His64 and His67 are included as Zn(II) ligands in addition to one Br$^-$ from solvent (Figure 9). The bond distances are in good agreement with those determined experimentally (Table 1). This model suggests that His64 completes the coordination sphere as the second His ligand in addition to His67. A previous study, involving mutation of His64 to Cys, resulted in a six-coordinate $[Zn(His)_3(Cys)_2Br]$ complex, [48] supporting His64 as a ligand. In the model, it appears that a putative and indirect role of Glu63 involves the formation of a second-shell H-bond between the carboxylate group of this residue and Cys35-Sγ. A similar interaction, involving a metal-bound cysteine thiolate and a second shell residue acting as an H-bond donor has been reported in the case of the copper center in plastocyanin. [78]
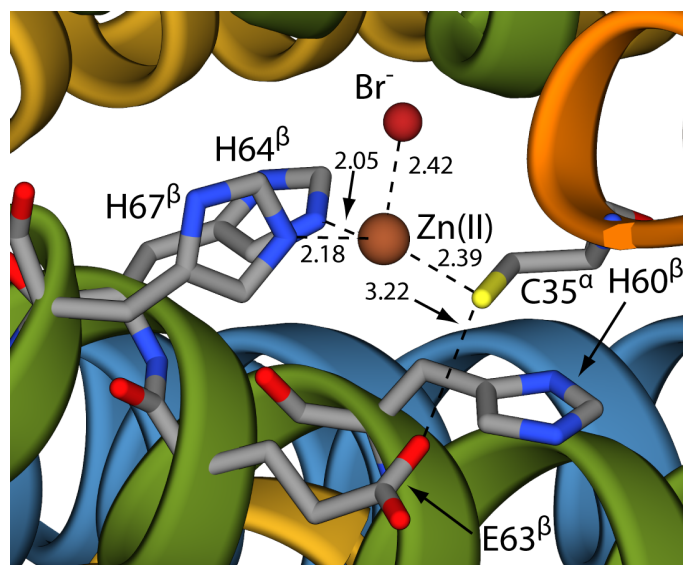
Figure 9. Results of the Zn-2b modeling (see supporting information). The *Ec*RcnR backbone is reported as ribbons colored accordingly to the protein chain, as in Figure 7. Putative metal binding residues are reported as sticks colored according to atom types. The Zn(II) and Br⁻ ions are shown as brown and dark red spheres, respectively. The reported distances are in Angstroms.

DISCUSSION

RcnR is one of only a few metallosensors for which high-coordination number sensing sites have been identified (*e.g.*, NmtR, MntR).[10, 79] Establishing the full primary coordination sphere of metals bound to *Ec*RcnR is important for understanding its cellular function as a Ni- and Co-responsive metal sensor protein. Knowledge of the complete set of ligands will also help to explain the unusual features of Ni-coordination, in particular a six-coordinate, high-spin ($S = 1$) complex that features Cys thiolate coordination at 2.65 Å, and the basis by which *Ec*RcnR senses both Ni(II) and Co(II) with different sets of ligands.

Metal-site structures

The results shown above associate Glu34 and Glu63 with cognate metal binding by demonstrating that altering either glutamate residue to alanine or cysteine causes significant changes to the cognate metal site structures, but not to the non-cognate Zn(II) site structure. In the case of Co(II), the structural changes observed in the glutamate variants are the ones anticipated for loss of a ligand (E34A; E63A) and a ligand substitution (E34C; E63C), namely loss of an N/O-donor ligand and incorporation of Br⁻ from the buffer and substitution of an O/N-donor ligand by the Cys34 S-donor in the mutant protein, respectively. Thus, Glu34 and Glu63 are clearly established as Co(II) ligands in WT-*Ec*RcnR. This completes the coordination sphere for Co(II), which has now been shown to bind the N-terminus, His3, Glu34, Cys35, Glu63, and His64.[47, 48] It is worth noting that the ligation of Co(II) by *Ec*RcnR resembles a tris-bidentate chelate complex in that it involves coordination of neighboring pairs of residues the His3/N-terminal amine, Glu34/Cys35, and Glu63/His64.

The nature of the structural changes observed for the Ni(II) complexes of E34A- and E34C-*Ec*RcnR are more ambiguous. Alteration of Glu34 to alanine shows formation of what is best described as a seven-coordinate complex with an $(N/O)_6S$ ligand donor-atom set. One possible explanation is that Glu34 is a Ni(II) ligand, and the vacancy created in E34A-*Ec*RcnR is filled either by a water molecule in preference to bromide, or by causing Glu63 to become bidentate to fill the vacancy. The combination of these two changes would result in a seven-coordinate complex, with Glu63 becoming bidentate in part to compensate for the increased positive charge on the metal. Another possibility is that Glu34 is not a ligand, but that modification of Glu34 perturbs the position of Glu63, possibly via alteration of an H-bonding network, such that Glu63 becomes bidentate, resulting in a complex that is seven-coordinate in terms of donor-atoms, but involves coordination of only six protein residues. Modeling of the WT-*Ec*RcnR Ni site does

indicate the possibility that Glu63 may bind in a bidentate fashion (*vide supra*). A similar situation was observed for Ni(II) H3E-*Ec*RcnR mutation, which also adopted a 7-coordinate site that was hypothesized to result from bidentate glutamate binding.[47] Further, conversion of monodentate carboxylate ligands to bidentate carboxylate ligands has been observed upon mutation of Asp8 to Met in a Mn(II) site in the manganese metallosensor, MntR,[2] an alteration that does not affect the Mn(II) response.

The results for the Ni(II) complex of the "ligand substitution" variant E34C-*Ec*RcnR do not directly help resolve the role of Glu34 in coordination of Ni(II) by WT-*Ec*RcnR. This variant results in multiple structural changes in the Ni(II) site, namely the loss of a N/O-donor ligand and substitution of another by Cys34, yielding a five-coordinate complex with two S-donor ligands $((N/O)_3S_2)$. This change is not consistent with a single ligand substitution, and therefore obscures the role of Glu34 as a ligand by this criterion. However, it is possible that the ligand substituted is a bidentate Glu34, which would yield this result.

One likely reason for the large structural perturbation of the Ni(II) site in the Glu → Cys variants comes from the studies of the Ni(II) complexes of the Glu63 variants. The XAS results for the E63A-RcnR Ni(II) complex show the expected results for a loss of ligand mutation where one N/O-donor replaced by a bromide ion from the buffer, and thus clearly establishes Glu63 as a Ni ligand. The structure of the of E63C-*Ec*RcnR Ni(II) complex is similar to the structure found for Ni(II) E34C-*Ec*RcnR, namely a 5-coordinate structure containing two S-donor ligands that involves the loss of one N/O-donor as well as coordination of the second S-donor (Cys63), resulting in a five-coordinate complex with $(N/O)_3S_2$-donor ligands. The change in coordination number/geometry that accompanied coordination of Cys63 suggested a change in electronic structure, possibly involving a conversion to a low-spin configuration that is associated with

lower coordination numbers. This is supported by susceptibility measurements using the Evans NMR method, in which WT-*Ec*RcnR contains a paramagnetic Ni(II) center, consistent with the six-coordinate structure, but E63C-*Ec*RcnR is ~80% diamagnetic, and thus largely consistent with a low-spin five-coordinate complex.

All Ni(II) complexes with an octahedral geometry are high-spin and paramagnetic with $S = 1$. In contrast, all four-coordinate planar complexes of Ni(II) are low-spin, with $S = 0$. Five-coordinate pyramidal complexes are roughly evenly divided between high- and low-spin electronic configurations, depending on the relative strength of the apical and basal ligand fields. The role of cysteine thiolate ligands in determining the spin-state of Ni(II) has been explored using a mutagenic approach in NiSOD, where it was concluded that both cysteine ligands present in the NiSOD active site were required to maintain a low-spin configuration.[80] Loss of either Cys ligand led to conversion to a high-spin complex with no Cys ligation. In E34C-*Ec*RcnR, the addition of a second S-donor ligand results in Ni(II) complexes that undergo a spin conversion to a low-spin configuration and lose a N/O-donor ligand (the reverse of the situation described above for NiSOD). This may also be relevant to the Ni(II) site structure in InrS, a related transcriptional regulator in the RcnR family that contains a low-spin, four-coordinate planar site that is supported by two Cys thiolate-donors.[50] The change in structure that occurs with the spin-state change also points out a limitation in our mutation strategy in that the ligand substitution of an N/O-donor for an S-donor, which is easily detected by EXAFS analysis, can have unintended structural consequences as a result of a change in the spin-state of Ni(II).

The six-coordinate high-spin monothiolate Ni(II) complex formed with WT-RcnR is very unusual. With respect to metal coordination by WT-RcnR, the results presented above indicate a Ni(II) site in WT-*Ec*RcnR features coordination by the N-terminus, Cys35, Glu63, His64, and

two other N/O-donors, one of which might be Glu34. The similar results obtained for the Ni(II) complexes of E34C-RcnR and E63C-RcnR are consistent with similar roles as ligands for the two glutamate residues, although this role for Glu34 is still ambiguous because the results of XAS analysis for E34A-RcnR are not conclusive. It has been previously noted that few high-spin Ni(II) thiolate complexes have been characterized,[35] and the existing examples feature very long (> 2.5 Å) Ni-S distances, like that of the WT-*Ec*RcnR Ni(II) complex, and are generally supported by bidentate coordination, presumably to prevent facile substitution of the weak S-donor ligands.[81, 82] This supporting role may be the function of the neighboring Glu34 residue, which could act to support the high-spin six-coordinate mono-thiolate Ni(II) complex that utilizes the only Cys residue in the protein. For Ni, the computational models suggest that a similar structure to Co, mentioned above, is obtained, where coordination by the Ser2 amide O atom replaces the His3 imidazole, forming a true five-membered chelate ring with the terminal Ser-NH$_2$.

Implications for Function

The present and previous studies of RcnR mutants have revealed discrepancies between functional responses to metal compared to effects on metal coordination. The available structure/function data from XAS and LacZ studies for the cognate metal complexes of *Ec*RcnR are summarized in Table 4, which indicates whether a residue is or is not a metal ligand (XAS), and whether the residue contributes to a transcriptional response to metal binding (LacZ). There are three main outcomes of these sets of data. First, XAS demonstrates that Co and Ni ions bind different, but overlapping, ligand sets. Second, LacZ assays reveal that there are residues important for metal coordination that when mutated show little effect on the transcriptional response for at least one metal, and *vice versa*. A response to metal in the LacZ assay by an

RcnR mutant requires a metal-binding affinity tight enough to detect the metal *in vivo*, as well as the capability of metal-binding to regulate DNA-binding allosterically. The consequence of a weakened affinity mutant is greater metal accumulation because induction of efflux by RcnA is impaired, but the feedback does not extrapolate with ever weakening affinities, as recently shown for the Ni-responsive RcnR homolog, InrS.[83] Thus, mutants with altered metal

Table 4. Analysis of structure-function relationships in metal-coordination by *Ec*RcnR

| Residue | Ni | | Co | | |
	XAS	LacZ[a]	XAS	LacZ	Refs.
S2-NH$_2$	Yes	Yes (A2*)	Yes	Yes (A2*)	35, 47
H3	No	Yes (C,L,E)	Yes	Yes (C,L,E)	35, 47
E34	maybe	No (A,C,Q)	Yes	No (A,C,Q)	this work,[35]
C35	Yes	No (A) Yes (L)	Yes	Yes (A,L)	35
H60	No	No (A,N,L) Partial (C)	No	Yes (A,C,N,L)	35, 48
E63	Yes	Partial (A,C,Q)	Yes	No (A) Partial (Q,C)	this work[35]

H64	Yes	Yes (C) Partial (L)	Yes	Yes(L) Partial (C)	35, 48
H67	No	No (C, L)	No	No (C, L)	35, 48

coordination geometry as determined by XAS that maintain a normal transcriptional response are predicted to have a metal-binding affinity within 20-30 fold of the wild-type protein and be capable of transmitting metal-binding site occupancy to DNA-binding residues.

Second coordination sphere interactions important in the allosteric response to metal binding can contribute structural features that cannot be directly probed by XAS. These interactions are known to play important roles in generating metal-specific responses in metalloregulators. Mutation of these residues will yield wild-type like XAS metal-site structures but be non-responsive to one or more metals in the LacZ assay. For example, mutation of a second sphere Glu residue (E81) is the Cu(I)-sensing CsoR protein has negligible effect on Cu(I)-affinity but a large effect on the allosteric response.[84] Furthermore, in the MerR family of transcriptional regulators, it has been shown that the metal discrimination *in vitro* between monovalent and divalent cations, and between different pools of monovalent and divalent cations, is conferred by second coordination sphere interactions and not through the primary metal coordination sphere.[9, 84]

Despite the obvious structural roles played by Glu34 and Glu63 in coordination of the cognate metals, neither residue is critical to the allosteric response to specific metal binding that

facilitates DNA release. Both Glu34 variants retain full metal-responsive transcriptional regulation to both cognate metals, and both Glu63 variants retain substantial, although sometimes partially diminished, responses. The lack of a correlation between ligation of specific Glu residues and transcriptional response in *Ec*RcnR indicates that not every ligand in the primary coordination sphere plays a critical role in the allosteric response involved in regulating transcription. This contrasts with the intensively studied Zn(II)-responsive CzrA protein, in which mutation of any of the four metal-ligands affects function in some way.[85] Thus, identification of a residue as a metal ligand does not infer functional importance, and identification of ligands by functional assay alone is also limited. In *Ec*RcnR, where the ligand selection of the two cognate metals is different, Glu34 and Glu63 may provide a basis for differential response to these two metals.

Mechanistic considerations

A critical requirement for the allosteric response of *Ec*RcnR appears to be metal-coordination of N-terminus. Binding of the N-terminal amine and, in the case of Co(II), the His3 side chain imidazole, may be involved in positioning the N-terminus of the α1-helix over the metal-binding site, in analogy with studies of *Geobacillus thermodenitrificans* CsoR.[49] The allosteric response would not occur for non-cognate metals, since they do not bind these residues. This situation is similar to what has been recently determined for the Ni(II)/Co(II) responsive membrane-bound periplasmic regulator CnrX.[46, 86-88] Mutational studies on CnrX indicate that binding of Met123 pulls the protein into a signal propagating active conformation. Non-cognate metals do not bind this residue and thus cannot facilitate this conformational change.

Remarkably, these studies show that the coordination number (and even spin-state!) of the cognate metal ion is relatively unimportant to the allosteric response in EcRcnR. However, coordination number is important for discriminating cognate from non-cognate metals in EcRcnR.[47, 48] Resolving the details of the link between metal coordination and transcriptional response to metal binding will require determination of metal-affinities of individual mutants for both cognate and non-cognate metals and the corresponding changes in DNA-binding affinity that are linked to the transcriptional response monitored by the LacZ assay.

ASSOCIATED CONTENT

Supplementary materials and methods, tables, and discussion of modeling results, XAS of E34A- and E34C-RcnR bound to Co(II) in Cl buffer, pre-edge features of Ni(II) complexes, Evans magnetic susceptibility measurements, lacZ titrations, and SEC, fluorescence anisotropy data, and tables with additional fits for WT and mutant *Ec*RcnR proteins. This material is available free of charge via the Internet at http://pubs.acs.org.

AUTHOR INFORMATION

Corresponding Author

*Phone: (413) 545-4876. E-mail: mmaroney@chem.umass.edu.

Present Addresses

†Department of Pharmaceutical Sciences, University of Nebraska Medical Center, 986025 Nebraska Medical Center, Omaha, Nebraska, 68198-6025, United States

Author Contributions

The manuscript was written through contributions of all authors. All authors have given approval to the final version of the manuscript.

ABBREVIATIONS

RcnR, resistance to cobalt and nickel regulator; Amp, ampicillin; cam, chloramphenicol; CsoR, copper-sensitive operon repressor; XAS, X-ray absorption spectroscopy; XANES, X-ray absorption near-edge spectroscopy; EXAFS, extended X-ray absorption fine structure; InrS, internal nickel-responsive sensor; ICP-OES, inductively coupled plasma optical emission spectroscopy; IPTG, isopropyl β-D-1-thiogalactopyranoside; NikR, nickel-responsive regulator of the *nik* operon; HEPES: (4-(2-hydroxyethyl)-1-piperazineethanesulfonic acid; TCEP, tris(2-carboxyethyl)phosphine hydrochloride; SlyD, sensitive to lysis D; HypA, hydrogenase protein A; RicR, regulated in copper repressor; CstR, CsoR-like sulfur transferase repressor; FrmR, formaldehyde regulator.

REFERENCES

1.   Rosenzweig, A. C. Metallochaperones: Bind and Deliver. *Chem. Biol.* **2002,** 9 (02), 673-677.

2.   Waldron, K. J.; Rutherford, J. C.; Ford, D.; Robinson, N. J. Metalloproteins and metal sensing. *Nature* **2009,** 460 (7257), 823-830.

3.   Yannone, S. M.; Hartung, S.; Menon, A. L.; Adams, M. W. W.; Tainer, J. A. Metals in biology: Defining metalloproteomes. *Curr. Opin. Biotech.* **2012,** 23 (1), 89-95.

4.   Andrews, N. C. Metal transporters and disease. *Curr. Opin. Chem. Biol.* **2002,** 6, 181-186.

5.   De Domenico, I.; McVey Ward, D.; Kaplan, J. Regulation of iron acquisition and storage: consequences for iron-linked disorders. *Nature reviews. Molecular cell biology* **2008,** 9 (1), 72-81.

6.   Fantino, J.-R.; Py, B.; Fontecave, M.; Barras, F. A genetic analysis of the response of Escherichia coli to cobalt stress. *Environmental microbiology* **2010,** 12 (10), 2846-2857.

7.   Hagar, W.; Theil, E. C.; Vichinsky, E. P. Diseases of iron metabolism. *Pediatric clinics of North America* **2002,** 49 (5), 893-909.

8.   Hamza, I.; Gitlin, J. D. Copper chaperones for cytochrome c oxidase and human disease. *Journal of bioenergetics and biomembranes* **2002,** 34 (5), 381-388.

9.   Ma, Z.; Jacobsen, F. E.; Giedroc, D. P. Coordination chemistry of bacterial metal transport. *Chem. Rev.* **2009,** 109, 4644-4681.

10.   Pennella, M. A.; Shokes, J. E.; Cosper, N. J.; Scott, R. A.; Giedroc, D. P. Structural elements of metal selectivity in metal sensor proteins. *Proc. Nat. Acad. Sci. USA* **2003,** 100 (7), 3713-3718.

11.   Foster, A. W.; Osman, D.; Robinson, N. J. Metal preferences and metallation. *J. of Biol. Chem.* **2014,** 289 (41), 28095-28103.

12.   Guerra, A. J.; Giedroc, D. P. Metal site occupancy and allosteric switching in bacterial metal sensor proteins. *Arch. of Biochem. Biophys.* **2012,** 519 (2), 210-222.

13.   Pennella, M. A.; Giedroc, D. P. Structural determinants of metal selectivity in prokaryotic metal-responsive transcriptional regulators. *BioMetals* **2005,** 18 (4), 413-428.

14.   Tottey, S.; Harvie, D. R.; Robinson, N. J. Understanding how cells allocate metals using metal sensors and metallochaperones. *Accounts of Chemical Research* **2005,** 38 (10), 775-783.

15.   Waldron, K. J.; Robinson, N. J. How do bacterial cells ensure that metalloproteins get the correct metal? *Nature reviews. Microbiology* **2009,** 7 (1), 25-35.

16.   Kobayashi, M.; Shimizu, S. Cobalt proteins. *European Journal of Biochemistry* **1999,** 261 (1), 1-9.

17.   Ko, Y.; Ashok, S.; Ainala, S. K.; Sankaranarayanan, M.; Chun, A. Y.; Jung, G. Y.; Park, S. Coenzyme B 12 can be produced by engineered Escherichia coli under both anaerobic and aerobic conditions. *Biotechnology Journal* **2014,** 9 (12), 1526-1535.

18.   Li, Y. Production of vitamin B 12 in recombinant Escherichia coli : An important step for heterologous production of structurally complex small molecules. *Biotechnology Journal* **2014,** 9 (12), 1478-1479.

19.   Scarlett, F. A.; Turner, J. M. Microbial metabolism of amino alcohols. Ethanolamine catabolism mediated by coenzyme B12-dependent ethanolamine ammonia-lyase in *Escherichia coli* and *Klebsiella aerogenes. Journal of general microbiology* **1976,** 95 (1), 173-176.

20.   Boer, J. L.; Mulrooney, S. B.; Hausinger, R. P. Nickel-dependent metalloenzymes. *Archives of Biochemistry and Biophysics* **2014,** 544, 142-152.

21.   Kaluarachchi, H.; Chan Chung, K. C.; Zamble, D. B. Microbial nickel proteins. *Natural product reports* **2010,** 27 (5), 681-694.

22.   Peters, J. W.; Schut, G. J.; Boyd, E. S.; Mulder, D. W.; Shepard, E. M.; Broderick, J. B.; King, P. W.; Adams, M. W. W. [FeFe]- and [NiFe]-hydrogenase diversity, mechanism, and maturation. *Biochimica et Biophysica Acta (BBA) - Molecular Cell Research* **2015,** 1853 (6), 1350-1369.

23.   Ragsdale, S. W. Nickel-based enzyme systems. *Journal of Biological Chemistry* **2009,** 284 (28), 18571-18575.

24.   De Pina, K.; Navarro, C.; McWalter, L.; Boxer, D. H.; Price, N. C.; Kelly, S. M.; Mandrand-Berthelot, M. A.; Wu, L. F. Purification and characterization of the periplasmic nickel-binding protein NikA of Escherichia coli K12. *European Journal of Biochemistry* **1995,** 227 (3), 857-865.

25.   Navarro, C.; Wu, L.-F.; Mandrand-Berthelot, M.-A. The nik operon of *Escherichia coli* encodes a periplasmic binding-protein-dependent transport system for nickel. *Mol. Microbiol.* **1993,** 9, 1181-1191.

26.   Atanassova, A.; Zamble, D. B. Escherichia coli HypA is a zinc metalloprotein with a weak affinity for nickel. *Journal of Bacteriology* **2005,** 187 (14), 4689-4697.

27.   Johnson, R. C.; Hu, H. Q.; Merrell, D. S.; Maroney, M. J. Dynamic HypA zinc site is essential for acid viability and proper urease maturation in Helicobacter pylori. *Metallomics* **2015,** 7 (4), 674-682 DOI: 10.1039/c4mt00306c.

28.   Mehta, N.; Olson, J. W.; Maier, R. J. Characterization of Helicobacter pylori nickel metabolism accessory proteins needed for maturation of both urease and hydrogenase. *Journal of Bacteriology* **2003,** 185 (3), 726-734.

29.   Chan Chung, K. C.; Zamble, D. B. The Escherichia coli metal-binding chaperone SlyD interacts with the large subunit of [NiFe]-hydrogenase 3. *FEBS Letters* **2011,** 585 (2), 291-294.

30.   Kaluarachchi, H.; Altenstein, M.; Sugumar, S. R.; Balbach, J.; Zamble, D. B.; Haupt, C. Nickel binding and [NiFe]-hydrogenase maturation by the metallochaperone SlyD with a single metal-binding site in Escherichia coli. *Journal of molecular biology* **2012,** 417 (1-2), 28-35.

31.   Blériot, C.; Effantin, G.; Lagarde, F.; Mandrand-Berthelot, M. A.; Rodrigue, A. RcnB is a periplasmic protein essential for maintaining intracellular Ni and Co concentrations in *Escherichia coli. Journal of Bacteriology* **2011,** 193 (15), 3785-3793.

32.   Rodrigue, A.; Effantin, G. Identification of rcnA (yohM), a Nickel and Cobalt Resistance Gene in *Escherichia coli*. **2005,** 187 (8), 2912-2916.

33.   Chivers, P. T.; Sauer, R. T. NikR is a ribbon-helix-helix DNA-binding protein. *Protein Sci*. **1999,** 8 (11), 2494-2500.

34.   De Pina, K.; Desjardin, V.; Mandrand-Berthelot, M. A.; Giordano, G.; Wu, L. F. Isolation and characterization of the nikR gene encoding a nickel-responsive regulator in *Escherichia coli. Journal of bacteriology* **1999,** 181 (2), 670-674.

35.   Iwig, J. S.; Leitch, S.; Herbst, R. W.; Maroney, M. J.; Chivers, P. T. Ni(II) and Co(II) sensing by *Escherichia coli* RcnR. *Journal of the American Chemical Society* **2008,** 130 (24), 7592-7606.

36.   Iwig, J. S.; Rowe, J. L.; Chivers, P. T. Nickel homeostasis in Escherichia coli - the rcnR-rcnA efflux pathway and its linkage to NikR function. *Molecular microbiology* **2006,** 62 (1), 252-262.

37.   Higgins, K. A.; Giedroc, D. Insights into Protein Allostery in the CsoR/RcnR Family of Transcriptional Repressors. *Chem Lett* **2014,** 43 (1), 20-25 DOI: 10.1246/cl.130965.

38.   Festa, R. A.; Jones, M. B.; Butler-Wu, S.; Sinsimer, D.; Gerads, R.; Bishai, W. R.; Peterson, S. N.; Darwin, K. H. A novel copper-responsive regulon in *Mycobacterium tuberculosis. Molecular microbiology* **2011,** 79 (1), 133-148.

39.	Liu, T.; Ramesh, A.; Ma, Z.; Ward, S. K.; Zhang, L.; George, G. N.; Talaat, A. M.; Sacchettini, J. C.; Giedroc, D. P. CsoR is a novel Mycobacterium tuberculosis copper-sensing transcriptional regulator. *Nature chemical biology* **2007,** 3 (1), 60-68.

40.	Foster, A. W.; Patterson, C. J.; Pernil, R.; Hess, C. R.; Robinson, N. J. Cytosolic Ni(II) Sensor in Cyanobacterium: Nickel Detection Follows Nickel Affinity Across Four Families of Metal Sensors. *Journal of Biological Chemistry* **2012,** 287 (15), 12142-12151.

41.	Grossoehme, N.; Kehl-Fie, T. E.; Ma, Z.; Adams, K. W.; Cowart, D. M.; Scott, R. A.; Skaar, E. P.; Giedroc, D. P. Control of Copper Resistance and Inorganic Sulfur Metabolism by Paralogous Regulators in *Staphylococcus aureus*. *Journal of Biological Chemistry* **2011,** 286 (15), 13522-13531.

42.	Herring, C. D.; Blattner, F. R. Global transcriptional effects of a suppressor tRNA and the inactivation of the regulator frmR. *Journal of Bacteriology* **2004,** 186 (20), 6714-6720.

43.	Denby, K. J., Iwig, J., Bisson, C., Westwood J., Rolfe, M. D., Sedelnikova, S. E., Higgins, K., Maroney, M. J., Baker, P. J., Chivers, P. T., and Green, J. The mechanism of a formaldehyde-sensing transcriptional regulator. *Sci. Rep.* **2016,** 6, DOI: 10.1038/srep38879.

44.	Iwig, J. S.; Chivers, P. T. DNA recognition and wrapping by *Escherichia coli* RcnR. *Journal of molecular biology* **2009,** 393 (2), 514-526.

45.	Cavet, J. S. A Nickel-Cobalt-sensing ArsR-SmtB Family Repressor. Contributions of Cytosol and Effector Binding Sites to Metal Selectivity. *Journal of Biological Chemistry* **2002,** 277 (41), 38441-38448.

46.	Trepreau, J.; Girard, E.; Maillard, A. P.; De Rosny, E.; Petit-Haertlein, I.; Kahn, R.; Coves, J. Structural basis for metal sensing by CnrX. *J. Mol. Biol.* **2011,** 408 (4), 766-779.

47.	Higgins, K. A.; Chivers, P. T.; Maroney, M. J. Role of the N-terminus in determining metal-specific responses in the *E. coli* Ni- and Co-responsive metalloregulator, RcnR. *Journal of the American Chemical Society* **2012,** 134 (16), 7081-7093.

48.	Higgins, K. A.; Hu, H. Q.; Chivers, P. T.; Maroney, M. J. Effects of select histidine to cysteine mutations on transcriptional regulation by *Escherichia coli* RcnR. *Biochemistry* **2013,** 52 (1), 84-97.

49.	Chang, F.-M. J.; Coyne, H. J.; Cubillas, C.; Vinuesa, P.; Fang, X.; Ma, Z.; Ma, D.; Helmann, J. D.; Garcia-de los Santos, A.; Wang, Y.-X.; Dann, C. E.; Giedroc, D. P. Cu(I)-mediated Allosteric Switching in a Copper-sensing Operon Repressor (CsoR). *Journal of Biological Chemistry* **2014,** 289 (27), 19204-19217.

50.	Foster, A. W.; Pernil, R.; Patterson, C. J.; Robinson, N. J. Metal specificity of cyanobacterial nickel-responsive repressor InrS: Cells maintain zinc and copper below the detection threshold for InrS. *Molecular Microbiology* **2014,** 92 (4), 797-812.

51.   Wilmot, C. M. Fighting toxic copper in a bacterial pathogen. *Nat Chem Biol* **2007,** 3 (1), 15-16 DOI: 10.1038/nchembio0107-15.

52.   Musiani, F.; Zambelli, B.; Bazzani, M.; Mazzei, L.; Ciurli, S. Nickel-responsive transcriptional regulators. *Metallomics* **2015,** 7 (9), 1305-1318 DOI: 10.1039/c5mt00072f.

53.   Webb, S. M. SIXPack a Graphical User Interface for XAS Analysis Using IFEFFIT. *Physica Scripta* **2005,** T115, 1011-1014.

54.   Newville, M. Data analysis. *Journal of Synchrotron Radiation* **2001,** 8, 322-324.

55.   Ravel, B.; Newville, M. *ATHENA , ARTEMIS, HEPHAESTUS*: data analysis for X-ray absorption spectroscopy using *IFEFFIT*. *Journal of Synchrotron Radiation* **2005,** 12 (4), 537-541.

56.   Banaszak, K.; Martin-Diaconescu, V.; Bellucci, M.; Zambelli, B.; Rypniewski, W.; Maroney, M. J.; Ciurli, S. Crystallographic and X-ray absorption spectroscopic characterization of *Helicobacter pylori* UreE bound to Ni(2)(+) and Zn(2)(+) reveals a role for the disordered C-terminal arm in metal trafficking. *The Biochemical journal* **2012,** 441 (3), 1017-1026 DOI: 10.1042/BJ20111659.

57.   Blackburn, N. J.; Hasnain, S. S.; Pettingill, T. M.; Strange, R. W. Copper K-extended X-ray absorption fine structure studies of oxidized and reduced dopamine beta-hydroxylase: Confirmation of a sulfur ligand to copper(I) in the reduced enzyme. *Journal of Biological Chemistry* **1991,** 266, 23120-23127.

58.   Ferreira, G. C.; Franco, R.; Mangravita, A.; George, G. N. Unraveling the substrate-metal binding site of ferrochelatase: an X-ray absorption spectroscopic study. *Biochemistry* **2002,** 41 (15), 4809-4818.

59.   Engh, R. A.; Huber, R. Accurate bond and angle parameters for X-ray protein structure refinement. *Acta Crystallographica Section A* **1991,** 47 (4), 392-400.

60.   Evans, D. F. The Determination of the Paramagnetic Susceptibility of Substances in Solution by Nuclear Magnetic Resonance. *J Chem Soc* **1959,** (Jun), 2003-2005 DOI: Doi 10.1039/Jr9590002003.

61.   Schubert, E. Utilizing the Evans method with a superconducting NMR spectrometer in the undergraduate laboratory. *J. Chem. Ed.* **1992,** 69, 62.

62.   Piguet, C. Paramagnetic susceptibility by NMR: the solvent correction removed for large paramagentic molecules. *J. Chem. Ed.* **1997,** 74, 815-816.

63.   Miller, J. *Experiments in Molecular Genetics*. Cold Spring Harbor Laboratory: Cold Spring Harbor, New York, 1972; p 466.

64.   Kuzmic, P. Program DYNAFIT for the analysis of enzyme kinetic data: application to HIV proteinase. *Anal Biochem* **1996,** 237 (2), 260-273 DOI: 10.1006/abio.1996.0238.

65.   Marti-Renom, M. A.; Stuart, A. C.; Fiser, A.; Sanchez, R.; Melo, F.; Sali, A. Comparative protein structure modeling of genes and genomes. *Annu Rev Biophys Biomol Struct* **2000,** 29, 291-325.

66.   Martin-Diaconescu, V.; Bellucci, M.; Musiani, F.; Ciurli, S.; Maroney, M. J. Unraveling the Helicobacter pylori UreG zinc binding site using X-ray absorption spectroscopy (XAS) and structural modeling. *J. Biol. Inorg. Chem.* **2012,** 17 (3), 353-361 DOI: 10.1007/s00775-011-0857-9.

67.   Sali, A.; Sali, A. Statistical potential for assessment and prediction of protein structures. *Protein Science* **2006**, 2507-2524.

68.   Laskowski, R. A.; MacArthur, M. W.; Moss, D. S.; Thornton, J. M. PROCHECK: a program to check the stereochemical quality of protein structures. *Journal of Applied Crystallography* **1993,** 26 (November), 283-291.

69.   Pettersen, E. F.; Goddard, T. D.; Huang, C. C.; Couch, G. S.; Greenblatt, D. M.; Meng, E. C.; Ferrin, T. E. UCSF Chimera - A visualization system for exploratory research and analysis. *Journal of Computational Chemistry* **2004,** 25 (13), 1605-1612.

70.   Hu, V. W.; Chan, S. I.; Brown, G. S. X-ray absorption edge studies on oxidized and reduced cytochrome c oxidase. *Proceedings of the National Academy of Sciences* **1977,** 74 (9), 3821-3825.

71.   Shulman, G. R.; Yafet, Y.; Eisenberger, P.; Blumberg, W. E. Observations and interpretation of x-ray absorption edges in iron compounds and proteins. *Proceedings of the National Academy of Sciences of the United States of America* **1976,** 73 (5), 1384-1388.

72.   Clark-Baldwin, K.; Tierney, D. L.; Govindaswamy, N.; Gruff, E.; Kim, C.; Berg, J. M.; Koch, S.; Penner-Hahn, J. E. The Limitations of X-ray Absorption Spectroscopy for Determining the Structure of Zinc Sites in Proteins. When Is a Tetrathiolate Not a Tetrathiolate? *Journal of the American Chemical Society* **1998,** 120 (33), 8401-8409.

73.   Jacquamet, L.; Aberdam, D.; Adrait, A.; Hazemann, J.-l.; Latour, J.-m.; Michaud-soret, I. X-ray Absorption Spectroscopy of a New Zinc Site in the Fur Protein from *Escherichia coli*. *Biochemistry* **1998,** 1 (97), 2564-2571.

74.   Wirt, M. D.; Sagi, I.; Chen, E.; Frisbie, S. M.; Lee, R.; Chance, M. R. Geometric conformations of intermediates of B12 catalysis by x-ray edge spectroscopy: cobalt(I) B12, cobalt(II) B12, and base-off adenosylcobalamin. *Journal of the American Chemical Society* **1991,** 113 (14), 5299-5304.

75.   Roe, A. L.; Schneider, D. J.; Mayer, R. J.; Pyrz, J. W.; Widom, J.; Que Jr, L. J. X-ray absorption spectroscopy of iron-tyrosinate proteins. *Journal of the American Chemical Society* **1984,** 106 (6), 1676-1681.

76.   Scheuring, E. M.; Clavin, W.; Wirt, M. D.; Miller, L. M.; Fischetti, R. F.; Lu, Y.; Mahoney, N.; Xie, A. H.; Wu, J. J.; Chance, M. R. Time-resolved X-ray absorption spectroscopy of photoreduced base-off Cob(II)alamin compared to the Co(II) species in *Clostridium thermoaceticum*. *Journal of Physical Chemistry* **1996,** 100 (9), 3344-3348.

77.   Colpas, G. J.; Maroney, M. J.; Bagyinka, C.; Kumar, M.; Willis, W. S.; Suib, S. L.; Mascharak, P. K.; Baidya, N. X-ray spectroscopic studies of nickel complexes, with application to the structure of nickel sites in hydrogenases. *Inorganic Chemistry* **1991,** 30 (5), 920-928.

78.   Musiani, F.; Carloni, P.; Ciurli, S. The asn 38-cys 84 H-bond in plastocyanin. *J Phys Chem B* **2004,** 108 (22), 7495-7499 DOI: 10.1021/jp037834z.

79.   Glasfeld, A.; Guedon, E.; Helmann, J. D.; Brennan, R. G. Structure of the manganese-bound manganese transport regulator of *Bacillus subtilis*. *Nat Struct Biol* **2003,** 10 (8), 652-657 DOI: 10.1038/nsb951.

80.   Ryan, K. C.; Johnson, O. E.; Cabelli, D. E.; Brunold, T. C.; Maroney, M. J. Nickel superoxide dismutase: structural and functional roles of Cys2 and Cys6. *Journal of biological inorganic chemistry : JBIC : a publication of the Society of Biological Inorganic Chemistry* **2010,** 15 (5), 795-807.

81.   Rosenfield, S. G.; Berends, H. P.; Gelmini, L.; Stephan, D. W.; Mascharak, P. K. New Octahedral Thiolato Complexes of Divalent Nickel: Syntheses, Structures and Properties of (Et$_4$N)[Ni(SC$_5$H$_4$N)$_3$] and (Ph$_4$P)[Ni{SC$_4$H$_3$N$_2$}$_3$]-CH$_3$CN. *Inorg. Chem.* **1987,** 26, 2792-2797.

82.   Ragunathan, K. G.; Bharadwaj, P. K. Nickel(II) Complexes with Tripodal Ligands - Synthesis, X-Ray Structural and Spectroscopic Studies. *J Chem Soc Dalton* **1992,** (15), 2417-2422 DOI: 10.1039/Dt9920002417.

83.   Pennella, M. A.; Arunkumar, A. I.; Giedroc, D. P. Individual metal ligands play distinct functional roles in the zinc sensor *Staphylococcus aureus* CzrA. *J Mol Biol* **2006,** 356 (5), 1124-1136 DOI: 10.1016/j.jmb.2005.12.019.

84.   Osman, D.; Cavet, J. S. Bacterial metal-sensing proteins exemplified by ArsR-SmtB family repressors. *Natural product reports* **2010,** 27 (5), 668-680.

85.   Pompidor, G.; Maillard, A. P.; Girard, E.; Gambarelli, S.; Kahn, R.; Coves, J. X-ray structure of the metal-sensor CnrX in both the apo- and copper-bound forms. *FEBS Letters* **2008,** 582 (28), 3954-3958.

86.   Trepreau, J.; Grosse, C.; Mouesca, J.-M.; Sarret, G.; Girard, E.; Petit-Haertlein, I.; Kuennemann, S.; Desbourdes, C.; de Rosny, E.; Maillard, A. P.; Nies, D. H.; Coves, J. Metal

sensing and signal transduction by CnrX from *Cupriavidus metallidurans* CH34: role of the only methionine assessed by a functional, spectroscopic, and theoretical study. *Metallomics : integrated biometal science* **2014,** 6 (2), 263-273.

87.	Maillard, A. P.; Kunnemann, S.; Grosse, C.; Volbeda, A.; Schleuder, G.; Petit-Hartlein, I.; de Rosny, E.; Nies, D. H.; Coves, J. Response of CnrX from *Cupriavidus metallidurans* CH34 to nickel binding. *Metallomics* **2015,** 7 (4), 622-631.

88.	Ma, Z.; Cowart, D. M.; Ward, B. P.; Arnold, R. J.; DiMarchi, R. D.; Zhang, L. M.; George, G. N.; Scott, R. A.; Giedroc, D. P. Unnatural Amino Acid Substitution as a Probe of the Allosteric Coupling Pathway in a Mycobacterial Cu(I) Sensor. *Journal of the American Chemical Society* **2009,** 131 (50), 18044-18045 DOI: 10.1021/ja908372b.

Table of Contents Material

Synopsis

E. coli RcnR is a Ni(II)- and Co(II)-responsive transcriptional regulator involved in metal efflux. This work reports structure/function investigations of metal site glutamate protein variants. While the glutamate residues play a structural role in binding the cognate metals, they are not required for function. The flexibility of the metal site structures is striking, and includes spin-state changes in Ni(II) complexes that cause a conversion from high- to low-spin, but are unimportant to allosteric response.

TOC Figure
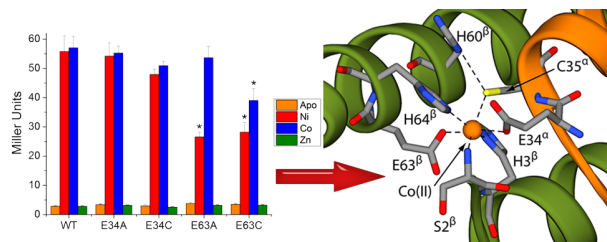
Supplemental Material

Glutamate Ligation in the Ni(II) and Co(II) Responsive *E. coli* Transcriptional Regulator, RcnR

Carolyn E. Carr, Francesco Musiani, Hsin-Ting Huang, Peter T. Chivers, Stefano Ciurli, and Michael J. Maroney

Table S12. Additional Fits for Co(II) E63A-RcnR in Buffer with 20 mM Hepes, 300 mM NaBr and 10 % Glycerol at pH 7.0.

Table S13. Additional Fits for Co(II) E63A-RcnR in Buffer with 20 mM Hepes, 300 mM NaCl and 10 % Glycerol at pH 7.0.

Table S14. Additional Fits for Zn(II) E63A-RcnR in Buffer with 20 mM Hepes, 300 mM NaBr and 10 % Glycerol at pH 7.0.

Table S15. Additional Fits for Ni(II) E63C-RcnR in Buffer with 20 mM Hepes, 300 mM NaBr and 10 % Glycerol at pH 7.0.

Table S16. Additional Fits for Co(II) E63C-RcnR in Buffer with 20 mM Hepes, 300 mM NaBr and 10 % Glycerol at pH 7.0.

Table S17. Additional Fits for Zn(II) E63C-RcnR in Buffer with 20 mM Hepes, 300 mM NaBr and 10 % Glycerol at pH 7.0.

Table S18. Results of LacZ transcription reporter assays**.**

Figure S1: XAS data for E63A-RcnR complexed to Ni(II) in NaCl buffer.

Figure S2: XAS data for E63A-RcnR complexed to Co(II) in NaCl buffer.

Figure S3: Pre-edge XANES features of metal complexes of *Ec*RcnR proteins.

Figure S4: ^{1}H NMR spectra of the DSS reference peak in solution with the Ni(II) complexes of WT- and E63C- RcnR in 20 mM HEPES, 100 mM NaCl, 1 mM TCEP, 10% glycerol, pH 7.0 in 90% H_2O/10% D_2O.

Figure S5: LacZ titrations of WT-, E34A-, and E34C-RcnR with Ni(II) and Co(II)**.**

Figure S6: Size-exclusion chromatograms for WT-RcnR and Glu variants.

Figure S7: Anisotropy change upon titration of DNA (10 nM) with apo-RcnR.

Figure S8. Details of one of the three modeled Zn(II) binding sites on *Ec*RcnR model structure.

Supplementary details of molecular modeling for *Ec*RcnR

Additional data regarding EXAFS fits and additional fits are shown in the tables below. (The best fits for the data are shown in bold and other alternative fits are shown in italics)

Table S1. Additional Fits for Ni(II) WT-RcnR in Buffer with 20 mM Hepes, 300 mM NaBr and 10 % Glycerol at pH 7.0.

Fourier-transform window: $k = 2 - 12.5$ Å^{-1}. Data range fit: r = 1- 4 Å.

N	r (Å)	σ^2 (x10^{-3} Å^2)	ΔE_0 (eV)	R factor	χ^2	Red χ^2	nvar
5N/O	2.07(1)	6(1)	2(2)	0.1749	1655.572	84.297	3
4N/O	2.07(1)	4(1)					
1N/O	2.31(0.11)	14(23)	4(2)	0.1569	1484.604	84.163	5
5N/O	2.07(1)	5(1)					
1S	2.00(0.11)	21(18)	4(3)	0.1652	1563.630	88.643	5
5N/O	2.09(2)	11(2)					
1Im	2.05(2)	1(1)	3(2)	0.1440	1157.916	65.643	5
4N/O	2.08(2)	5(2)					
1Im	1.88(4)	5(4)					
1Im	2.03(3)	1(2)	-1(2)	0.1093	1034.944	66.174	7
3N/O	2.08(2)	4(2)					
1Im	2.11(3)	2(3)					
1Im	1.99(3)	3(3)					
1Im	1.86(3)	0(3)	-1(2)	0.0969	917.509	67.268	9
4N/O	*2.10(1)*	*8(1)*					
1S	*2.63(1)*	*6(2)*					
1Im	*2.05(1)*	*1(1)*	*4(1)*	*0.0499*	*472.106*	*30.187*	*7*
3N/O	*2.09(1)*	*5(2)*					
1S	*2.63(1)*	*6(2)*					
1Im	*2.17(5)*	*8(8)*					
1Im	*2.04(2)*	*2(2)*	*5(1)*	*0.0456*	*431.668*	*31.648*	*9*
3N/O	*2.09(1)*	*5(2)*					
1S	*2.63(1)*	*6(2)*					
1Im 0°	*2.05(2)*	*2(2)*					
1Im 5°	*2.19(4)*	*7(6)*	*5(1)*	*0.0461*	*436.280*	*31.986*	*9*
3N/O	*2.11(2)*	*7(3)*					
1S	*2.62(2)*	*6(2)*					
1Im 0°	*2.06(2)*	*2(1)*					
1Im 10°	*2.04(5)*	*5(3)*	*4(1)*	*0.0442*	*418.444*	*30.678*	*9*

3N/O	2.10(2)	8(3)					
1S	2.62(2)	6(2)					
1Im 5°	2.06(2)	1(1)					
1Im 10°	2.05(6)	6(6)	4(1)	0.0502	475.207	34.840	9
2N/O	2.08(1)	2(1)					
1S	2.62(2)	5(2)					
1Im	2.02(0.26)	6(32)					
1Im	2.20(7)	3(11)					
1Im	2.06(0.18)	2(7)	4(2)	0.0499	472.104	40.560	11
2N/O	2.07(2)	2(2)					
1N/O	2.21(6)	7(11)					
1S	2.63(2)	5(2)					
1Im 0°	2.13(9)	6(14)					
1Im 0°	2.03(7)	3(7)	5(1)	0.0405	382.917	32.898	11
2N/O	*2.08(2)*	*2(2)*					
1N/O	*2.24(5)*	*5(8)*					
1S	*2.63(2)*	*5(2)*					
1Im 0°	*2.13(4)*	*2(5)*					
1Im 5°	*2.02(4)*	*1(4)*	*5(1)*	*0.0406*	*383.940*	*32.986*	*11*
2N/O	**2.07(2)**	**2(2)**					
1N/O	**2.21(3)**	**3(4)**					
1S	**2.63(2)**	**6(2)**					
1Im 0°	**2.07(3)**	**3(2)**					
1Im 10°	**2.02(6)**	**6(5)**	**4(1)**	**0.0381**	**360.950**	**31.010**	**11**
2N/O	*2.07(2)*	*2(2)*					
1N/O	*2.21(4)*	*4(6)*					
1S	*2.63(2)*	*6(2)*					
1Im 5°	*2.08(3)*	*3(3)*					
1Im 10°	*2.05(8)*	*7(8)*	*4(1)*	*0.0445*	*421.170*	*36.184*	*11*
1N/O	2.07(3)	0(2)					
2N/O	2.14(4)	10(8)					
1S	2.63(2)	5(2)					
1Im 0°	2.12(0.10)	6(17)					
1Im 0°	2.03(9)	3(7)	4(1)	0.0406	383.995	32.990	11
1N/O	2.06(3)	1(2)					
2N/O	2.14(5)	9(9)					
1S	2.63(2)	6(2)					
1Im 0°	2.06(6)	4(5)					
1Im 5°	2.09(0.19)	10(20)	4(1)	0.0422	399.215	34.298	11
1N/O	*2.06(3)*	*1(2)*					
2N/O	*2.15(3)*	*8(6)*	*3(1)*	*0.0377*	*356.576*	*30.635*	*11*

1S	*2.62(2)*	*6(2)*					
1Im 0°	*2.07(2)*	*3(2)*					
1Im 10°	*2.02(6)*	*6(5)*					
1N/O	*2.06(3)*	*1(2)*					
2N/O	*2.15(4)*	*9(7)*					
1S	*2.62(2)*	*6(2)*					
1Im 5°	*2.07(3)*	*3(3)*					
1Im 10°	*2.05(8)*	*7(7)*	*4(1)*	*0.0441*	*417.198*	*35.843*	*11*

Table S2. Additional Fits for Co(II) WT-RcnR in Buffer with 20 mM Hepes, 300 mM NaBr and 10 % Glycerol at pH 7.0.

Fourier-transform window: k = 2 - 12.5 Å$^{-1.}$ Data range fit: r = 1- 4 Å.

N	r (Å)	σ^2 (x10^{-3} Å^2)	ΔE_0 (eV)	R factor	χ^2	Red χ^2	nvar
5N/O	2.10(2)	12(2)	1(2)	0.2092	453.594	27.003	3
4N/O	2.04(2)	8(2)					
1N/O	2.18(2)	1(1)	-2(2)	0.1457	315.975	21.353	5
3N/O	2.01(2)	5(2)					
2N/O	2.16(2)	2(1)	-2(2)	0.1577	341.980	23.110	5
5N/O	2.01(4)	15(3)					
1S	2.28(2)	6(2)	-8(4)	0.1582	342.931	23.174	5
5N/O	2.07(3)	15(3)					
1Im	2.13(4)	6(4)	0(2)	0.1498	300.393	20.300	5
4N/O	2.06(3)	18(4)					
1Im	2.02(1)	1(1)					
1Im	2.16(1)	2(1)	-1(1)	0.0635	137.746	10.763	7
3N/O	2.07(3)	16(5)					
1Im	1.93(4)	2(5)					
1Im	2.04(2)	3(3)					
1Im	2.17(2)	4(2)	-3(1)	0.0500	108.393	10.038	9
4N/O	2.03(7)	22(6)					
1S	2.28(2)	5(2)					
1Im 0°	2.00(2)	4(2)	-7(3)	0.0952	206.426	16.130	7
3N/O	2.08(6)	21(10)					
1S	2.29(4)	13(7)					
1Im 0°	2.00(2)	0(2)					
1Im 0°	2.15(2)	1(2)	-2(2)	0.0631	136.739	12.664	9
3N/O	2.08(2)	8(2)					
1S	2.74(7)	20(12)					
1Im 0°	1.58(4)	16(5)					
1Im 5°	2.20(2)	1(2)	5(2)	5(2)	172.275	15.955	9
3N/O	2.04(6)	14(7)					
1S	2.29(5)	14(10)					
1Im 0°	2.01(4)	6(4)					
1Im 10°	2.15(3)	2(2)	-4(3)	0.0795	174.012	16.115	9
3N/O	2.05(6)	15(7)	-4(3)	0.0785	170.090	15.752	9

1S	2.29(5)	13(9)					
1Im 5°	2.01(3)	5(3)					
1Im 10°	2.15(3)	2(2)					
2N/O	2.08(6)	18(11)					
1S	2.31(3)	12(6)					
1Im 0°	2.01(3)	4(2)					
1Im 0°	2.14(3)	4(2)					
1Im 0°	1.90(4)	2(4)	-5(2)	0.0416	90.239	10.257	11
2N/O	2.07(8)	20(13)					
1S	2.31(4)	13(7)					
1Im 0°	1.94(5)	3(6)					
1Im 0°	2.16(3)	3(2)					
1Im 5°	2.03(4)	2(3)	-4(2)	0.0467	101.334	11.518	11
2N/O	2.00(5)	11(7)					
1S	2.35(0.15)	33(33)					
1Im 0°	2.01(3)	1(2)					
1Im 0°	2.17(2)	1(2)					
1Im 10°	2.13(3)	3(3)	-2(2)	0.047	101.817	11.573	11
2N/O	2.09(9)	24(18)					
1S	2.30(3)	10(5)					
1Im 0°	2.15(3)	3(2)					
1Im 5°	1.92(5)	3(6)					
1Im 5°	2.02(3)	3(3)	-4(2)	0.0459	99.588	11.320	11
2N/O	2.00(5)	11(6)					
1S	2.35(0.15)	33(33)					
1Im 10°	2.01(3)	0(2)					
1Im 5°	2.17(2)	1(2)					
1Im 5°	2.12(4)	3(3)	-2(2)	0.0445	96.586	10.978	11
2N/O	1.94(3)	5(3)					
1S	2.38(7)	21(14)					
1Im 0°	2.13(4)	6(4)					
1Im 10°	2.15(2)	5(1)					
1Im 10°	2.02(2)	4(2)	-3(2)	0.039	84.593	9.615	11
2N/O	1.94(3)	5(2)					
1S	2.38(7)	22(14)					
1Im 5°	2.14(4)	5(4)					
1Im 10°	2.15(2)	5(1)					
1Im 10°	2.02(2)	4(2)	-3(2)	0.0392	84.893	9.649	11
2N/O	2.01(5)	11(7)					
1S	2.33(0.13)	31(28)					
1Im 0°	2.16(3)	0(2)					
1Im 5°	2.01(2)	0(2)	-2(2)	0.0454	98.399	11.184	11

1Im 10°	2.14(3)	3(2)					
2N/O	2.01(5)	9(9)					
1N/O	2.17(3)	0(3)					
1S	2.22(0.11)	23(25)					
1Im 0°	2.15(3)	0(3)					
1Im 0°	2.01(3)	0(2)	-2(2)	0.0454	98.491	11.195	11
1N/O							
2N/O							
1S							
1Im 0°							
1Im 0°			No Fit	No Fit	No Fit	No Fit	11
2N/O	1.96(3)	7(4)					
1N/O	2.16(2)	0(2)					
1S	1.85(9)	35(28)					
1Im 0°	2.16(2)	1(2)					
1Im 5°	2.02(2)	2(1)	-1(1)	0.0347	75.261	8.554	11
1N/O	1.95(4)	3(5)					
2N/O	2.16(5)	3(3)					
1S	2.20(8)	14(14)					
1Im 0°	2.15(2)	1(2)					
1Im 5°	2.02(3)	1(2)	-2(2)	0.039	84.536	9.609	11
2N/O	1.99(2)	6(3)					
1N/O	2.20(1)	2(1)					
1S	2.20(5)	18(10)					
1Im 0°	2.08(3)	4(3)					
1Im 10°	2.08(2)	1(2)	-3(2)	0.0304	65.943	7.495	11
1N/O	**1.97(4)**	**2(3)**					
2N/O	**2.20(4)**	**0(2)**					
1S	**2.20(6)**	**5(6)**					
1Im 0°	**2.09(4)**	**4(3)**					
1Im 10°	**2.09(3)**	**2(3)**	**-2(2)**	**0.0405**	**87.704**	**9.969**	**11**
2N/O	1.99(3)	6(3)					
1N/O	2.20(1)	2(1)					
1S	2.20(5)	18(11)					
1Im 5°	2.09(3)	4(3)					
1Im 10°	2.08(3)	1(2)	-3(2)	0.0317	68.823	7.823	11
1N/O	*1.97(4)*	*2(3)*					
2N/O	*2.20(4)*	*0(2)*					
1S	*2.20(6)*	*5(6)*					
1Im 5°	*2.09(4)*	*4(3)*					
1Im 10°	*2.09(3)*	*2(3)*	*-2(2)*	*0.0417*	*90.515*	*10.288*	*11*

1N/O							
1N/O							
1S							
1Im 0°							
1Im 0°							
1Im 5°			No Fit	No Fit	No Fit	No Fit	13
1N/O	1.98(4)	2(4)					
1N/O	2.19(2)	2(2)					
1S	2.22(6)	15(10)					
1Im 0°	2.09(5)	4(5)					
1Im 0°	1.96(0.13)	12(17)					
1Im 10°	2.08(3)	2(3)	-4(2)	0.0305	66.103	9.724	13
1N/O							
1N/O							
1S							
1Im 0°							
1Im 5°							
1Im 5°			No Fit	No Fit	No Fit	No Fit	13
1N/O	1.98(4)	2(4)					
1N/O	2.19(2)	2(2)					
1S	2.22(6)	15(9)					
1Im 10°	2.10(5)	3(5)					
1Im 5°	1.97(0.14)	12(18)					
1Im 5°	2.08(3)	2(3)	-4(2)	0.0314	68.037	10.009	13
1N/O	1.99(3)	2(4)					
1N/O	2.19(2)	3(1)					
1S	2.22(4)	15(9)					
1Im 0°	2.07(3)	3(3)					
1Im 10°	2.07(3)	1(2)					
1Im 10°	1.91(5)	6(6)	-5(2)	0.0266	57.620	8.476	13
1N/O	1.99(4)	2(4)					
1N/O	2.19(2)	3(1)					
1S	2.22(5)	15(9)					
1Im 5°	2.08(3)	2(3)					
1Im 10°	2.07(3)	0(2)					
1Im 10°	1.91(5)	6(6)	-5(2)	0.028	60.666	8.924	13
1N/O	1.98(4)	1(4)					
1N/O	2.19(2)	2(2)					
1S	2.23(6)	16(11)					
1Im 0°	2.08(4)	3(4)					
1Im 5°	1.92(8)	9(9)					
1Im 10°	2.08(3)	1(2)	-4(2)	0.0293	63.571	9.352	13

Table S3. Additional Fits for Zn(II) WT-RcnR in Buffer with 20 mM Hepes, 300 mM NaBr and 10 % Glycerol at pH 7.0.

Fourier-transform window: k = 2 - 12.5 Å$^{-1..}$ Data range fit: r = 1- 4 Å.

N	r (Å)	σ^2 (x10^{-3} Å^2)	ΔE_0 (eV)	R factor	χ^2	Red χ^2	nvar
3N/O	2.16(2)	3(2)	11(0)	0.4315	8845.087	526.561	3
4N/O	2.14(3)	5(2)	9(3)	0.4366	8950.887	532.859	3
2N/O	2.08(2)	1(2)					
1N/O	2.21(2)	6(2)	8(3)	0.2987	6123.046	413.779	5
3N/O	2.06(4)	6(3)					
1S	2.31(2)	0(1)	1(4)	0.1646	3374.422	228.035	5
3N/O	2.08(3)	5(2)					
1Br	2.43(2)	4(1)	1(4)	0.1393	2855.550	192.971	5
3N/O	2.01(7)	11(4)					
1S	2.24(6)	4(3)					
1Br	2.41(2)	5(2)	-7(8)	0.0837	1716.114	134.094	7
4N/O	2.09(4)	9(4)					
1Im	2.20(3)	1(3)	4(4)	0.3746	7678.663	518.904	5
3N/O	2.05(6)	12(8)					
1Im	2.22(3)	5(2)					
1Im	2.09(3)	5(3)	1(3)	0.3018	6187.927	483.513	7
2N/O	2.11(5)	4(6)					
1Im	2.21(2)	10(2)					
1Im	2.08(2)	11(2)					
1Im	1.96(3)	8(3)	-1(3)	0.2126	4358.762	403.669	9
2N/O	1.99(4)	7(4)					
1S	2.30(1)	1(1)					
1Im	2.06(2)	1(2)	-1(3)	0.0879	1811.714	141.564	7
1N/O	2.00(2)	2(2)					
1S	2.29(1)	2(1)					
1Im	2.05(2)	3(1)					
1Im	1.89(3)	0(3)	-5(2)	0.0616	1262.334	116.906	9
0N/O							
1S	2.29(1)	0(1)					
1Im	1.92(3)	4(3)					
1Im	2.16(4)	4(4)					
1Im	2.04(2)	7(3)	-2(2)	0.0641	1314.055	121.696	9

1N/O	1.95(2)	3(2)					
1S	2.29(2)	2(1)					
1Br	2.42(1)	7(2)					
1Im	2.05(2)	0(1)	-4(2)	0.0226	464.225	42.992	9
0N/O							
1S	2.29(2)	4(2)					
1Br	2.41(1)	5(1)					
1Im	2.07(2)	2(1)					
1Im	1.95(2)	0(2)	-5(1)	0.0163	333.354	30.872	9
3N/O	2.01(6)	15(7)					
1S	2.30(1)	0(1)					
1Im	2.05(2)	0(2)	-2(3)	0.1034	2118.990	165.574	7
2N/O	2.47(1)	1(1)					
1S	2.29(2)	3(2)					
1Im	1.94(2)	1(2)					
1Im	2.07(2)	3(1)	-6(2)	0.0265	544.224	50.401	9
1N/O	1.99(3)	0(4)					
1S	2.28(1)	1(1)					
1Im	2.47(3)	2(4)					
1Im	2.04(2)	3(1)					
1Im	1.88(3)	1(3)	-7(2)	0.0413	846.293	96.193	11
2N/O	1.98(4)	10(4)					
1S	2.29(2)	3(2)					
1Br	2.41(1)	6(1)					
1Im 0°	2.05(2)	1(1)	-4(2)	0.0277	568.128	52.615	9
1N/O	1.94(4)	10(6)					
1S	2.30(2)	5(2)					
1Br	2.41(1)	5(1)					
1Im 0°	1.97(2)	1(3)					
1Im 0°	2.08(2)	1(2)	-4(1)	0.0114	234.559	26.661	11
1N/O	**1.94(3)**	**7(4)**					
1S	**2.30(2)**	**7(3)**					
1Br	**2.41(1)**	**5(1)**					
1Im 0°	**1.99(2)**	**0(3)**					
1Im 5°	**2.10(2)**	**1(2)**	**-4(1)**	**0.0117**	**240.469**	**27.333**	**11**
1N/O	1.93(2)	1(1)					
1S	2.29(2)	6(3)					
1Br	2.42(1)	5(1)					
1Im 0°	2.05(1)	0(1)					
1Im 10°	2.11(3)	3(2)	-3(1)	0.0102	208.695	23.721	11
1N/O	1.94(2)	1(1)	-3(1)	0.0139	285.062	32.401	11

1S	*2.29(2)*	*7(3)*					
1Br	*2.42(1)*	*5(1)*					
1Im 5°	*2.06(1)*	*0(1)*					
1Im 10°	*2.12(3)*	*2(3)*					
0N/O							
1S	2.29(2)	5(2)					
1Br	2.41(1)	5(1)					
1Im	2.08(4)	0(4)					
1Im	1.97(9)	3(9)					
1Im	1.99(0.26)	12(23)	-5(2)	0.0126	257.385	29.255	11
0N/O							
1S	*2.18(3)*	*3(3)*					
1Br	*2.39(2)*	*3(1)*					
1Im 0°	*2.33(4)*	*1(4)*					
1Im 5°	*1.05(6)*	*7(6)*					
1Im 10°	*1.90(5)*	*5(4)*	*-19(4)*	*0.0451*	*925.059*	*105.146*	*11*

Table S4. Additional Fits for Ni(II) E34A-RcnR in Buffer with 20 mM Hepes, 300 mM NaBr and 10 % Glycerol at pH 7.0.

Fourier-transform window: k = 2 - 12.5 Å^{-1}. Data range fit: r = 1- 4 Å.

N	r (Å)	σ^2 (x10^{-3} Å^2)	ΔE_0 (eV)	R factor	χ^2	Red χ^2	nvar
6N/O	2.08(2)	3(1)	5(3)	0.2457	1552.706	92.435	3
5N/O	2.12(2)	1(2)					
1N/O	2.00(2)	6(2)	6(3)	0.2146	1356.183	91.647	5
4N/O	2.05(2)	2(2)					
2N/O	2.18(2)	3(2)	5(3)	0.2199	1389.823	93.921	5
5N/O	2.05(3)	2(2)					
1S	2.29(4)	2(4)	1(4)	0.2388	1509.005	101.975	5
6N/O	2.07(3)	4(2)					
1S	2.26(7)	6(10)	2(4)	0.2442	1542.976	104.270	5
5N/O	2.09(2)	2(2)					
1Im	2.00(0.13)	6(16)	4(3)	0.2492	1574.932	106.430	5
4N/O	2.09(3)	1(3)					
1Im	2.02(7)	1(5)					
1Im	2.19(7)	1(6)	6(3)	0.2596	1640.476	128.184	7
3N/O	2.08(3)	1(3)					
1Im	2.04(8)	7(7)					
1Im	1.92(9)	2(10)					
1Im	2.18(7)	6(5)	5(5)	0.2610	1649.528	152.764	9
4N/O	2.11(2)	1(1)					
1S	2.64(2)	2(1)					
1Im	2.00(2)	2(1)	7(2)	0.0958	605.087	47.280	7
3N/O	2.09(1)	2(1)					
1S	2.65(1)	2(1)					
1Im	2.18(3)	3(2)					
1Im	1.99(1)	2(1)	8(2)	0.0886	560.134	51.875	9
2N/O	2.10(1)	5(1)					
1S	2.65(1)	4(1)					
1Im	2.00(3)	9(3)					
1Im	2.27(3)	11(2)					
1Im	2.14(1)	4(1)	10(2)	0.0729	460.634	52.358	11

3N/O	2.13(2)	3(2)					
1N/O	2.01(2)	6(3)					
1S	2.64(2)	1(2)					
1Im	2.03(2)	0(2)	7(2)	0.0906	572.708	53.039	9
2N/O	2.05(2)	4(2)					
2N/O	2.17(2)	4(3)					
1S	2.64(2)	1(2)					
1Im	2.03(2)	1(2)	7(2)	0.0821	518.688	48.036	9
1N/O	2.02(3)	5(3)					
3N/O	2.14(2)	2(3)					
1S	2.64(2)	1(2)					
1Im	2.02(2)	1(2)	6(2)	0.0834	527.062	48.812	9
2N/O	2.08(1)	10(1)					
1N/O	2.23(2)	12(2)					
1S	2.60(2)	3(2)					
1Im	1.94(2)	8(1)					
1Im	2.11(2)	3(2)	7(1)	0.0354	223.731	25.300	11
1N/O	2.04(1)	13(1)					
2N/O	2.19(2)	9(2)					
1S	2.60(2)	3(2)					
1Im	1.94(2)	9(1)					
1Im	2.10(2)	3(2)	7(1)	0.0319	201.818	22.939	11
1N/O							
1N/O							
1S							
1Im							
1Im							
1Im			No Fit	No Fit	No Fit	No Fit	13
5N/O	2.10(1)	1(1)					
1S	2.64(1)	1(1)					
1Im	2.00(4)	1(4)	6(2)	0.0834	526.817	41.164	7
4N/O	2.10(1)	1(1)					
1S	2.64(1)	2(1)					
1Im	2.19(5)	1(6)					
1Im	1.99(3)	2(3)	7(2)	0.0790	499.166	46.228	9
3N/O	2.10(1)	3(1)					
1S	2.65(1)	3(1)					
1Im	2.15(4)	9(2)					
1Im	2.29(4)	7(3)					
1Im	2.00(3)	7(2)	9(2)	0.0677	427.865	48.633	11
3N/O	2.09(1)	7(1)	7(1)	0.0355	224.452	25.512	9

1N/O	2.26(2)	10(2)					
1S	2.61(2)	3(2)					
1Im	2.11(2)	6(2)					
1Im	1.95(2)	8(1)					
2N/O	**2.07(1)**	**9(1)**					
2N/O	**2.22(2)**	**7(2)**					
1S	**2.61(2)**	**3(1)**					
1Im	**1.94(2)**	**8(1)**					
1Im	**2.11(2)**	**7(1)**	**7(1)**	**0.0324**	**204.827**	**23.281**	**9**
1N/O	2.04(2)	11(1)					
3N/O	2.19(2)	4(2)					
1S	2.61(2)	3(1)					
1Im	2.10(2)	7(1)					
1Im	1.94(2)	9(1)	7(1)	0.0330	208.709	23.723	9
2N/O	2.17(2)	9(3)					
1N/O	2.03(2)	13(2)					
1S	2.61(3)	2(3)					
1Im	2.10(3)	10(2)					
1Im	1.94(3)	10(2)					
1Im	2.25(5)	5(4)	7(2)	0.0444	280.274	41.230	11
1N/O	2.04(2)	13(1)					
2N/O	2.19(2)	9(2)					
1S	2.60(2)	4(2)					
1Im	2.10(2)	9(1)					
1Im	2.63(0.12)	6(17)					
1Im	1.94(2)	10(1)	6(2)	0.0294	185.958	27.355	11
0N/O							
3N/O	2.10(1)	3(1)					
1S	2.64(2)	3(1)					
1Im	2.29(4)	7(3)					
1Im	2.15(4)	9(3)					
1Im	2.00(3)	7(2)	8(2)	0.0782	494.166	56.169	11
4N/O	2.11(2)	1(2)					
2S	2.65(2)	3(1)					
1Im	2.04(4)	0(3)	8(2)	0.1036	654.627	51.151	7
3N/O	2.10(2)	1(2)					
2S	2.65(2)	2(2)					
1Im	2.20(4)	2(3)					
1Im	2.03(4)	2(2)	9(2)	0.0963	608.280	56.333	9
2N/O							
2S							
1Im			No Fit	No Fit	No Fit	No Fit	11

1Im							
1Im							
4N/O	2.08(3)	4(2)					
1S	2.62(3)	4(2)					
1Br	2.17(6)	4(5)					
1Im	1.95(3)	5(2)	5(3)	0.0777	491.244	45.495	9
3N/O	2.09(2)	8(1)					
1S	2.62(2)	6(1)					
1Br	2.19(3)	2(2)					
1Im	2.12(2)	7(1)					
1Im	1.96(2)	9(1)	6(1)	0.0326	206.273	23.446	11
2N/O	2.05(2)	9(2)					
1S	2.50(5)	14(4)					
1Br	2.44(4)	11(3)					
1Im	1.92(4)	8(3)					
1Im	2.25(6)	7(6)					
1Im	2.08(5)	10(5)	5(3)	0.0439	277.505	40.823	13
2N/O	2.06(2)	11(2)					
1N/O	2.16(2)	1(2)					
1S	2.63(2)	6(1)					
1Br	2.21(3)	3(2)					
1Im	2.13(4)	5(3)					
1Im	1.96(3)	8(2)	6(1)	0.0232	146.547	21.558	13
1N/O	2.03(2)	14(2)					
2N/O	2.15(2)	13(2)					
1S	2.63(2)	7(1)					
1Br	2.22(2)	4(2)					
1Im	1.95(3)	8(2)					
1Im	2.10(3)	7(3)	6(1)	0.0245	155.001	22.802	13

Table S5. Additional Fits for Co(II) E34A-RcnR in Buffer with 20 mM Hepes, 300 mM NaBr and 10 % Glycerol at pH 7.0.

Fourier-transform window: k = 2 - 12.5 Å^{-1}. Data range fit: r = 1- 4 Å.

N	r (Å)	σ^2 (x10^{-3} Å^2)	ΔE_0 (eV)	R factor	χ^2	Red χ^2	nvar
5N/O	2.11(1)	7(1)	-1(2)	0.1055	350.133	20.844	3
2N/O	2.03(1)	1(1)					
2N/O	2.17(1)	1(1)	-3(2)	0.0867	287.478	19.427	5
3N/O	2.05(2)	3(1)					
2N/O	2.18(2)	1(2)	-3(2)	0.0879	291.440	19.695	5
4N/O	2.11(2)	5(1)					
1S	2.55(0.19)	29(31)	-1(3)	0.1201	398.413	26.924	5
4N/O	2.11(1)	5(1)					
2S	2.56(0.13)	34(21)	-1(2)	0.1125	373.266	25.224	5
4N/O	2.12(1)	5(1)					
1Im	2.01(3)	3(2)	-2(2)	0.0878	291.265	19.683	5
3N/O	2.11(1)	3(1)					
1Im	2.00(2)	0(1)					
1Im	2.18(3)	1(2)	-2(1)	0.0577	191.260	14.945	7
2N/O	2.11(1)	1(1)					
1Im	2.24(5)	0(8)					
1Im	2.13(5)	2(7)					
1Im	1.99(3)	2(3)	-1(2)	0.0635	210.774	19.520	9
3N/O	2.10(2)	3(1)					
1S	2.37(6)	15(9)					
1Im	1.98(3)	2(2)	-5(3)	0.0986	326.951	25.547	7
2N/O	2.10(1)	1(1)					
1S	2.54(0.10)	25(16)					
1Im	2.01(2)	1(1)					
1Im	2.18(2)	1(2)	-2(2)	0.0609	202.055	18.713	9
1N/O	2.10(2)	2(2)					
1S	2.57(0.12)	22(18)					
1Im	1.98(3)	5(3)					
1Im	2.23(3)	5(3)					
1Im	2.11(4)	7(3)	-1(2)	0.0797	264.283	30.040	11
3N/O	2.12(2)	4(2)	-2(3)	0.1152	382.136	29.859	7

1Br	2.47(7)	18(8)					
1Im	2.03(4)	3(3)					
2N/O	2.10(2)	1(2)					
1Br	2.36(0.26)	34(41)					
1Im	2.01(2)	1(2)					
1Im	2.18(3)	1(2)	-2(2)	0.0790	261.935	24.258	9
1N/O							
1Br							
1Im							
1Im							
1Im			No Fit	No Fit	No Fit	No Fit	11
4N/O	2.11(2)	7(2)					
1Br	2.87(3)	12(4)					
1Im	2.08(6)	7(8)	-3(2)	0.0626	207.807	16.238	7
3N/O	2.11(1)	5(2)					
1Br	2.86(3)	12(4)					
1Im	2.18(2)	0(2)					
1Im	2.02(2)	0(2)	-3(1)	0.0405	134.237	12.432	9
2N/O	2.11(2)	3(2)					
1Br	2.85(4)	12(4)					
1Im	2.26(5)	1(6)					
1Im	2.15(3)	4(4)					
1Im	2.01(3)	3(2)	-1(2)	0.043	142.526	16.200	11
4N/O	2.11(2)	7(2)					
1Br	2.68(5)	15(8)					
1Im	2.12(8)	9(10)	-1(2)	0.0747	247.876	19.369	7
3N/O	2.11(1)	3(1)					
1Br	2.63(6)	20(10)					
1Im	2.01(2)	1(1)					
1Im	2.19(2)	0(2)	-1(1)	0.0411	136.363	12.629	9
2N/O	2.11(1)	1(1)					
1Br	2.66(5)	14(7)					
1Im	2.27(4)	3(3)					
1Im	2.01(3)	3(2)					
1Im	2.14(3)	5(3)	1(2)	0.0445	147.625	16.780	11
3N/O	2.06(1)	3(1)					
2N/O	2.19(2)	1(2)					
1S	2.69(5)	15(7)	-1(1)	0.0659	218.642	17.084	7
3N/O	2.05(1)	3(1)					
2N/O	2.18(2)	1(2)	-(2)	0.0641	212.709	16.621	7

1Br	2.88(3)	12(3)					
2N/O	*2.09(1)*	*1(1)*					
1Br	*2.47(4)*	*4(4)*					
1S	*2.51(4)*	*1(5)*					
1Im	*2.16(2)*	*1(1)*					
1Im	*2.00(2)*	*1(1)*	*-2(1)*	*0.0283*	*93.823*	*10.664*	*11*
1N/O	**2.02(1)**	**5(1)**					
1N/O	**2.16(1)**	**6(1)**					
1Br	**2.50(3)**	**3(3)**					
1S	**2.54(4)**	**1(4)**					
1Im	**2.02(7)**	**6(9)**					
1Im	**2.16(8)**	**6(11)**	**-2(2)**	**0.017**	**56.437**	**8.302**	**13**

Table S6. Additional Fits for Zn(II) E34A-RcnR in Buffer with 20 mM Hepes, 300 mM NaBr and 10 % Glycerol at pH 7.0.

Fourier-transform window: k = 2 - 12.5 Å^{-1}. Data range fit: r = 1- 4 Å.

N	r (Å)	σ^2 (x10^{-3} Å^2)	ΔE_0 (eV)	R factor	χ^2	Red χ^2	nvar
3N/O	2.12(3)	5(2)	9(4)	0.4437	7115.043	423.569	3
4N/O	2.11(3)	7(2)	7(4)	0.4189	6717.437	399.899	3
2N/O	2.05(2)	1(2)					
1N/O	2.19(2)	5(1)	6(3)	0.2835	4546.172	307.218	5
3N/O	2.03(2)	4(2)					
1S	2.30(2)	1(1)	0(3)	0.1607	2576.731	174.129	5
3N/O	2.05(2)	5(1)					
1Br	2.42(2)	5(1)	-1(3)	0.1359	2178.544	147.220	5
3N/O	2.02(4)	7(3)					
1S	2.25(7)	7(5)					
1Br	2.42(2)	6(2)	-4(5)	0.0912	1461.919	114.232	7
3N/O	2.04(5)	9(7)					
1Im	2.04(4)	2(3)					
1Im	2.18(3)	4(2)	2(3)	0.2829	4535.757	354.416	7
2N/O	2.04(6)	6(7)					
1Im	2.04(4)	2(4)					
1Im	2.18(3)	4(2)	3(3)	0.2898	4645.917	363.101	7
2N/O	2.00(3)	3(2)					
1S	2.30(1)	1(1)					
1Im	2.07(3)	1(3)	-1(2)	0.0969	1554.363	121.455	7
1N/O	1.99(2)	3(2)					
1S	2.29(1)	0(1)					
1Im	1.92(4)	1(3)					
1Im	2.08(3)	2(2)	-3(2)	0.0677	1085.818	100.559	9
0N/O							
1S	2.28(2)	2(2)					
1Im	2.20(3)	6(3)					
1Im	2.07(3)	8(2)					
1Im	1.94(2)	6(2)	0(2)	0.0888	1424.699	131.943	9
1N/O	*1.97(2)*	*0(2)*	*-3(2)*	*0.0314*	*503.492*	*46.629*	*9*

1S	*2.28(2)*	*3(1)*					
1Br	*2.43(2)*	*8(2)*					
1Im	*2.06(2)*	*1(2)*					
0N/O							
1S							
1Br							
1Im							
1Im			No Fit	No Fit	No Fit	No Fit	9
3N/O	2.01(5)	12(5)					
1S	2.30(2)	1(1)					
1Im	2.04(3)	1(2)	-2(3)	0.1236	1981.261	154.812	7
2N/O	2.01(3)	3(2)					
1S	2.31(2)	0(1)					
1Im	2.39(0.18)	14(24)					
1Im	2.09(4)	1(3)	1(3)	0.0879	1410.000	130.582	9
1N/O	1.98(2)	2(3)					
1S	2.28(2)	0(2)					
1Im	1.90(5)	2(4)					
1Im	2.49(4)	2(5)					
1Im	2.06(3)	1(2)	-6(3)	0.0525	842.548	95.767	11
2N/O	*1.99(4)*	*7(6)*					
1S	*2.28(3)*	*5(3)*					
1Br	*2.42(1)*	*7(1)*					
1Im	*2.04(3)*	*2(2)*	*-3(1)*	*0.0411*	*659.846*	*61.109*	*9*
1N/O	**1.98(4)**	**7(6)**					
1S	**2.28(3)**	**9(4)**					
1Br	**2.43(1)**	**6(1)**					
1Im	**2.11(2)**	**2(2)**					
1Im	**1.98(2)**	**1(2)**	**-3(1)**	**0.0193**	**310.138**	**35.252**	**11**
0N/O							
1S	*2.26(2)*	*8(3)*					
1Br	*2.43(1)*	*6(1)*					
1Im	*1.95(2)*	*4(2)*					
1Im	*2.07(2)*	*6(3)*					
1Im	*2.19(3)*	*3(4)*	*-1(1)*	*0.0236*	*378.924*	*43.070*	*11*

Table S7. Additional Fits for Ni(II) E34C-RcnR in Buffer with 20 mM Hepes, 300 mM NaBr and 10 % Glycerol at pH 7.0.

Fourier-transform window: k = 2 - 12.5 Å^{-1}. Data range fit: r = 1- 4 Å.

N	r (Å)	σ^2 (x10^{-3} Å^2)	ΔE_0 (eV)	R factor	χ^2	Red χ^2	nvar
3N/O	2.08(1)	3(1)	6(2)	0.1438	1888.576	112.430	3
2N/O	2.03(1)	1(1)					
1N/O	2.16(1)	4(1)	5(2)	0.1028	1350.516	91.264	5
3N/O	2.04(3)	6(2)					
1S	2.26(3)	6(3)	-1(3)	0.1177	1545.655	104.451	5
3N/O	2.08(1)	4(1)					
1Br	2.42(3)	12(3)	5(2)	0.1003	1317.964	89.065	5
4N/O	2.08(2)	8(2)					
1Im	2.08(3)	4(4)	5(1)	0.0787	1033.763	69.859	5
3N/O	2.08(2)	5(2)					
1Im	2.12(4)	2(3)					
1Im	1.98(4)	5(5)	3(2)	0.0662	868.828	67.889	7
3N/O	2.08(1)	5(2)					
1S	2.67(3)	10(4)					
1Im	2.10(3)	4(4)	6(1)	0.0536	704.259	55.029	7
2N/O	2.07(2)	3(2)					
1S	2.66(3)	11(4)					
1Im	2.16(2)	1(2)					
1Im	2.01(2)	0(2)	5(1)	0.0507	666.220	61.699	9
1N/O	2.04(3)	0(2)					
1S	2.29(3)	8(5)					
1Im	1.84(4)	1(3)					
1Im	1.97(3)	6(2)					
1Im	2.10(3)	5(2)	-3(2)	0.0567	745.026	84.683	11
2N/O	2.07(3)	3(3)					
2S	2.25(3)	12(4)					
1Im	1.97(6)	6(6)	-2(3)	0.0928	1219.001	95.250	7
1N/O	2.05(5)	2(4)					
2S	2.25(2)	9(3)					
1Im	1.86(6)	7(8)					
1Im	2.00(5)	3(5)	-5(3)	0.0788	1035.529	95.901	9

0N/O							
2S	2.26(2)	9(3)					
1Im	1.95(3)	5(3)					
1Im	2.08(3)	5(3)					
1Im	1.83(4)	0(4)	-5(2)	0.0945	1240.673	114.900	9
1N/O	**2.04(2)**	**1(2)**					
1S	**2.29(2)**	**3(2)**					
1S	**2.56(3)**	**9(3)**					
1Im	**1.94(3)**	**2(3)**					
1Im	**2.08(3)**	**1(2)**	**0(2)**	**0.0253**	**284.442**	**32.331**	**11**
2N/O	2.07(3)	5(2)					
1S	2.29(3)	8(4)					
1S	2.59(3)	10(3)					
1Im	1.98(9)	9(12)					
1Im	2.07(6)	4(6)	1(2)	0.0246	322.621	36.670	11
3N/O	2.09(3)	9(4)					
1S	2.27(3)	9(5)					
1S	2.61(3)	10(4)					
1Im	2.05(2)	4(2)	2(1)	0.0308	405.004	37.508	9
4N/O	2.08(1)	8(2)					
1S	2.67(2)	10(3)					
1Im	2.10(2)	4(3)	5(1)	0.0461	605.016	47.275	7
3N/O	2.07(1)	6(2)					
1S	2.66(3)	10(4)					
1Im	2.01(4)	4(4)					
1Im	2.14(3)	2(3)	5(1)	0.0457	599.699	55.539	9
2N/O	2.07(2)	3(2)					
1S	2.64(5)	16(8)					
1Im	2.02(2)	4(3)					
1Im	1.90(3)	2(5)					
1Im	2.15(2)	4(2)	2(1)	0.0451	592.877	67.389	11

Table S8. Additional Fits for Co(II) E34C-RcnR in Buffer with 20 mM Hepes, 300 mM NaBr and 10 % Glycerol at pH 7.0.

Fourier-transform window: k = 2 - 12.5 Å$^{-1..}$ Data range fit: r = 1- 4 Å.

N	r (Å)	σ^2 (x10^{-3} Å^2)	ΔE_0 (eV)	R factor	χ^2	Red χ^2	nvar
4N/O	2.13(2)	6(1)	2(2)	0.1818	824.120	49.061	3
2N/O	2.02(1)	1(1)					
2N/O	2.16(1)	2(1)	-2(1)	0.0654	296.676	20.049	5
4N/O	2.02(3)	9(2)					
1S	2.28(1)	2(1)	-11(3)	0.1024	464.391	31.382	5
3N/O	2.14(1)	1(1)					
1Im	2.00(2)	0(1)	-1(2)	0.1369	620.466	41.929	5
2N/O	2.13(2)	2(2)					
1Im	2.15(2)	2(2)					
1Im	2.00(1)	2(1)	-1(2)	0.0794	359.777	28.112	7
1N/O	2.13(2)	2(2)					
1Im	2.20(3)	5(3)					
1Im	2.07(3)	6(4)					
1Im	1.96(3)	4(3)	-2(2)	0.0944	428.079	39.645	9
4N/O	2.13(2)	7(3)					
1S	2.71(7)	16(11)					
1Im	2.12(0.11)	10(13)	1(2)	0.1332	604.007	47.196	7
3N/O	2.12(2)	5(2)					
1S	2.65(7)	20(12)					
1Im	2.00(2)	1(1)					
1Im	2.16(2)	1(1)	-1(1)	0.0569	258.112	23.904	9
2N/O	2.12(2)	2(2)					
1S	2.43(0.17)	34(39)					
1Im	2.03(6)	3(7)					
1Im	1.95(7)	1(10)					
1Im	2.17(4)	3(4)	-3(2)	0.0568	257.417	29.259	11
4N/O	2.13(1)	3(1)					
1Br	3.03(3)	10(4)					
1Im	1.97(2)	1(1)	-2(2)	0.1071	485.416	37.930	7
3N/O	2.13(2)	5(2)					
1Br	2.40(4)	16(5)					
1Im	1.99(2)	1(1)	-1(1)	0.0491	222.727	20.627	9

1Im	2.16(2)	1(2)					
2N/O	2.13(2)	2(2)					
1Br	2.79(7)	17(9)					
1Im	2.06(8)	1(25)					
1Im	1.97(0.14)	1(13)					
1Im	2.18(6)	2(9)	-2(2)	0.0570	258.242	29.353	11
3N/O	2.12(2)	3(2)					
2S	2.28(4)	15(7)					
1Im	1.97(2)	1(2)	-7(4)	0.1138	515.725	40.298	7
2N/O	2.13(2)	2(2)					
2S	2.48(0.13)	42(22)					
1Im	1.99(2)	2(1)					
1Im	2.15(2)	2(2)	-2(2)	0.0658	298.453	27.640	9
1N/O	2.13(2)	2(2)					
2S	2.43(9)	32(17)					
1Im	1.94(3)	3(4)					
1Im	2.05(4)	6(4)					
1Im	2.18(3)	5(3)	-4(2)	0.0694	314.657	35.765	11
2N/O	*2.09(3)*	*6(3)*					
1S	*2.31(2)*	*3(2)*					
1S	*2.55(3)*	*8(3)*					
1Im	*2.12(2)*	*1(2)*					
1Im	*1.97(2)*	*0(1)*	*-5(1)*	*0.0221*	*100.026*	*11.369*	*11*
2N/O	2.13(2)	2(2)					
1S	2.31(4)	10(7)					
1Br	2.74(5)	13(4)					
1Im	2.11(3)	1(3)					
1Im	1.97(2)	2(1)	-4(2)	0.0545	247.205	28.098	11
1N/O	**1.99(3)**	**1(3)**					
1N/O	**2.14(2)**	**4(2)**					
1S	**2.36(4)**	**7(4)**					
1S	**2.61(4)**	**8(4)**					
1Im	**2.17(4)**	**1(3)**					
1Im	**2.01(3)**	**1(2)**	**-3(1)**	**0.0153**	**69.320**	**10.197**	**11**

Table S9. Additional Fits for Zn(II) E34C-RcnR in Buffer with 20 mM Hepes, 300 mM NaBr and 10 % Glycerol at pH 7.0.

Fourier-transform window: $k = 2 - 12.5$ Å^{-1}. Data range fit: r = 1- 4 Å.

N	r Å	σ^2 (x10^{-3} Å^2)	ΔE_0 (eV)	R factor	χ^2	Red χ^2	nvar
3N/O	2.15(2)	3(2)	11(3)	0.3757	16179.618	963.196	3
2N/O	2.07(2)	2(2)					
1N/O	2.20(2)	6(1)	8(3)	0.2225	9581.358	647.483	5
3N/O	2.04(2)	5(2)					
1S	2.30(1)	1(1)	1(3)	0.1050	4523.383	305.678	5
3N/O	2.08(2)	4(1)					
1Br	2.42(1)	4(1)	2(3)	0.1053	4536.062	306.535	5
2N/O	2.10(4)	2(4)					
1Im	2.20(4)	2(3)	10(4)	0.3698	15924.596	1076.142	5
1N/O	2.14(4)	2(4)					
1Im	2.03(3)	3(2)					
1Im	2.17(4)	3(3)	7(3)	0.3145	13541.170	1058.082	7
0N/O							
1Im	2.19(2)	11(2)					
1Im	1.95(2)	9(2)					
1Im	2.06(2)	12(2)	2(3)	0.2696	11611.669	907.314	7
2N/O	2.03(4)	6(4)					
1S	2.30(1)	0(1)					
1Im	2.06(4)	3(4)	0(2)	0.0704	3136.057	245.046	7
1N/O	*2.00(2)*	*4(1)*					
1S	*2.28(1)*	*2(1)*					
1Im	*2.05(2)*	*2(1)*					
1Im	*1.89(2)*	*1(2)*	*-5(2)*	*0.0422*	*1818.475*	*168.133*	*9*
0N/O							
1S	2.28(1)	0(1)					
1Im	2.06(2)	8(2)					
1Im	1.94(2)	5(2)					
1Im	2.19(2)	6(2)	0(2)	0.0533	2293.913	212.442	9
1N/O	1.99(4)	2(4)					
2S	2.28(1)	3(1)					
1Im	2.01(7)	6(8)	-4(2)	0.0879	3783.882	295.665	7
0N/O			-3(3)	0.0788	3392.953	265.119	9

2S	2.28(1)	4(1)					
1Im	2.08(0.13)	9(26)					
1Im	1.99(7)	2(3)					
1N/O	*2.00(2)*	*1(2)*					
1S	*2.29(1)*	*0(0)*					
1S	*2.67(2)*	*6(2)*					
1Im	*2.06(2)*	*2(2)*	*-1(2)*	*0.0241*	*1039.284*	*96.249*	*9*
0N/O							
1S	2.29(1)	0(1)					
1S	2.65(2)	4(2)					
1Im	1.98(3)	0(4)					
1Im	2.09(4)	0(5)	-2(2)	0.0431	1855.774	171.865	9
1S							
1Br							
1Im							
1Im			No Fit	No Fit	No Fit	No Fit	9
2N/O	2.08(3)	4(3)					
1Br	2.42(1)	4(1)					
1Im	2.05(6)	5(6)	1(3)	0.0837	3604.945	281.684	7
1N/O	2.09(2)	1(2)					
1Br	2.42(1)	4(1)					
1Im	2.11(2)	2(2)					
1Im	1.97(2)	2(1)	-1(2)	0.0514	2215.402	205.171	9
0N/O							
1Br	2.42(1)	5(1)					
1Im	2.05(3)	8(4)					
1Im	2.17(3)	7(4)					
1Im	1.94(3)	5(3)	-1(2)	0.0883	3803.605	352.256	9
3N/O	2.05(6)	14(6)					
1S	2.29(1)	0(1)					
1Im	2.04(2)	2(3)	0(3)	0.0816	3512.219	274.438	7
2N/O	2.03(4)	5(3)					
1S	2.30(1)	0(1)					
1Im	2.35(0.20)	18(31)					
1Im	2.08(5)	3(5)	1(3)	0.0651	2804.774	259.753	7
1N/O	*1.99(2)*	*2(2)*					
1S	*2.27(1)*	*1(1)*					
1Im	*2.48(3)*	*1(3)*					
1Im	*1.87(3)*	*1(2)*					
1Im	*2.03(2)*	*1(2)*	*-7(2)*	*0.0281*	*1210.605*	*137.602*	*7*

2N/O	2.20(0.14)	31(62)					
2S	2.28(2)	3(1)					
1Im	2.00(3)	2(2)	-2(4)	0.0827	3563.194	278.421	7
1N/O	2.10(0.17)	19(44)					
2S	2.25(2)	5(1)					
1Im	1.96(3)	4(3)					
1Im	2.48(2)	1(2)	-7(3)	0.0559	2408.448	223.049	7
0N/O							
2S	2.28(2)	4(1)					
1Im	2.19(0.57)	21(162)					
1Im	1.99(7)	2(5)					
1Im	2.11(0.32)	8(31)	-1(4)	0.0746	3212.544	297.517	7
2N/O	*2.02(2)*	*6(2)*					
1S	*2.29(1)*	*0(0)*					
1S	*2.66(1)*	*6(2)*					
1Im	*2.06(2)*	*2(2)*	*-1(1)*	*0.0178*	*763.019*	*70.664*	*9*
1N/O	2.01(2)	1(3)					
1S	2.29(1)	0(1)					
1S	2.66(2)	6(2)					
1Im	2.01(0.12)	9(13)					
1Im	2.09(6)	3(5)	-1(2)	0.0143	617.408	70.177	11
0N/O							
1S	*2.28(1)*	*1(1)*					
1S	*2.65(2)*	*6(2)*					
1Im	*2.06(2)*	*7(2)*					
1Im	*2.19(2)*	*5(2)*					
1Im	*1.94(2)*	*4(2)*	*0(1)*	*0.0264*	*1136.554*	*129.185*	*11*
1N/O	2.01(2)	2(3)					
1S	2.29(1)	1(1)					
1S	2.66(1)	6(2)					
1Im	2.04(0.19)	9(18)					
1Im	2.07(0.11)	5(7)	-1(2)	0.0140	601.649	68.386	11
1N/O	**2.02(3)**	**6(5)**					
1S	**2.29(1)**	**3(2)**					
1Br	**2.41(1)**	**7(1)**					
1Im	**1.99(3)**	**3(5)**					
1Im	**2.11(4)**	**3(5)**	**-2(1)**	**0.0107**	**461.706**	**52.479**	**11**

Table S10. Additional Fits for Ni(II) E63A-RcnR in Buffer with 20 mM Hepes, 300 mM NaBr and 10 % Glycerol at pH 7.0.

Fourier-transform window: $k = 2 - 12.5$ Å^{-1}. Data range fit: r = 1- 4 Å.

N	r (Å)	σ^2 (x10^{-3} Å^2)	ΔE_0 (eV)	R factor	χ^2	Red χ^2	nvar
4N/O	2.06(2)	7(1)	2(2)	0.1797	732.929	43.632	3
2N/O	2.00(2)	1(2)					
2N/O	2.14(3)	2(3)	2(2)	0.1587	647.306	43.743	5
3N/O	2.03(2)	3(2)					
1N/O	2.17(3)	1(3)	2(2)	0.1582	645.246	43.604	5
4N/O	2.06(2)	7(1)					
1S	2.52(7)	16(9)	3(2)	0.1524	621.351	41.989	5
4N/O	2.06(2)	7(1)					
2S	2.53(7)	25(11)	3(2)	0.1477	602.468	40.713	5
4N/O	2.06(2)	6(2)					
1Br	2.26(0.11)	22(15)	3(2)	0.1724	702.935	47.502	5
4N/O	2.06(2)	6(2)					
2Br	2.24(0.13)	30(18)	2(2)	0.1714	699.116	47.244	5
4N/O	2.07(1)	6(1)					
1S	2.57(3)	3(2)					
1Br	2.52(3)	1(2)	5(2)	0.1063	433.496	33.873	7
3N/O	2.09(2)	7(3)					
1Im	2.02(3)	2(2)	2(2)	0.1108	451.706	30.525	5
2N/O	2.08(3)	6(3)					
1Im	2.13(3)	0(3)					
1Im	1.99(2)	1(2)	3(1)	0.0837	341.146	26.657	7
1N/O	2.08(3)	2(4)					
1Im	2.21(7)	4(13)					
1Im	2.11(4)	3(5)					
1Im	1.98(2)	3(3)	4(2)	0.0939	382.767	35.448	9
3N/O	*2.05(2)*	*7(2)*					
1S	*2.53(2)*	*5(2)*					
1Br	*2.47(2)*	*0(2)*					
1Im	*2.06(2)*	*1(3)*	*3(1)*	*0.0477*	*194.521*	*18.015*	*9*
2N/O	2.02(6)	16(12)					
1S	2.42(5)	5(4)	1(1)	0.0366	149.361	16.977	11

1Br	2.37(4)	1(4)					
1Im 0°	2.12(3)	1(3)					
1Im 0°	1.98(3)	3(2)					
2N/O	1.98(5)	14(9)					
1S	2.41(4)	7(3)					
1Br	2.36(4)	3(3)					
1Im 0°	1.98(2)	5(2)					
1Im 5°	2.13(3)	3(2)	0(2)	0.0371	151.093	17.174	11
2N/O	**2.02(2)**	**3(2)**					
1S	**2.50(4)**	**2(4)**					
1Br	**2.44(4)**	**3(4)**					
1Im 0°	**2.03(3)**	**2(3)**					
1Im 10°	**2.16(2)**	**1(2)**	**3(1)**	**0.0348**	**142.043**	**16.145**	**11**
2N/O	*2.02(2)*	*2(2)*					
1S	*2.51(4)*	*1(4)*					
1Br	*2.45(5)*	*4(5)*					
1Im 5°	*2.05(3)*	*2(4)*					
1Im 10°	*2.16(2)*	*0(2)*	*3(1)*	*0.0390*	*158.892*	*18.060*	*11*
1N/O	2.02(9)	7(12)					
1S	2.41(6)	6(6)					
1Br	2.36(6)	2(6)					
1Im	1.89(0.10)	16(18)					
1Im	2.12(4)	2(4)					
1Im	1.98(4)	4(4)	0(2)	0.0362	147.448	21.690	13
1N/O	1.99(4)	2(4)					
1N/O	2.13(4)	4(4)					
1S	2.59(9)	15(20)					
1Br	2.19(0.13)	15(15)					
1Im 0°	2.14(6)	4(10)					
1Im 0°	2.01(4)	0(4)	3(2)	0.0341	138.994	20.447	13
1N/O	1.99(2)	3(3)					
1N/O	2.14(2)	4(3)					
1S	2.49(9)	1(10)					
1Br	2.44(0.11)	7(12)					
1Im 0°	2.04(4)	0(4)					
1Im 5°	1.92(0.11)	10(17)	1(2)	0.0377	153.658	22.604	13
1N/O	1.98(3)	2(2)					
1N/O	2.12(4)	2(4)					
1S	2.53(0.17)	25(30)					
1Br	2.25(9)	16(12)					
1Im 0°	2.03(3)	3(3)					
1Im 10°	2.14(3)	1(3)	3(1)	0.0286	116.464	17.132	13

1N/O	1.99(2)	2(2)					
1N/O	1.99(0.12)	23(30)					
1S	2.46(4)	3(3)					
1Br	2.40(4)	1(3)					
1Im 5°	2.03(3)	1(3)					
1Im 10°	2.14(2)	1(2)	2(2)	0.0298	121.719	17.905	13

Table S11. Additional Fits for Ni(II) E63A-RcnR in Buffer with 20 mM Hepes, 300 mM NaCl and 10 % Glycerol at pH 7.0.

Fourier-transform window: k = 2 - 12.5 Å^{-1}. Data range fit: r = 1- 4 Å.

N	r(Å)	σ^2 (x10^{-3} Å^2)	ΔE_0 (eV)	R factor	χ^2	Red χ^2	nvar
4N/O	2.08(1)	5(1)	4(2)	0.1401	2817.942	167.756	3
2N/O	2.03(3)	2(3)					
2N/O	2.14(3)	2(4)	4(2)	0.1316	2646.506	178.844	5
3N/O	2.05(2)	2(2)					
1N/O	2.17(4)	0(4)	4(2)	0.1320	2654.462	179.382	5
4N/O	2.08(1)	5(1)					
1S	2.59(3)	9(4)	6(1)	0.0862	1732.886	117.104	5
4N/O	2.08(1)	5(1)					
2S	2.59(3)	16(4)	6(1)	0.0761	1530.630	103.436	5
3N/O	2.09(2)	4(2)					
1Im	2.03(6)	5(6)	4(2)	0.1225	2464.494	166.544	5
2N/O	2.08(2)	1(2)					
1Im	2.15(4)	1(4)					
1Im	1.99(3)	1(3)	4(2)	0.1240	2494.573	194.921	7
1N/O	2.07(2)	2(2)					
1Im	2.17(4)	4(4)					
1Im	2.04(6)	3(7)					
1Im	1.94(7)	0(11)	3(3)	0.1489	2995.272	277.395	9
4N/O	*2.09(1)*	*7(2)*					
1S	*2.60(2)*	*9(3)*					
1Im	*2.06(4)*	*5(4)*	*5(1)*	*0.0493*	*991.533*	*77.477*	*7*
3N/O	*2.08(1)*	*4(2)*					
1S	*2.60(2)*	*8(3)*					
1Im	*2.01(3)*	*3(3)*					
1Im	*2.17(4)*	*4(4)*	*5(1)*	*0.0461*	*926.610*	*85.814*	*9*
2N/O	2.08(2)	1(2)					
1S	2.58(4)	9(4)					
1Im	2.05(8)	0(13)					
1Im	1.96(0.10)	3(15)					
1Im	2.19(4)	1(6)	4(2)	0.0542	1089.150	123.797	11
3N/O	2.08(1)	5(2)					
2S	2.60(3)	17(4)	5(1)	0.0556	1117.943	87.354	7

1Im	2.07(4)	6(5)					
2N/O							
2S							
1Im							
1Im			No Fit	No Fit	No Fit	No Fit	9
1N/O	2.06(2)	2(2)					
2S	2.54(5)	19(6)					
1Im	2.04(4)	5(4)					
1Im	2.17(3)	5(3)					
1Im	1.93(4)	1(6)	3(2)	0.0743	1495.056	169.934	11
3N/O	2.08(1)	4(2)					
1S	2.43(6)	14(8)					
1S	2.62(3)	6(3)					
1Im	2.04(5)	6(5)	4(1)	0.0438	881.627	81.648	9
2N/O	2.07(1)	0(1)					
1S	2.40(4)	7(5)					
1S	2.60(3)	3(2)					
1Im	1.96(3)	0(2)					
1Im	2.12(3)	1(2)	3(2)	0.0327	658.034	74.795	11
2N/O	*2.08(1)*	*1(2)*					
1S	*2.42(5)*	*9(5)*					
1S	*2.61(3)*	*4(3)*					
1Im 0°	*2.12(3)*	*1(3)*					
1Im 5°	*1.97(3)*	*0(2)*	*4(2)*	*0.0338*	*680.523*	*77.351*	*11*
2N/O	**2.06(3)**	**3(3)**					
1S	**2.38(5)**	**9(6)**					
1S	**2.59(3)**	**5(3)**					
1Im 0°	**2.01(8)**	**9(7)**					
1Im 10°	**2.08(5)**	**3(6)**	**3(2)**	**0.0377**	**757.520**	**86.103**	**11**
2N/O	2.06(3)	3(3)					
1S	2.39(5)	10(7)					
1S	2.59(3)	5(3)					
1Im 5°	2.01(9)	8(8)					
1Im 10°	2.09(5)	3(5)	3(2)	0.0389	781.398	88.817	11
1N/O	2.05(2)	6(2)					
1S	2.35(3)	0(3)					
1S	2.56(3)	0(2)					
1Im	2.11(3)	4(2)					
1Im	1.95(3)	4(2)					
1Im	1.88(6)	5(10)	0(2)	0.0274	551.623	81.147	13
1N/O	2.06(2)	6(2)	1(2)	0.0235	472.054	69.442	13

1N/O	1.94(7)	11(12)					
1S	2.38(3)	0(3)					
1S	2.58(3)	1(2)					
1Im	1.95(2)	5(2)					
1Im	2.11(2)	3(2)					
1N/O	*2.11(3)*	*5(3)*					
1N/O	*1.99(3)*	*4(3)*					
1S	*2.40(5)*	*5(6)*					
1S	*2.60(4)*	*3(4)*					
1Im 0°	*1.97(7)*	*7(7)*					
1Im 10°	*2.10(6)*	*3(6)*	*2(2)*	*0.0326*	*654.856*	*96.333*	*13*
3N/O	2.07(2)	4(2)					
1Cl	2.39(5)	13(7)					
1Cl	2.59(3)	6(3)					
1Im	2.04(5)	6(5)	4(2)	0.0451	906.107	83.915	9
2N/O	2.06(1)	0(1)					
1Cl	2.37(4)	6(4)					
1Cl	2.57(3)	4(2)					
1Im	2.11(3)	1(3)					
1Im	1.95(3)	0(2)	2(2)	0.033	663.374	75.402	11
1N/O	2.04(2)	6(2)					
1Cl	2.32(3)	0(3)					
1Cl	2.53(3)	1(2)					
1Im	1.88(5)	5(10)					
1Im	1.95(4)	4(2)					
1Im	2.10(3)	4(2)	0(2)	0.0255	513.237	75.500	13

Table S12. Additional Fits for Co(II) E63A-RcnR in Buffer with 20 mM Hepes, 300 mM NaBr and 10 % Glycerol at pH 7.0.

Fourier-transform window: $k = 2 - 12.5$ Å^{-1}. Data range fit: r = 1- 4 Å.

N	r (Å)	σ^2 (x10^{-3} Å^2)	ΔE_0 (eV)	R factor	χ^2	Red χ^2	nvar
4N/O	2.10(2)	7(1)	-1(2)	0.1779	927.112	55.192	3
2N/O	2.06(2)	1(2)					
2N/O	2.19(3)	2(3)	0(2)	0.1445	753.081	50.891	5
3N/O	2.08(2)	2(1)					
1N/O	2.23(3)	1(2)	1(2)	0.1424	742.049	50.146	5
4N/O	2.12(2)	7(1)					
1S	2.69(3)	7(3)	1(2)	0.1446	753.552	50.923	5
4N/O	2.11(2)	7(1)					
2S	2.65(6)	22(9)	1(2)	0.1477	769.687	52.013	5
4N/O	2.09(2)	7(1)					
1Br	2.47(4)	13(4)	-2(3)	0.1574	820.441	55.443	5
4N/O	2.11(2)	7(2)					
2Br	2.45(5)	22(8)	-1(3)	0.1647	858.469	58.013	5
3N/O	2.13(2)	6(3)					
1Im	2.04(4)	3(3)	-1(3)	0.1428	744.367	50.302	5
2N/O	2.12(3)	4(3)					
1Im	2.18(6)	4(6)					
1Im	2.03(4)	1(2)	0(3)	0.1448	754.740	58.974	7
1N/O	2.10(3)	0(3)					
1Im	1.98(4)	3(4)					
1Im	2.23(4)	4(3)					
1Im	2.10(4)	5(4)	-1(3)	0.1532	798.402	73.941	9
4N/O	2.14(2)	9(2)					
1S	2.69(2)	7(2)					
1Im	2.06(2)	3(2)	1(1)	0.0738	384.662	30.057	7
3N/O	2.13(2)	7(2)					
1S	2.69(2)	7(2)					
1Im	2.24(4)	4(4)					
1Im	2.06(2)	1(2)	2(1)	0.0599	312.371	28.929	9
2N/O	2.12(2)	4(3)					
1S	2.69(2)	6(2)					
1Im	2.02(3)	3(3)	2(1)	0.0614	320.088	36.382	11

1Im	2.15(3)	5(3)					
1Im	2.29(3)	3(3)					
4N/O	2.14(3)	10(3)					
1Br	2.45(3)	14(4)					
1Im	2.06(3)	2(2)	0(2)	0.0973	506.872	39.606	7
3N/O	2.13(3)	7(3)					
1Br	2.46(3)	13(4)					
1Im	2.07(3)	2(2)					
1Im	2.27(5)	4(5)	1(2)	0.0884	460.928	42.687	9
2N/O	2.12(3)	5(4)					
1Br	2.46(3)	10(3)					
1Im	2.16(5)	4(4)					
1Im	2.03(4)	2(3)					
1Im	2.31(4)	3(4)	2(2)	0.0821	427.924	48.640	11
3N/O	*2.09(1)*	*5(1)*					
1S	*2.52(2)*	*4(2)*					
1Br	*2.47(2)*	*1(2)*					
1Im	*2.05(3)*	*4(3)*	*-2(1)*	*0.0306*	*159.429*	*14.765*	*9*
2N/O	2.09(1)	2(1)					
1S	2.51(2)	5(2)					
1Br	2.46(2)	1(2)					
1Im 0°	2.03(6)	4(4)					
1Im 0°	2.09(9)	12(15)	-2(1)	0.0192	100.191	11.388	11
2N/O	2.09(1)	2(1)					
1S	2.51(2)	5(2)					
1Br	2.46(1)	1(2)					
1Im 0°	2.04(4)	4(4)					
1Im 5°	2.06(0.11)	13(13)	-2(1)	0.0196	102.101	11.605	11
2N/O	2.09(1)	2(1)					
1S	2.51(2)	5(2)					
1Br	2.46(2)	2(2)					
1Im 0°	2.04(3)	3(3)					
1Im 10°	2.06(0.16)	16(18)	-2(1)	0.0215	111.945	12.724	11
2N/O	**2.08(2)**	**2(2)**					
1S	**2.50(2)**	**4(2)**					
1Br	**2.45(2)**	**1(2)**					
1Im 5°	**2.03(3)**	**4(3)**					
1Im 10°	**2.16(6)**	**7(7)**	**-2(1)**	**0.0262**	**136.435**	**15.508**	**11**
1N/O	2.09(1)	3(1)					
1S	2.49(3)	5(2)					
1Br	2.45(3)	2(2)	-2(2)	0.0193	100.834	14.833	13

1Im	2.09(0.40)	17(33)					
1Im	2.00(4)	0(4)					
1Im	2.15(0.12)	4(9)					
1N/O	2.10(3)	3(2)					
1N/O	2.02(6)	7(12)					
1S	2.51(2)	7(2)					
1Br	2.46(2)	3(2)					
1Im 0°	2.02(3)	0(3)					
1Im 0°	2.17(6)	6(7)	-2(1)	0.0159	82.942	12.201	13
1N/O	2.10(1)	2(1)					
1N/O	2.06(9)	15(17)					
1S	2.50(2)	5(3)					
1Br	2.46(2)	1(2)					
1Im 0°	2.13(3)	3(5)					
1Im 5°	2.00(3)	1(2)	-2(1)	0.0157	82.077	12.074	13
1N/O	*2.04(2)*	*5(2)*					
1N/O	*2.15(1)*	*6(2)*					
1S	*2.53(2)*	*8(2)*					
1Br	*2.49(2)*	*4(2)*					
1Im 0°	*2.06(2)*	*1(2)*					
1Im 10°	*1.93(3)*	*0(3)*	*-3(1)*	*0.0163*	*84.780*	*12.472*	*13*
1N/O	*2.03(2)*	*5(2)*					
1N/O	*2.15(2)*	*6(2)*					
1S	*2.53(3)*	*8(3)*					
1Br	*2.49(3)*	*4(3)*					
1Im 5°	*2.07(3)*	*2(3)*					
1Im 10°	*1.92(3)*	*0(3)*	*-3(1)*	*0.0244*	*127.285*	*18.724*	*13*

Table S13. Additional Fits for Co(II) E63A-RcnR in Buffer with 20 mM Hepes, 300 mM NaCl and 10 % Glycerol at pH 7.0.

Fourier-transform window: k = 2 - 12.5 Å^{-1}. Data range fit: r = 1- 4 Å.

N	r (Å)	σ^2 (x10^{-3} Å^2)	ΔE_0 (eV)	R factor	χ^2	Red χ^2	nvar
4N/O	2.11(2)	10(2)	2(3)	0.2148	768.246	45.735	3
2N/O	2.01(2)	2(1)					
2N/O	2.16(2)	1(1)	-1(2)	0.1464	523.743	35.393	5
3N/O	2.04(2)	5(2)					
1N/O	2.18(2)	1(1)	-1(2)	0.1497	535.611	36.195	5
4N/O	2.04(7)	14(4)					
2S	2.30(4)	14(6)	-7(5)	0.1900	679.584	45.925	5
3N/O	2.12(2)	5(2)					
1Im	1.97(2)	1(2)	-2(2)	0.1810	647.412	43.750	5
2N/O	2.10(2)	7(3)					
1Im	2.16(2)	1(1)					
1Im	1.99(2)	0(1)	-1(1)	0.0695	248.452	19.414	7
1N/O	2.10(3)	2(3)					
1Im	1.96(2)	2(2)					
1Im	2.21(2)	3(4)					
1Im	2.09(3)	4(4)	-1(2)	0.0684	244.587	22.651	9
4N/O	2.09(2)	10(2)					
1S	2.75(4)	12(5)					
1Im	2.20(3)	3(3)	2(2)	0.1317	470.965	36.800	7
3N/O	2.10(3)	12(4)					
1S	2.44(0.18)	42(36)					
1Im	1.99(2)	0(1)					
1Im	2.15(2)	1(1)	-1(1)	0.0532	190.416	17.635	9
2N/O	2.10(3)	8(4)					
1S	2.39(8)	27(20)					
1Im	2.15(3)	1(3)					
1Im	1.99(4)	0(3)					
1Im	1.97(0.16)	12(22)	-3(2)	0.0458	163.648	18.601	11
3N/O	2.07(2)	6(2)					
2S	2.71(8)	29(13)					
1Im	2.20(2)	1(2)	3(2)	0.1557	556.990	43.522	7
2N/O	2.09(3)	8(3)	-2(1)	0.0506	181.153	16.777	9

2S	2.44(9)	40(15)					
1Im	2.15(2)	1(1)					
1Im	1.99(2)	0(1)					
1N/O	2.09(3)	3(3)					
2S	2.41(6)	32(12)					
1Im	2.17(3)	1(4)					
1Im	2.04(0.17)	1(18)					
1Im	1.96(0.18)	2(19)	-3(2)	0.0424	151.705	17.243	11
3N/O	2.09(8)	19(10)					
1S	2.45(8)	13(9)					
1S	2.28(3)	5(3)					
1Im	1.98(3)	3(2)	-7(3)	0.1041	372.421	34.490	9
2N/O	2.08(3)	10(4)					
1S	2.41(5)	13(5)					
1S	2.68(5)	12(5)					
1Im	2.15(2)	1(1)					
1Im	1.99(2)	0(1)	-2(1)	0.0356	127.368	14.477	11
2N/O	2.08(4)	12(5)					
1S	2.41(6)	14(6)					
1S	2.69(6)	13(6)					
1Im 0°	2.15(2)	1(1)					
1Im 5°	2.00(2)	1(1)	-1(1)	0.0371	132.615	15.074	11
2N/O	2.04(9)	19(14)					
1S	2.51(9)	13(9)					
1S	2.31(4)	6(5)					
1Im 0°	1.97(2)	3(2)					
1Im 10°	2.09(4)	2(3)	-6(2)	0.0621	221.978	25.231	11
2N/O	2.05(9)	20(14)					
1S	2.50(9)	15(11)					
1S	2.31(4)	7(5)					
1Im 5°	1.97(2)	2(2)					
1Im 10°	2.10(4)	2(2)	-5(3)	0.0602	215.435	24.487	11
1N/O	2.08(3)	3(3)					
1S	2.38(4)	10(6)					
1S	2.63(7)	16(8)					
1Im	1.99(3)	1(2)					
1Im	1.98(0.18)	15(24)					
1Im	2.15(3)	1(2)	-3(2)	0.0323	115.496	16.990	13
1N/O	**1.95(5)**	**5(6)**					
1N/O	**2.11(3)**	**0(3)**					
1S	**2.66(5)**	**8(4)**					
1S	**2.42(4)**	**8(4)**	**-2(2)**	**0.0259**	**92.765**	**13.646**	**13**

1Im 0°	**2.00(2)**	**2(2)**					
1Im 0°	**2.15(2)**	**2(1)**					
1N/O	1.95(4)	3(5)					
1N/O	2.12(2)	1(3)					
1S	2.43(4)	9(4)					
1S	2.68(5)	10(4)					
1Im 0°	2.16(2)	1(1)					
1Im 5°	2.01(2)	2(2)	-2(2)	0.0264	94.424	13.890	13
1N/O	1.97(2)	1(1)					
1N/O	2.15(3)	0(3)					
1S	2.74(6)	10(6)					
1S	2.47(7)	15(7)					
1Im 0°	2.15(6)	9(8)					
1Im 10°	2.10(3)	2(3)	0(2)	0.0349	124.764	18.353	13
1N/O	1.97(2)	1(1)					
1N/O	2.15(3)	0(3)					
1S	2.74(6)	11(6)					
1S	2.46(7)	15(7)					
1Im 5°	2.15(6)	8(8)					
1Im 10°	2.10(3)	2(3)	0(2)	0.0362	129.633	19.070	13

Table S14. Additional Fits for Zn(II) E63A-RcnR in Buffer with 20 mM Hepes, 300 mM NaBr and 10 % Glycerol at pH 7.0.

Fourier-transform window: $k = 2 - 12.5$ Å^{-1}. Data range fit: r = 1- 4 Å.

N	r (Å)	σ^2 (x10^{-3} Å^2)	ΔE_0 (eV)	R factor	χ^2	Red χ^2	nvar
3N/O	2.11(2)	4(3)	9(0)	0.4878	12537.136	746.354	3
2N/O	2.04(2)	2(2)					
1N/O	2.18(2)	6(1)	7(3)	0.3149	8093.365	546.928	5
3N/O	2.01(2)	4(2)					
1S	2.28(2)	0(1)	-1(3)	0.1795	4612.858	311.725	5
3N/O	2.02(2)	5(1)					
1Br	2.39(1)	4(1)	-2(3)	0.1077	2768.076	187.059	5
3N/O	1.99(2)	6(1)					
2Br	2.38(1)	7(1)	-6(3)	0.0855	2198.809	148.590	5
3N/O	2.00(4)	8(4)					
1S	2.20(6)	7(6)					
1Br	2.39(2)	4(1)	-7(6)	0.0727	1868.540	146.004	7
2N/O	2.05(4)	2(4)					
1Im	2.17(4)	2(3)	7(5)	0.4533	11651.030	787.346	5
1N/O	2.01(9)	3(10)					
1Im	2.02(4)	3(4)					
1Im	2.16(3)	5(2)	3(4)	0.3769	9687.515	756.964	7
0N/O							
1Im	1.93(2)	9(2)					
1Im	2.05(2)	13(2)					
1Im	2.17(2)	11(2)	1(3)	0.2961	7611.428	594.743	7
2N/O	1.98(3)	3(3)					
1S	2.28(1)	0(1)					
1Im	2.06(3)	0(3)	-1(3)	0.1195	3072.526	240.081	7
1N/O	1.97(2)	2(2)					
1S	2.28(1)	0(1)					
1Im	2.27(0.21)	19(49)					
1Im	2.08(3)	1(2)	1(4)	0.0919	2362.216	218.767	9
0N/O							
1S	2.26(2)	1(2)					
1Im	2.17(3)	7(3)					
1Im	1.92(3)	6(2)	-1(3)	0.1163	2990.307	276.935	9

1Im	2.04(3)	9(2)					
1N/O	*2.00(2)*	*3(3)*					
1Br	*2.40(1)*	*3(0)*					
1Im	*2.08(2)*	*3(1)*					
1Im	*1.95(2)*	*2(1)*	*-3(2)*	*0.0248*	*637.587*	*59.048*	*9*
0N/O							
1Br	2.40(1)	4(1)					
1Im	2.11(8)	3(9)					
1Im	2.02(5)	4(12)					
1Im	1.92(5)	3(8)	-4(2)	0.0456	1172.707	108.606	9
1S							
1Br							
1Im							
1Im			No Fit	No Fit	No Fit	No Fit	9
1N/O	1.94(2)	0(2)					
1S	2.26(2)	4(2)					
1Br	2.40(1)	6(1)					
1Im	2.05(2)	1(2)	-4(2)	0.0258	663.242	61.423	9
3N/O	1.98(5)	9(5)					
1S	2.28(2)	0(1)					
1Im	2.03(3)	1(3)	-2(3)	0.1521	3909.045	305.445	7
2N/O	1.96(4)	5(4)					
1S	2.27(2)	1(1)					
1Im	2.47(3)	0(3)					
1Im	2.03(4)	1(3)	-4(3)	0.0974	2504.430	231.938	9
1N/O	1.96(3)	3(2)					
1S	2.27(2)	1(1)					
1Im	2.26(8)	1(8)					
1Im	2.07(3)	2(3)					
1Im	2.50(4)	0(5)	0(4)	0.0741	1904.869	216.515	11
3N/O	*2.00(2)*	*7(2)*					
1Br	*2.40(1)*	*4(1)*					
1Im	*2.07(2)*	*1(2)*	*-2(2)*	*0.0489*	*1257.311*	*98.244*	*7*
2N/O	*1.99(2)*	*8(3)*					
1Br	*2.40(1)*	*4(0)*					
1Im	*1.97(2)*	*1(2)*					
1Im	*2.09(1)*	*3(1)*	*-3(1)*	*0.0207*	*532.166*	*49.284*	*9*
1N/O	2.00(2)	2(3)					
1Br	2.39(1)	3(1)					
1Im	1.95(2)	2(2)	-5(2)	0.0210	540.926	61.484	11

1Im	2.08(2)	3(2)					
1Im	1.90(0.13)	18(28)					
1S	**2.23(2)**	**9(3)**					
1Br	**2.40(1)**	**4(1)**					
1Im	**2.05(1)**	**6(2)**					
1Im	**2.17(2)**	**2(3)**					
1Im	**1.93(1)**	**4(1)**	**-3(1)**	**0.0107**	**273.787**	**31.120**	**11**
1N/O	1.99(3)	5(4)					
1S	2.24(3)	14(5)					
1Br	2.40(1)	4(0)					
1Im	1.96(1)	0(1)					
1Im	2.08(1)	2(1)	-4(1)	0.0096	245.725	27.930	11

Table S15. Additional Fits for Ni(II) E63C-RcnR in Buffer with 20 mM Hepes, 300 mM NaBr and 10 % Glycerol at pH 7.0.

Fourier-transform window: k = 2 - 12.5 Å^{-1}. Data range fit: r = 1- 4 Å.

N	r (Å)	σ^2 (x10^{-3} Å^2)	ΔE_0 (eV)	R factor	χ^2	Red χ^2	nvar
3N/O	2.07(1)	5(1)	5(2)	0.1736	984.371	50.122	3
2N/O	2.03(1)	0(1)					
1N/O	2.15(1)	2(1)	4(2)	0.1260	714.481	40.504	5
3N/O	2.03(3)	7(2)					
1S	2.25(3)	7(3)	-2(3)	0.1373	778.912	44.157	5
3N/O	2.06(1)	5(1)					
1Br	2.41(2)	12(3)	4(2)	0.1222	693.351	39.306	5
3N/O	2.05(2)	6(1)					
1S	2.39(8)	14(11)					
1Br	2.38(4)	10(3)	2(2)	0.1014	575.242	36.781	7
2N/O	2.08(2)	4(3)					
1Im	2.04(5)	4(4)	4(2)	0.1256	654.141	44.205	5
1N/O	2.07(2)	0(2)					
1Im	2.14(2)	2(2)					
1Im	1.99(2)	2(1)	4(2)	0.1019	531.145	41.503	7
0N/O							
1Im	2.15(3)	6(3)					
1Im	1.94(4)	2(7)					
1Im	2.03(3)	6(4)	2(2)	0.1806	940.923	73.522	7
3N/O	2.09(3)	8(5)					
1S	2.23(3)	9(7)					
1Im	2.01(4)	4(3)	1(3)	0.0805	419.524	32.781	7
2N/O	2.05(4)	5(3)					
1S	2.25(2)	6(3)					
1Im	1.86(6)	7(6)					
1Im	1.99(4)	2(3)	-4(3)	0.0648	337.501	31.256	9
1N/O	2.04(3)	0(3)					
1S	2.27(3)	7(4)					
1Im	1.95(3)	5(2)					
1Im	2.08(3)	4(3)					
1Im	1.82(3)	0(3)	-4(2)	0.0514	267.874	30.448	11
2N/O	2.07(3)	3(3)	-2(3)	0.1008	525.393	41.053	7

2S	2.24(4)	16(5)					
1Im	1.97(4)	4(4)					
1N/O	2.04(5)	2(4)					
2S	2.24(2)	9(2)					
1Im	1.97(4)	2(3)					
1Im	1.83(5)	7(6)	-7(3)	0.0834	434.643	40.253	9
0N/O							
2S	2.25(2)	9(3)					
1Im	1.93(4)	5(3)					
1Im	2.06(4)	4(3)					
1Im	1.80(4)	0(4)	-6(3)	0.0993	517.321	47.910	9
2N/O	2.05(3)	5(3)					
1S	2.57(3)	9(4)					
1S	2.30(3)	7(3)					
1Im	2.02(4)	4(4)	1(2)	0.0533	277.762	25.724	9
1N/O	**2.04(2)**	**1(2)**					
1S	**2.30(3)**	**4(3)**					
1S	**2.55(4)**	**8(4)**					
1Im	**1.94(4)**	**2(3)**					
1Im	**2.08(4)**	**2(4)**	**0(2)**	**0.0371**	**193.475**	**21.991**	**11**
1N/O	*2.04(3)*	*0(3)*					
1S	*2.30(3)*	*5(3)*					
1S	*2.55(4)*	*9(4)*					
1Im 0°	*2.07(4)*	*2(5)*					
1Im 5°	*1.94(5)*	*2(4)*	*0(2)*	*0.0404*	*301.825*	*34.307*	*11*
1N/O	*2.01(3)*	*2(4)*					
1S	*2.55(4)*	*8(4)*					
1S	*2.30(3)*	*6(3)*					
1Im 0°	*2.00(5)*	*6(5)*					
1Im 10°	*2.08(4)*	*3(4)*	*1(2)*	*0.0414*	*215.883*	*24.538*	*11*
1N/O	*2.01(4)*	*2(4)*					
1S	*2.56(4)*	*8(4)*					
1S	*2.30(3)*	*6(3)*					
1Im 5°	*2.02(5)*	*6(5)*					
1Im 10°	*2.09(4)*	*2(4)*	*1(2)*	*0.044*	*229.261*	*26.059*	*11*
0N/O							
1S	2.25(2)	4(3)					
1S	2.46(8)	15(11)					
1Im	2.10(5)	2(6)					
1Im	1.98(4)	3(5)					
1Im	1.88(6)	2(7)	-2(3)	0.0735	382.869	43.518	11

2N/O	2.05(3)	5(3)					
1S	2.39(7)	10(8)					
1Br	2.38(4)	9(3)					
1Im	2.03(4)	4(4)	2(2)	0.0533	277.498	25.699	9
1N/O	*2.04(2)*	*0(2)*					
1S	*2.38(5)*	*5(7)*					
1Br	*2.36(4)*	*7(4)*					
1Im	*2.09(4)*	*2(3)*					
1Im	*1.95(3)*	*1(3)*	*1(2)*	*0.0407*	*212.124*	*24.111*	*11*

Table S16. Additional Fits for Co(II) E63C-RcnR in Buffer with 20 mM Hepes, 300 mM NaBr and 10 % Glycerol at pH 7.0.

Fourier-transform window: k = 2 - 12.5 Å^{-1}.. Data range fit: r = 1- 4 Å.

N	r (Å)	σ^2 (x10^{-3} Å^2)	ΔE_0 (eV)	R factor	χ^2	Red χ^2	nvar
4N/O	2.11(2)	7(1)	1(2)	0.1935	2011.959	119.775	3
2N/O	2.00(1)	0(1)					
2N/O	2.15(1)	2(1)	-3(2)	0.0819	851.577	57.547	5
3N/O	2.04(1)	2(1)					
1N/O	2.17(1)	4(1)	-3(2)	0.0743	772.474	52.202	5
4N/O	2.02(4)	11(2)					
1S	2.26(2)	3(1)	-10(4)	0.1308	1360.539	91.942	5
3N/O	2.12(1)	2(1)					
1Im	1.98(2)	0(1)	-2(2)	0.1286	1337.693	90.398	5
2N/O	*2.11(1)*	*2(1)*					
1Im	*1.99(1)*	*2(1)*					
1Im	*2.15(1)*	*2(1)*	*-1(1)*	*0.0413*	*429.120*	*33.531*	*7*
1N/O	2.11(1)	1(1)					
1Im	2.17(5)	2(3)					
1Im	2.01(0.10)	1(6)					
1Im	2.02(0.19)	5(24)	-2(2)	0.0524	545.405	50.510	9
4N/O	2.13(4)	16(6)					
1S	2.26(1)	2(1)					
1Im	1.99(2)	2(1)	-6(3)	0.0710	1268.964	99.154	7
3N/O	*2.13(3)*	*3(1)*					
1S	*2.18(4)*	*9(8)*					
1Im	*2.15(2)*	*1(1)*					
1Im	*1.99(1)*	*2(1)*	*-2(1)*	*0.0298*	*309.507*	*28.664*	*9*
2N/O	2.14(4)	2(2)					
1S	2.22(4)	9(9)					
1Im	1.99(2)	2(2)					
1Im	2.13(3)	2(4)					
1Im	2.24(7)	5(13)	-1(2)	0.0301	313.324	35.614	11
3N/O	2.13(2)	2(2)					
2S	2.22(2)	13(6)					
1Im	1.97(2)	0(1)	-7(3)	0.0898	933.386	72.933	7
2N/O	2.11(1)	2(1)	-2(2)	0.0398	413.761	38.319	9

2S	2.45(0.33)	67(64)					
1Im	1.99(1)	2(1)					
1Im	2.15(2)	2(1)					
1N/O	2.11(2)	1(2)					
2S	2.37(8)	35(20)					
1Im	2.15(3)	3(2)					
1Im	1.97(0.11)	7(16)					
1Im	2.00(4)	2(2)	-4(2)	0.0438	455.024	51.720	11
3N/O	2.08(4)	13(5)					
1S	2.49(3)	8(4)					
1S	2.28(1)	2(1)					
1Im	2.00(2)	2(2)	-6(2)	0.0444	461.841	42.772	9
2N/O	**2.12(3)**	**9(4)**					
1S	**2.52(3)**	**9(3)**					
1S	**2.28(2)**	**5(2)**					
1Im	**2.14(2)**	**0(2)**					
1Im	**1.98(1)**	**1(1)**	**-3(1)**	**0.0177**	**184.485**	**20.969**	**11**
1N/O	2.86(7)	7(8)					
1S	2.28(2)	4(2)					
1S	1.78(5)	26(8)					
1Im	2.15(2)	5(2)					
1Im	2.01(2)	4(1)					
1Im	2.29(4)	1(4)	-1(2)	0.0318	331.179	48.718	13
1N/O	2.02(2)	1(2)					
1N/O	2.15(1)	4(1)					
1S	2.62(7)	16(7)					
1S	2.33(0.14)	31(23)					
1Im 0°	2.01(2)	0(2)					
1Im 0°	2.17(3)	2(3)	-2(1)	0.0109	112.991	16.622	13
1N/O	2.01(2)	2(2)					
1N/O	2.15(1)	4(1)					
1S	2.29(0.10)	23(16)					
1S	2.61(7)	17(7)					
1Im 0°	2.02(3)	0(2)					
1Im 5°	2.19(4)	1(3)	-2(1)	0.0131	135.771	19.973	13
1N/O	2.01(1)	3(1)					
1N/O	2.15(1)	5(1)					
1S	2.55(0.11)	19(11)					
1S	2.25(9)	19(15)					
1Im 0°	2.03(4)	6(4)					
1Im 10°	2.15(5)	5(5)	-3(2)	0.0142	147.649	21.720	13
1N/O	2.01(1)	4(1)	-1(2)	0.0169	175.881	25.873	13

1N/O	2.15(1)	5(1)
1S	2.11(7)	19(11)
1S	1.78(8)	31(11)
1Im 5°	2.07(5)	7(5)
1Im 10°	2.14(5)	4(4)

Table S17. Additional Fits for Zn(II) E63C-RcnR in Buffer with 20 mM Hepes, 300 mM NaBr and 10 % Glycerol at pH 7.0.

Fourier-transform window: k = 2 - 12.5 Å^{-1}. Data range fit: r = 1- 4 Å.

N	r (Å)	σ^2 (x10^{-3} Å^2)	ΔE_0 (eV)	R factor	χ^2	Red χ^2	nvar
3N/O	2.12(3)	4(2)	10(3)	0.3571	5175.240	308.089	3
2N/O	2.07(2)	2(2)					
1N/O	2.20(2)	5(1)	9(3)	0.2363	3425.147	231.462	5
2N/O	2.04(2)	1(1)					
1S	2.30(2)	1(1)	2(3)	0.1388	2012.234	135.982	5
2N/O	2.07(2)	2(2)					
1Br	2.44(2)	5(1)	4(4)	0.1960	2841.041	191.990	5
2N/O	2.02(4)	5(3)					
2S	2.29(6)	12(5)					
1Br	2.41(2)	7(2)	-2(5)	0.1081	1566.196	122.380	7
2N/O	2.02(3)	3(2)					
1S	2.30(4)	3(3)					
1Br	2.42(3)	9(4)	0(4)	0.1097	1590.348	124.267	7
2N/O	2.10(5)	5(6)					
1Im	2.14(9)	4(9)	9(4)	0.3601	5218.995	352.686	5
1N/O	2.04(8)	4(11)					
1Im	2.04(4)	3(3)					
1Im	2.17(4)	4(3)	5(3)	0.3240	4696.328	366.962	7
0N/O							
1Im	2.06(2)	12(2)					
1Im	2.18(2)	11(2)					
1Im	1.94(2)	9(2)	1(2)	0.2478	3591.218	280.611	7
2N/O	1.99(3)	5(3)					
1S	2.30(1)	1(1)					
1Im	2.06(2)	1(2)	0(2)	0.0813	1178.253	92.066	7
1N/O	1.99(2)	2(2)					
1S	2.29(1)	1(1)					
1Im	2.06(2)	2(1)					
1Im	1.90(3)	1(3)	-(2)	0.0599	867.962	80.383	9
0N/O							
1S	2.28(1)	2(1)					
1Im	1.93(2)	6(2)	0(2)	0.0648	939.232	86.983	9

1Im	2.18(3)	6(2)					
1Im	2.05(2)	8(2)					
1N/O	1.95(3)	2(3)					
2S	2.28(1)	5(1)					
1Im	2.04(2)	0(2)	-2(2)	0.0899	1303.568	101.858	7
0N/O							
2S	2.28(1)	5(1)					
1Im	1.93(5)	3(6)					
1Im	2.03(3)	1(3)	-3(2)	0.0872	1263.712	98.744	7
1N/O	1.98(2)	0(2)					
1S	2.30(1)	1(1)					
1S	2.67(3)	8(4)					
1Im	2.06(2)	1(1)	0(2)	0.0523	758.717	70.266	9
0N/O							
1S	2.30(2)	1(1)					
1S	2.65(3)	6(4)					
1Im	2.06(3)	2(3)					
1Im	1.96(4)	0(5)	-2(3)	0.0801	1160.477	107.473	9
1N/O	*1.96(3)*	*2(3)*					
1S	*2.30((3)*	*3(3)*					
1Br	*2.41(2)*	*9(3)*					
1Im	*2.05(2)*	*0(2)*	*-2()*	*0.0465*	*674.684*	*62.483*	*9*
0N/O							
1S	*2.29(3)*	*5(4)*					
1Br	*2.40(2)*	*7(2)*					
1Im	*2.06(3)*	*2(2)*					
1Im	*1.95(3)*	*0(3)*	*-3(2)*	*0.0484*	*701.595*	*64.975*	*9*
3N/O	2.00(5)	12(5)					
1S	2.30(1)	1(1)					
1Im	2.04(2)	0(2)	0(3)	0.0985	2485.307	194.197	7
2N/O	1.99(3)	4(3)					
1S	2.30(2)	0(1)					
1Im	2.07(3)	2(2)					
1Im	2.24(6)	2(6)	2(2)	0.0749	1085.512	100.530	9
1N/O	*1.94(2)*	*1(3)*					
1S	*2.28(1)*	*0(1)*					
1Im	*2.86(3)*	*2(2)*					
1Im	*2.04(2)*	*4(2)*					
1Im	*2.18(5)*	*1(5)*	*1(2)*	*0.0391*	*566.905*	*64.437*	*11*
2N/O	2.00(0.21)	31(25)	-2(4)	0.1075	1557.633	121.711	7

2S	2.28(2)	5(1)					
1Im	2.01(2)	1(2)					
1N/O	1.71(0.15)	25(28)					
2S	2.27(2)	4(1)					
1Im	1.91(4)	1(5)					
1Im	2.03(2)	2(3)	-4(3)	0.0819	1186.981	109.928	9
0N/O							
2S	2.26(1)	6(2)					
1Im	2.19(2)	6(2)					
1Im	1.93(2)	4(2)					
1Im	2.05(2)	7(2)	-1(2)	0.0620	898.057	83.170	9
2N/O	*1.99(2)*	*5(2)*					
1S	*2.30(1)*	*1(1)*					
1S	*2.66(2)*	*8(3)*					
1Im	*2.06(2)*	*0(1)*	*0(2)*	*0.0449*	*651.263*	*60.314*	*9*
1N/O	1.97(3)	1(3)					
1S	2.30(1)	1(1)					
1S	2.66(3)	7(4)					
1Im	2.09(0.16)	11(21)					
1Im	2.06(3)	0(2)	0(3)	0.0399	578.608	65.767	11
0N/O							
1S	2.29(1)	2(2)					
1S	2.65(4)	9(5)					
1Im	2.18(3)	5(3)					
1Im	2.05(2)	8(2)					
1Im	1.93(2)	5(2)	0(2)	0.0569	825.133	93.788	11
2N/O	*1.99(3)*	*8(4)*					
1S	*2.31(3)*	*5(4)*					
1Br	*2.40(2)*	*7(2)*					
1Im	*2.05(2)*	*1(2)*	*-1(2)*	*0.0447*	*647.744*	*59.988*	*9*
1N/O	1.96(4)	4(5)					
1S	2.31(3)	6(5)					
1Br	2.41(2)	7(3)					
1Im	2.05(3)	1(4)					
1Im	2.04(0.12)	8(14)	-1(2)	0.0317	459.497	52.228	11
0N/O							
1S	**2.29(3)**	**6(4)**					
1Br	**2.40(2)**	**8(3)**					
1Im	**2.17(3)**	**4(3)**					
1Im	**2.05(2)**	**7(2)**					
1Im	**1.93(2)**	**4(2)**	**-1(2)**	**0.0336**	**487.442**	**55.405**	**11**

1N/O	1.96(4)	4(4)					
2S	2.31(3)	12(3)					
1Br	2.40(1)	6(1)					
1Im	2.05(2)	0(2)	-2(2)	0.0430	622.716	57.670	9
0N/O							
2S	2.30(2)	13(3)					
1Br	2.40(1)	6(1)					
1Im	2.06(2)	1(2)					
1Im	1.95(3)	1(3)	-3(2)	0.0310	449.861	41.662	9
1N/O	1.95(3)	1(3)					
1S	2.26(4)	2(4)					
1S	2.46(8)	6(16)					
1Br	2.44(4)	5(6)					
1Im	2.04(2)	0(2)	-2(3)	0.0371	537.623	61.108	11

Table S18. Results of LacZ transcription reporter assays.

β-galactosidase results of Trials 1-4 and the internal replicates for WT- and E34A-RcnR.

	Miller Units							
	Trial 1A	Trial1B	Trial 2A	Trial 2B	Trial 3A	Trial 3B	Trial 4A	Trial 4B
Apo WT-RcnR	3.64	3.58	2.59	2.72	3.04	3.01	2.85	2.80
Co WT-RcnR	49.01	47.31	56.55	55.64	63.54	63.08	58.80	57.77
Ni WT-RcnR	40.45	43.23	38.61	40.13	66.96	61.70	61.89	60.21
Zn WT-RcnR	2.84	2.84	2.14	2.55	3.35	3.55	3.31	3.52
Apo E34A-RcnR	2.54	2.53	3.29	3.12	3.76	3.67	4.08	4.18
Co E34A-RcnR	52.72	51.15	51.64	50.08	58.98	62.33	58.10	57.37
Ni E34A-RcnR	46.89	47.49	45.21	46.19	63.11	61.43	59.67	63.90
Zn E34A-RcnR	2.85	2.82	3.42	2.94	3.43	3.16	3.38	3.68

β-galactosidase results of Trials 1-4 and the internal replicates for WT- and E34C-RcnR.

	Miller Units							
	Trial 1A	Trial1B	Trial 2A	Trial 2B	Trial 3A	Trial 3B	Trial 4A	Trial 4B
Apo WT-RcnR	2.21	2.32	1.98	2.01	3.11	3.16	3.65	3.63
Co WT-RcnR	57.75	54.13	50.85	48.44	59.68	59.59	66.55	66.12
Ni WT-RcnR	52.74	53.26	48.92	50.93	55.43	57.98	64.67	69.00
Zn WT-RcnR	2.34	2.29	2.08	1.96	3.17	3.18	3.09	3.31
Apo E34C-RcnR	2.10	1.79	2.64	3.41	2.96	2.92	4.04	4.13
Co E34C-RcnR	54.34	54.28	53.13	50.25	47.02	46.88	50.18	51.37
Ni E34C-RcnR	48.16	45.67	46.62	48.83	43.77	44.80	53.45	52.35
Zn E34C-RcnR	1.99	2.13	2.69	2.61	2.73	2.70	2.86	2.78

β-galactosidase results of Trials 1-4 and the internal replicates for WT- and E63A-RcnR.

	Miller Units							
	Trial 1A	Trial1B	Trial 2A	Trial 2B	Trial 3A	Trial 3B	Trial 4A	Trial 4B
Apo WT-RcnR	2.39	2.47	3.13	3.20	3.40	3.41	2.89	3.04
Co WT-RcnR	46.99	46.60	53.33	52.34	76.73	76.38	62.97	62.14
Ni WT-RcnR	43.31	43.15	51.47	50.57	85.53	78.76	63.88	63.44
Zn WT-RcnR	2.32	2.19	2.72	2.96	2.98	2.95	3.15	3.16
Apo E63A-RcnR	2.65	2.66	3.82	3.88	4.03	4.25	5.11	4.13
Co E63A-RcnR	42.26	42.58	56.22	55.47	25.84	25.15	60.25	59.31
Ni E63A-RcnR	22.95	23.13	27.98	27.68	56.08	57.21	30.18	29.97
Zn E63A-RcnR	2.65	2.59	3.72	3.59	2.72	3.28	3.58	3.49

β-galactosidase results of Trials 1-4 and the internal replicates for WT- and E63C-RcnR.

	Miller Units							
	Trial 1A	Trial1B	Trial 2A	Trial 2B	Trial 3A	Trial 3B	Trial 4A	Trial 4B
Apo WT-RcnR	2.67	2.65	2.83	2.86	2.81	2.71	2.73	2.73
Co WT-RcnR	58.71	59.06	59.43	58.38	52.07	50.20	50.38	49.01
Ni WT-RcnR	58.14	57.34	59.21	56.91	51.66	50.54	52.87	51.99
Zn WT-RcnR	2.38	2.33	2.47	2.47	2.54	2.49	2.46	2.34
Apo E63C-RcnR	4.13	4.17	3.94	3.72	3.01	3.14	3.05	2.97
Co E63C-RcnR	47.06	45.86	45.73	46.11	31.73	31.59	32.12	32.11
Ni E363C-RcnR	34.14	32.29	35.49	33.77	23.11	22.60	21.54	22.66
Zn E63C-RcnR	3.70	3.61	3.50	3.44	3.12	3.04	2.86	2.95

β-galactosidase results of Trials 1-4 and the internal replicates for WT- and E34A-RcnR titrated with different amounts of Co(OAc)$_2$.

μM Co(Ac)$_2$	0	10	30	50	70	90	110	130	180
WT-RcnR Trial One	5.06	14.94	47.87	60.84	67.93	77.05	81.01	82.69	86.69
WT-RcnR Trial Two	3.95	15.99	46.58	61.86	70.29	74.01	78.47	81.44	87.40
WT-RcnR Trial Three	2.00	9.18	35.86	44.74	44.89	59.11	61.89	65.19	71.35
WT-RcnR Trial Four	2.75	12.14	40.98	48.29	51.38	67.07	72.46	74.23	83.86
E34A-RcnR Trial One	6.47	14.07	48.69	45.00	49.77	52.73	55.88	53.42	55.05
E34A-RcnR Trial Two	7.44	17.28	53.85	70.81	78.87	77.01	82.57	85.20	84.26
E34A-RcnR Trial Three	2.62	7.42	35.92	45.40	49.79	62.90	64.75	72.74	66.17
E34A-RcnR Trial Four	2.21	6.45	33.59	42.64	45.44	56.27	57.52	60.89	67.31

β-galactosidase results of Trials 1-4 and the internal replicates for WT- and E34C-RcnR titrated with different amounts of Co(OAc)$_2$.

μM Co(Ac)$_2$	0	10	30	50	70	90	110	130	180
WT-RcnR Trial One	4.73	17.96	48.97	65.80	78.86	85.10	91.05	94.74	96.83
WT-RcnR Trial Two	4.44	15.19	50.57	70.69	85.32	94.81	94.46	94.37	104.13
WT-RcnR Trial Three	2.97	5.85	36.54	46.92	47.05	57.21	60.80	60.05	62.78
WT-RcnR Trial Four	2.84	6.00	38.99	45.70	46.42	51.42	53.90	58.37	60.60
E34C-RcnR Trial One	5.51	12.87	41.71	58.25	62.38	69.74	73.25	76.06	86.84
E34C-RcnR Trial Two	7.06	16.10	42.82	58.78	64.81	75.25	75.74	75.46	81.94
E34C-RcnR Trial Three	3.87	9.29	32.62	46.05	49.20	59.86	61.84	65.83	70.41
E34C-RcnR Trial Four	3.76	9.72	32.91	46.38	51.32	57.66	60.58	57.09	58.90

β-galactosidase results of Trials 1-4 and the internal replicates for WT- and E34A-RcnR titrated with different amounts of Ni(OAc)$_2$.

μM Ni(OAc)$_2$	0	100	200	300	400	500	600	700	900
WT-RcnR Trial One	4.48	4.70	5.49	11.99	25.70	45.72	58.82	72.11	78.99
WT-RcnR Trial Two	4.71	4.83	5.16	12.60	25.46	45.57	63.03	60.69	85.08
WT-RcnR Trial Three	4.93	5.14	6.45	19.80	42.04	69.96	81.85	95.46	108.63
WT-RcnR Trial Four	4.60	5.05	5.78	17.60	34.86	61.19	63.06	78.04	119.48
E34A-RcnR Trial One	3.81	4.20	4.78	10.03	21.63	38.71	54.16	61.68	73.32
E34A-RcnR Trial Two	3.72	4.03	4.87	10.89	21.60	38.98	51.36	78.11	86.23
E34A-RcnR Trial Three	9.15	10.01	13.35	20.23	45.20	80.23	91.34	104.6	114.31
E34A-RcnR Trial Four	6.63	7.24	8.59	14.91	28.43	47.68	56.23	78.07	104.60

β-galactosidase results of Trials 1-4 and the internal replicates for WT- and E34C-RcnR titrated with different amounts of Ni(OAc)$_2$.

μM Ni(OAc)$_2$	0	100	200	300	400	500	600	700	900
WT-RcnR Trial One	4.61	4.86	5.32	13.51	21.16	41.66	61.39	80.06	88.36
WT-RcnR Trial Two	4.13	4.26	4.52	11.30	16.99	37.30	50.17	71.49	84.45
WT-RcnR Trial Three	6.72	7.02	7.96	10.70	39.24	64.75	98.41	155.22	145.97
WT-RcnR Trial Four	5.50	4.93	5.13	6.83	26.87	55.84	71.37	99.06	117.77
E34C-RcnR Trial One	7.28	7.20	7.42	10.03	18.89	33.52	60.26	78.75	99.89
E34C-RcnR Trial Two	6.72	7.16	6.62	8.60	16.84	30.39	51.69	70.01	91.18
E34C-RcnR Trial Three	9.02	9.28	10.10	12.87	30.72	55.82	66.69	89.88	110.99
E34C-RcnR Trial Four	7.45	7.98	8.47	10.98	24.01	41.73	56.58	72.07	95.81
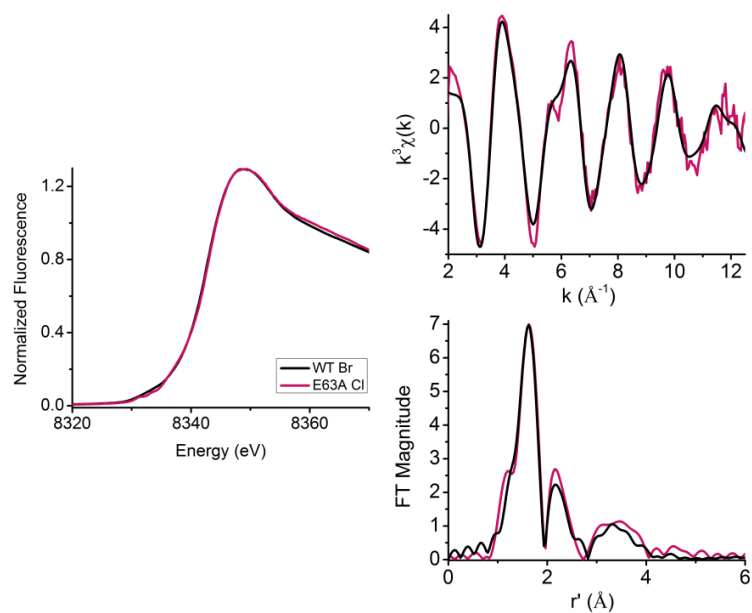
Figure S1: Left: XANES spectrum of E63A-RcnR (magenta) complexed to Ni(II) in 20 mM HEPES, 300 mM NaCl, and 10% glycerol at pH 7.0 and WT-RcnR (black) complexed to Ni(II) in 20 mM HEPES, 300 mM NaBr, and 10% glycerol at pH 7.0. Top Right: Unfiltered k^3-weighted XAS data (magenta) and fit (black). Bottom Right: Fourier filtered XAS data (magenta) and best fit (black).
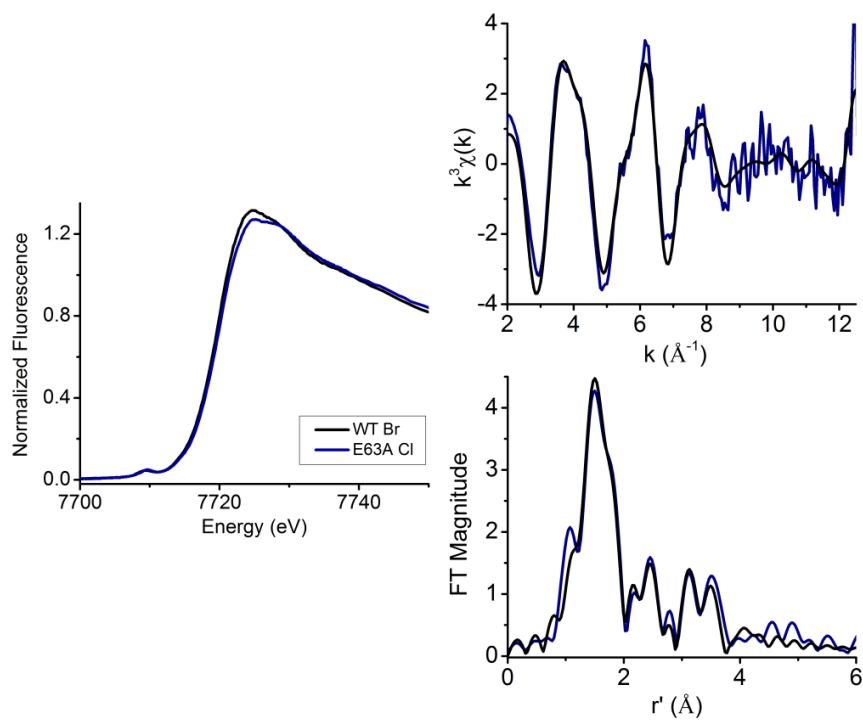
Figure S2: Left: XANES spectrum of E63A-RcnR (navy blue) complexed to Co(II) in 20 mM HEPES, 300 mM NaCl, and 10% glycerol at pH 7.0 and WT-RcnR (black) complexed to Co(II) in 20 mM Hepes, 300 mM NaBr, and 10% glycerol at pH 7.0. Top Right: Unfiltered k^3-weighted XAS data (navy blue) and fit (black). Bottom Right: Fourier filtered XAS data (navy blue) and best fit (black).
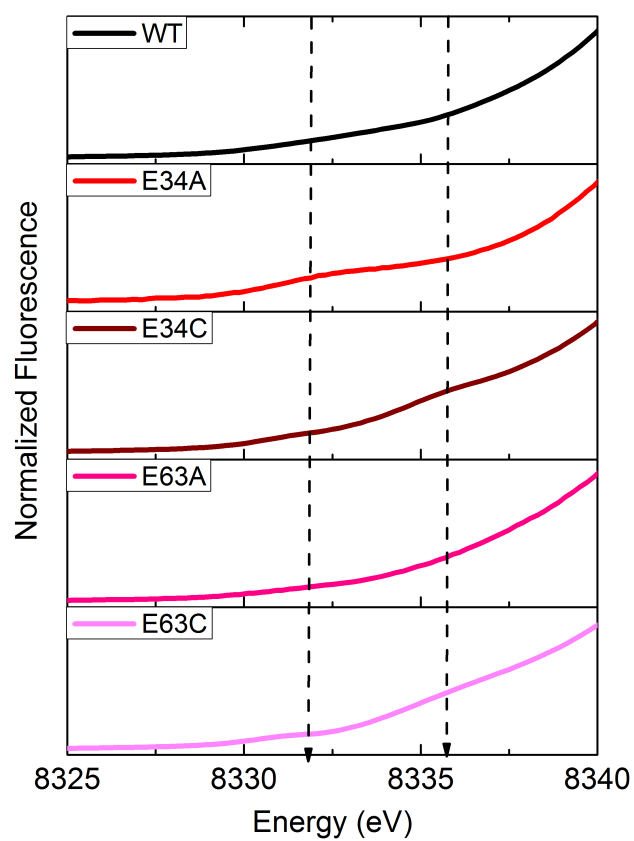
Figure S3: Stacked XANES pre-edge features of metal complexes of *Ec*RcnR proteins in buffer with 20 mM HEPES, 300 mM NaBr, 1 mM TCEP and 10% glycerol (pH 7.0). Dotted lines indicate approximate areas for the 1s → 3d and 1s → 4p_z transitions.
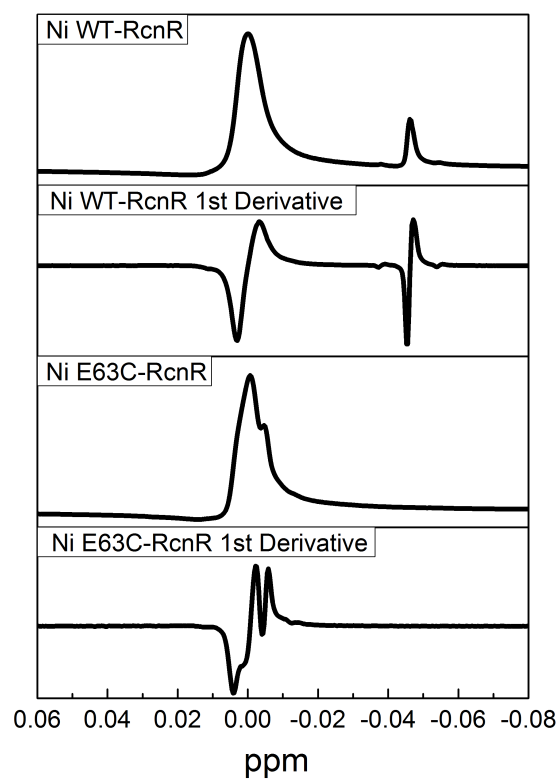
Figure S4: ^{1}H NMR spectra of the DSS reference peak in solution with the Ni(II) complexes of WT- and E63C-RcnR in 20 mM HEPES, 100 mM NaCl, 1 mM TCEP, 10% glycerol, pH 7.0 in 90% H_2O/10% D_2O.
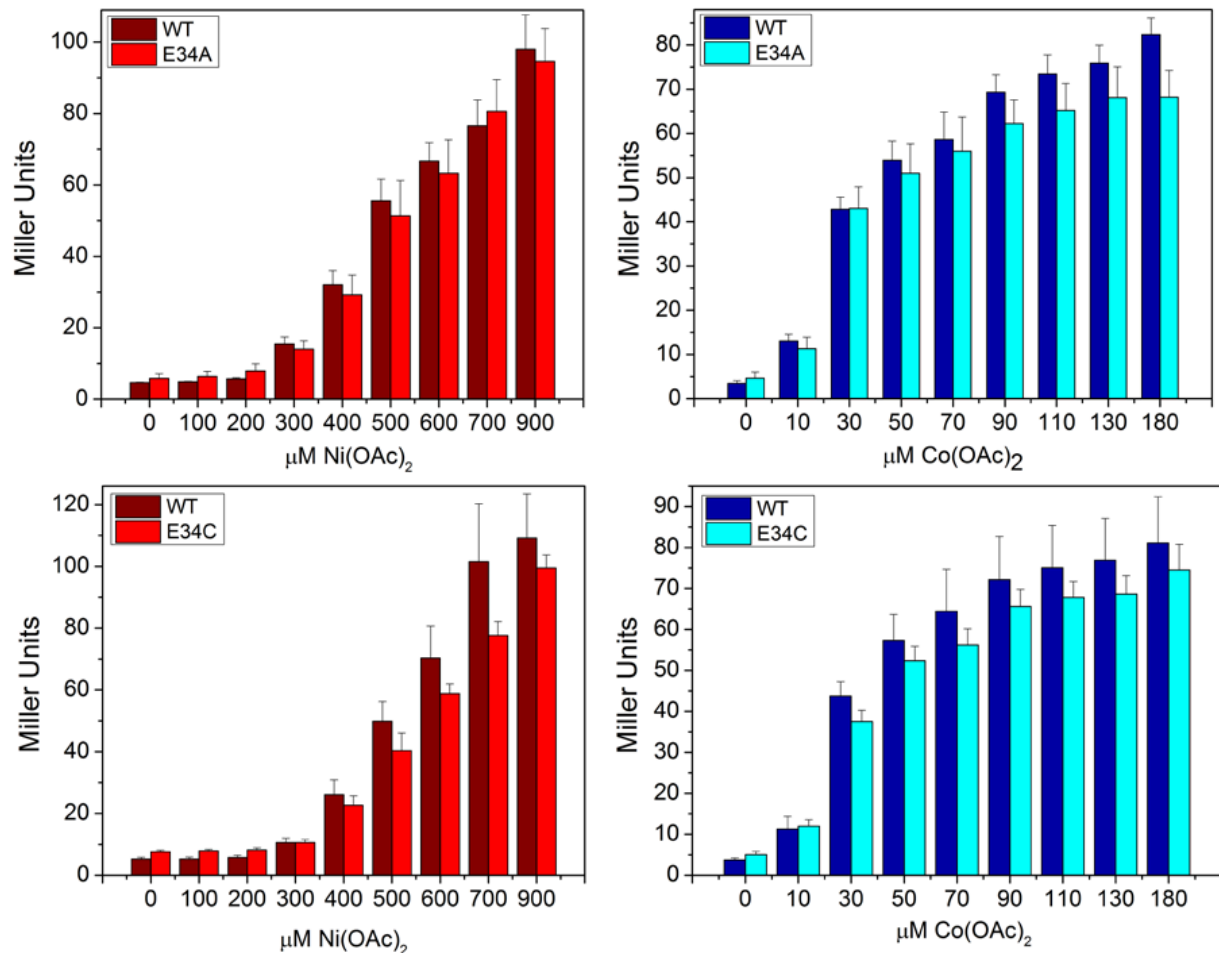
Figure S5. LacZ transcription reporter assays of titrations of WT-, E34A-, and E34C-RcnR with Ni(II) and Co(II shchowing the effect of the E34A-, and E34C-RcnR mutations on the expression of PrcnA in response to binding metal ions. The data is an average of four replicates. The error bars represent the standard deviation.
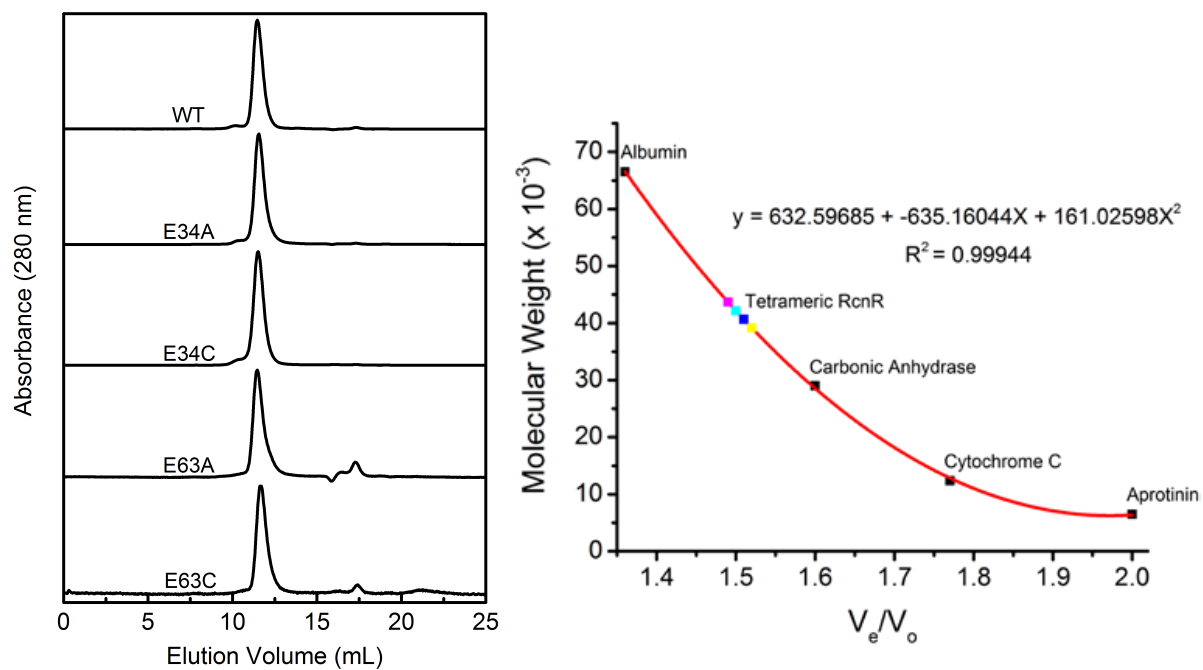
Figure S6: Size-exclusion chromatograms for WT-RcnR and Glu variants in 20 mM HEPES, 150 mM NaCl, 5 mM EDTA,1 mM TCEP, 10 % glycerol, pH 7.0 (left), and calibration curve (right) showing the the retention volume versus molecular mass for the standards and RcnR proteins (WT (green marker) E34A (blue marker), E34C (cyan marker), E63A (pink marker), and E63C (yellow marker). The red line represents the second order polynomial fit for the standards.
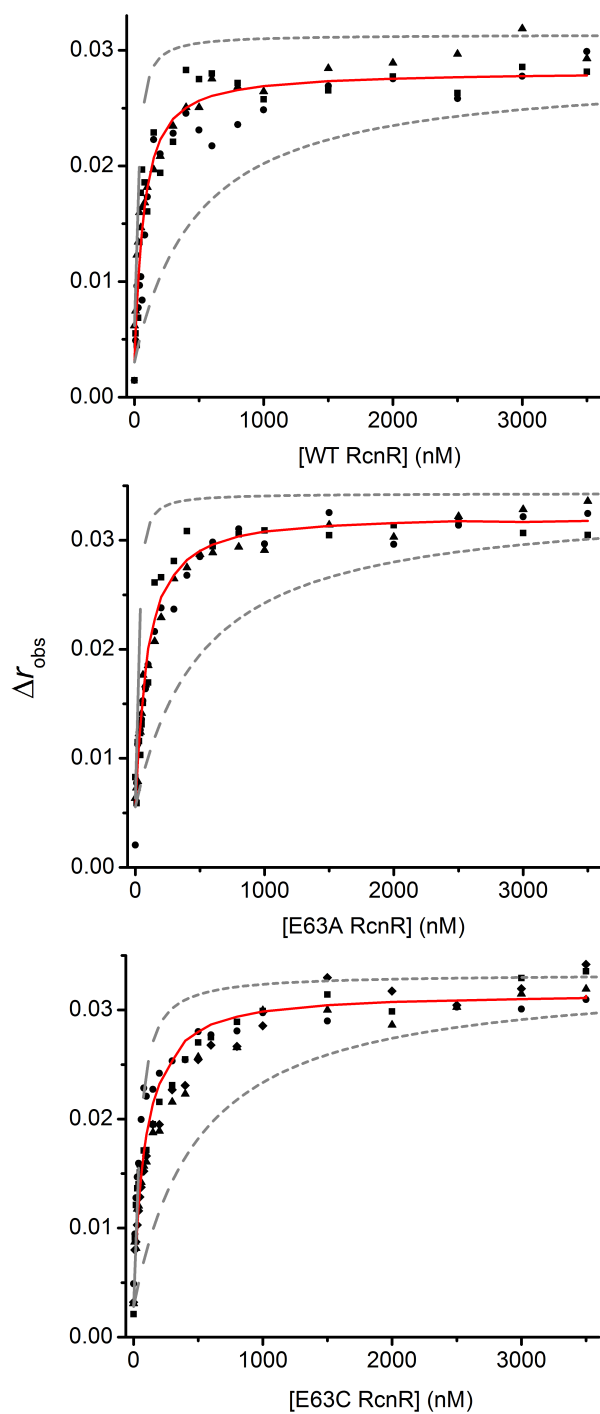
Figure S7: Anisotropy change upon titration of DNA (10 nM) with apo-RcnR (protomer concentration stated). Experiment performed aerobically in the presence of 1 mM TCEP and 5 mM EDTA.
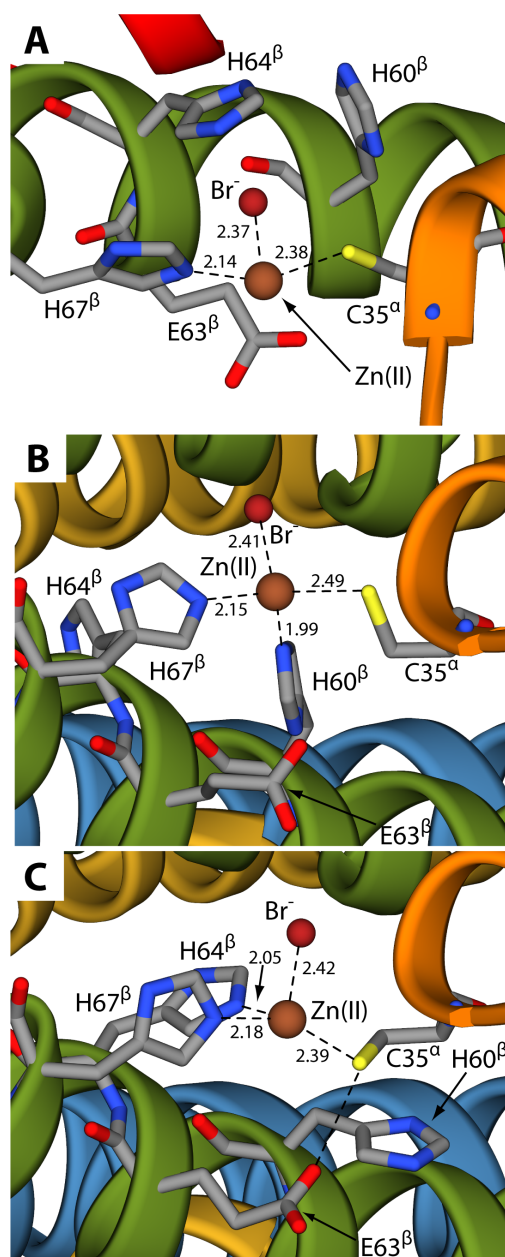
Figure S8. Details of one of the three modeled Zn(II) binding sites on *Ec*RcnR model structure. Panels **A**, **B**, and **C** report the results for Zn-1, Zn-2a, Zn-2b modeling, respectively. *Ec*RcnR backbone is reported as ribbons colored accordingly to the protein chain, as in Figure 7. Putative metal binding residues are reported as sticks colored accordingly to atom types. The Zn(II) and Br⁻ ions are showed as brown and dark red spheres, respectively. The reported distances are in Angstroms.

Supplementary details of molecular modelling for *Ec*RcnR

Zinc

The fitting of the XAS data for the Zn(II) complex with *Ec*RcnR is consistent with a (N/O)$_2$SBr or with a (N/O)$_3$SBr center with two histidine ligands, and contributions from one cysteine sulfur and one bromide derived from the buffer. The histidine and the cysteine ligands appear to be His67 and Cys35, while His3 and the N-terminal amine are not involved in Zn(II) binding. Thus, the aim of our modeling calculation was to identify other putative Zn(II) ligands in order to complete the coordination sphere of the ion and give hints on the coordination number. The present study also indicated that neither Glu34 nor Glu63 are ligands to Zn(II), with Glu63 having a marginal role in ordering the Zn(II) site. In the first modeling scheme (named Zn-1) we included four Zn(II) ions, each constrained to Cys35 from one chain and His67 from the second chain of each dimer. A Br$^-$ ion was also bound to each Zn(II) ion by using a distance restraint. The resulting modeled metal binding site is reported in Fig. S13A. The bond distances between the Zn(II) ion and the ligands are compatible with those reported in Table 1. The coordination geometry is clearly incomplete, but interestingly both His60 and His64 seems to be near to the Zn(II) ion to complete a hypothetical tetrahedral coordination sphere. Glu63 is in the close vicinity of the Zn(II).

We thus performed two new modeling schemes (named Zn-2a and Zn-2b, see Table 2) using the same restraints as in Zn-1, and including His60 or His64 bound to the Zn(II) ion, respectively. No torsional restraints were added to constraint the coordination geometry of the metal ion. The results of these calculations are shown in Fig. S13B,C. In the case of Zn-2a, the coordination geometry of the Zn(II) ion appear to be highly distorted. In particular, the angle formed by His60(Nε)-Zn(II)-Cys35(Sγ) is 77°. This angle is not compatible with any coordination geometry, even if one considers that there could be putative empty coordination site that should be occupied by an oxygen atom or by a nitrogen atom. On the other hand, the angles in the Zn-2b modelling are in good agreement with a distorted tetrahedral moiety. Glu64 Oε1 spontaneously positions at H-bond distance with the thiol group of Cys35. The bond distances are in good agreement with those determined experimentally (Table 1).